Enhancement of MEMS-Based Ultrasonic Transducers for Sensing Applications Using Machine Learning

by

Amirhossein MOSHREFI

THESIS PRESENTED TO ÉCOLE DE TECHNOLOGIE SUPÉRIEURE
IN PARTIAL FULFILLMENT FOR THE DEGREE OF
DOCTOR OF PHILOSOPHY
PH.D.

MONTREAL, 14, FEBRUARY, 2025

ÉCOLE DE TECHNOLOGIE SUPÉRIEURE
UNIVERSITÉ DU QUÉBEC

BOARD OF EXAMINERS (THESIS PH.D.)

THIS THESIS HAS BEEN EVALUATED

BY THE FOLLOWING BOARD OF EXAMINERS

Prof. Frederic Nabki, Thesis Supervisor
Electrical Engineering at École de technologie supérieure

Prof. Dominic Deslandes, President of the Board of Examiners
Electrical Engineering at École de technologie supérieure

Prof. Pierre Bélanger, Member of the jury
Mechanical Engineering at École de technologie supérieure

Prof. Yves Audet, Member of the jury
Electrical Engineering at Polytechnique Montréal

THIS THESIS WAS PRENSENTED AND DEFENDED

IN THE PRESENCE OF A BOARD OF EXAMINERS AND PUBLIC

ON 6, FEBRUARY, 2025

AT ÉCOLE DE TECHNOLOGIE SUPÉRIEUR

ACKNOWLEDGEMENTS

I am grateful to my supervisor, Professor Frederic Nabki, for his support, and guidance throughout my doctoral journey.

My gratitude extends to NSERC, ReSMiQ, and CMC for their support.

Lastly, I owe my gratitude to my family—Dad and Mom. Your constant support, love, and encouragement have been the foundation of my journey.

AMÉLIORATION DES TRANSDUCTEURS ULTRASONIQUES MEMS POUR LES APPLICATIONS DE DÉTECTION UTILISANT L'APPRENTISSAGE AUTOMATIQUE

Amirhossein MOSHREFI

RÉSUMÉ

Cette thèse présente une exploration approfondie de l'intégration de la transmission de signaux ultrasonores, du traitement de signaux ultrasonores par techniques d'intelligence artificielle et de méthodologies avancées de détection de pannes, mettant en évidence la synergie entre ces technologies à travers trois études interconnectées.

La première étude introduit un système télémétrique ultrasonore aéroporté de haute précision basé sur des transducteurs ultrasonores micromécaniques piézoélectriques (PMUTs). Utilisant à la fois des émetteurs (Tx) et des récepteurs (Rx) fabriqués avec des faisceaux piézoélectriques hautement sensibles, le système fonctionne sur le principe du temps de vol (ToF), où les ondes ultrasonores voyagent entre le Tx et le Rx pour détecter des obstacles ou calculer des distances. Amélioré par des modèles d'apprentissage profond—spécifiquement des réseaux de neurones convolutifs (CNN) avec validation croisée en k-plis—le télémètre atteint une précision supérieure par rapport aux méthodes traditionnelles, assurant des performances robustes dans des environnements variés. Cela le rend adapté à des applications en robotique, réalité augmentée et systèmes de sécurité industrielle.

La deuxième étude se concentre sur l'application du traitement des signaux ultrasonores pour la détection de pannes industrielles, n'employant que le récepteur (Rx). En se concentrant sur les pipelines et les systèmes moteurs, cette recherche utilise le Rx pour détecter des défauts mécaniques en capturant des signaux ultrasonores et en appliquant des techniques avancées d'extraction de caractéristiques dans les domaines temporel et fréquentiel. Des caractéristiques clés—incluant l'asymétrie, le kurtosis et le facteur de crête—sont extraites, et des méthodes de réduction de dimensionnalité comme l'analyse en composantes principales (ACP) et l'analyse discriminante linéaire (ADL) sont utilisées pour simplifier les données. Des classificateurs d'apprentissage automatique tels que les k-plus proches voisins (KNN), les machines à vecteurs de support (SVM) et les arbres de décision (AD) sont utilisés en conjonction avec des techniques d'apprentissage par ensemble comme le stacking et le boosting pour améliorer la précision et la fiabilité de la détection de pannes. La capacité du système à détecter et classifier les pannes en temps réel est en outre validée en déployant les modèles sur des microcontrôleurs (MCU), soulignant son potentiel pour des applications réelles.

La troisième étude explore l'utilisation de modèles d'apprentissage automatique par ensemble pour la détection de pannes en temps réel utilisant les ultrasons. En mettant l'accent sur la scalabilité et l'efficacité, cette recherche démontre l'utilisation de signaux ultrasonores pour la surveillance de systèmes industriels tels que les pipelines et les machines rotatives. Le Rx joue un rôle central en capturant les signaux ultrasonores, qui sont ensuite traités et analysés par des

algorithmes d'apprentissage automatique pour détecter des défauts comme les fuites, les blocages et les défaillances de roulements. L'étude compare plusieurs modèles d'apprentissage par ensemble—including gradient boosting (GB), classificateurs par vote et AdaBoost—and évalue leurs performances en utilisant une validation croisée en k-plis. Le déploiement de ces modèles sur des dispositifs à ressources limitées comme les MCU ARM Cortex-M4F démontre la faisabilité de la surveillance des pannes en temps réel sur des systèmes embarqués. Cette approche répond non seulement aux besoins industriels actuels, mais pave également la voie pour de futures innovations dans la détection sans fil et les systèmes de surveillance intelligents.

En conclusion, les recherches présentées dans ces études soulignent le rôle prometteur des ultrasons, améliorés par l'apprentissage automatique, dans l'augmentation de l'efficacité, de la sécurité et de la fonctionnalité des systèmes industriels. En intégrant des capteurs ultrasonores avec des techniques avancées d'apprentissage automatique, les systèmes développés fournissent une détection et un diagnostic des pannes en temps réel robustes, offrant des améliorations significatives par rapport aux méthodes de surveillance traditionnelles. La mise en œuvre réussie de ces technologies répond à des défis industriels pressants—tels que la détection précoce des pannes dans les pipelines et les machines—et jette les bases pour de futures innovations dans la détection sans fil, les systèmes embarqués et la surveillance en temps réel dans divers secteurs. Ce travail établit une base pour la poursuite de la recherche vers des solutions plus efficaces et évolutives pour l'automatisation industrielle, la maintenance prédictive et la surveillance de la sécurité.

Mots-clés : traitement des signaux ultrasonores, apprentissage automatique, systèmes embarqués, surveillance en temps réel, transducteurs ultrasoniques piézoélectriques micromécaniques (PMUTs), automatisation industrielle

ENHANCEMENT OF MEMS-BASED ULTRASONIC TRANSDUCERS FOR SENSING APPLICATIONS USING MACHINE LEARNING

Amirhossein MOSHREFI

ABSTRACT

This thesis presents an in-depth exploration of the integration of ultrasonic signal transmission, ultrasonic signal processing, and advanced fault detection methodologies, highlighting the synergy among these technologies through three interrelated studies.

The first study introduces a high-precision airborne ultrasonic rangefinder system based on piezoelectric micromachined ultrasonic transducers (PMUTs). Utilizing both transmitters (Tx) and receivers (Rx) fabricated with highly sensitive piezoelectric beams, the system operates on the time-of-flight (ToF) principle, where ultrasonic waves travel between the Tx and Rx to detect obstacles or calculate distances. Enhanced by deep learning models—specifically convolutional neural networks (CNNs) with k-fold cross-validation—the rangefinder achieves superior accuracy compared to traditional methods, ensuring robust performance in diverse environments. This makes it suitable for applications in robotics, augmented reality, and industrial safety systems.

The second study focuses on the application of ultrasonic signal processing for industrial fault detection, employing only the receiver (Rx). Concentrating on pipelines and motor systems, this research utilizes the Rx to detect mechanical faults by capturing ultrasonic signals and applying advanced feature extraction techniques in both time and frequency domains. Key features—including skewness, kurtosis and crest factor—are extracted, and dimensionality reduction methods like principal component analysis (PCA) and linear discriminant analysis (LDA) are employed to streamline the data. Machine learning classifiers such as k-nearest neighbors (KNN), support vector machines (SVM) and decision trees (DT) are used in conjunction with ensemble learning techniques like stacking and boosting to enhance accuracy and reliability in fault detection. The system's ability to detect and classify faults in real time is further validated by deploying the models on microcontroller units (MCUs), underscoring its potential for real-world applications.

The third study explores the use of ensemble machine learning models for real-time fault detection using ultrasonics. Emphasizing scalability and efficiency, this research demonstrates the use of ultrasonic signals for monitoring industrial systems such as pipelines and rotating machinery. The Rx plays a central role in capturing ultrasonic signals, which are then processed and analyzed by machine learning algorithms to detect faults like leaks, blockages, and bearing failures. The study compares several ensemble learning models—including gradient boosting (GB), voting classifiers, and AdaBoost—and evaluates their performance using k-fold cross-validation. Deployment of these models on resource-constrained devices like ARM Cortex-M4F MCUs demonstrates the feasibility of real-time fault monitoring on embedded systems. This approach not only addresses current industrial needs but also paves the way for future innovations in wireless sensing and smart monitoring systems.

In conclusion, the research presented in these studies underscores the promising role of ultrasonics, enhanced by machine learning, in augmenting industrial system efficiency, safety, and functionality. By integrating ultrasonic sensors with advanced machine learning techniques, the developed systems provide robust, real-time fault detection and diagnostics, offering significant improvements over traditional monitoring methods. The successful implementation of these technologies addresses pressing industrial challenges—such as early fault detection in pipelines and machinery—and lays the groundwork for future innovations in wireless sensing, embedded systems, and real-time monitoring across various sectors. This work establishes a strong foundation for ongoing research into more efficient, scalable solutions for industrial automation, predictive maintenance, and safety monitoring.

Keywords: ultrasonic signal processing, machine learning, embedded systems, real-time monitoring, piezoelectric micromachined ultrasonic transducers (PMUTs), industrial automation

TABLE OF CONTENTS

Page

LIST OF TABLES

Page

LIST OF FIGURES

LIST OF ABREVIATIONS

ADAS	Advanced Driver Assistance Systems
AI	Artificial Intelligence
AlN	Aluminum Nitride
AUC	Area Under Curve
CC	Cross-Correlation
CCRD	Central Composite Rotatable Design
CMUT	Capacitive Micromachined Ultrasonic Transducer
CNN	Convolutional Neural Network
CV	Cross Validation
DA	Data Analysis
DL	Deep Learning
DRIE	Deep Reactive Ion Etching
DT	Decision Tree
EMD	Empirical Mode Decomposition
FC	Fully Connected
FEA	Finite Element Analysis
FEM	Finite Element Method
FEM	Finite Element Modeling
FFT	Fast Fourier Transform
FN	False Negative
FP	False Positive
FPR	False Positive Rate
FRFT	Fractional Fourier Transform
FS	Feature Selection
FVM	Finite Volume Method
GB	Gradient Boosting
GMM	Gaussian Mixture Model
GNB	Gaussian Naive Bayes
GVF	Gradient Vector Flow

ICA	Independent Component Analysis
IoT	Internet of Things
IPF	Iterative Principal Factor
IQR	Interquartile Range
IR	Infrared
KNN	k-Nearest Neighbor
LCD	Liquid Crystal
LDA	Linear Discriminant Analysis
LDV	Laser Doppler Vibrometry
LR	Logistic Regression
MCU	Micro-controller Unit
ML	Machine Learning
MLP	Multilayer Perceptron
PCB	Printed Circuit Board
PCA	Principle Component Analysis
PMUT	Piezoelectric Micromachined Ultrasonic Transducer
PSG	Plasma-Enhanced Silicon Glass
QF	Quality Factor
RF	Random Forest
RF	Radio Frequency
RFE	Recursive Feature Elimination
ROC	Receiver Operating Characteristic
RS	Random Sampling
Rx	Receiver
SNR	Signal to Noise Ratio
SVM	Support Vector Machine
TEM	Transmission Electron Microscopy
t-SNE	t-distributed Stochastic Neighbor Embedding
TN	True Negative
ToF	Time of Flight

TP	True Positive
TPR	True Positive Rate
Tx	Transmitter
UMAP	Uniform Manifold Approximation and Projection
UWB	Ultra-Wideband
VMD	Variational Mode Decomposition
WDT	Wavelet Denoising Transform

LIST OF SYMBOLS

A	Surface Area
D	Dielectric Charge
E	Electric Field
f	Frequency
K_b	Boltzmann Constant
P	Probability Distribution
Q	Charge
S	Stress
T	Strain
V	Voltage
t	Thickness
ε	Dielectric Constant
μ	Average
ρ	Gradient Step Size
σ	Standard Deviation
ω	Angular Frequency

INTRODUCTION

In today's technological landscape, the demand for efficient, accurate, and scalable diagnostic and monitoring systems spans multiple sectors, including healthcare, manufacturing, and infrastructure. These industries require real-time, cost-effective solutions that can perform reliably under varied and often harsh conditions. Ultrasonic technology, with its non-invasive and high-resolution capabilities, has become a prominent tool to meet these needs. When combined with machine learning and wireless communication, ultrasonic systems offer a transformative approach to addressing challenges in fault detection, range measurement, and flow monitoring.

MEMS-based ultrasonic transducers are particularly well-suited for these applications due to their compact size, low power consumption, and ability to operate in non-contact configurations. Advances in real-time data processing have expanded their utility in precision diagnostics and monitoring. However, significant challenges remain, limiting the full potential of ultrasonic systems. These include bandwidth limitations, susceptibility to environmental noise, and the computational intensity of advanced signal processing algorithms. Furthermore, current solutions often face limitations in range and efficiency, and their hardware complexity can increase production costs, hindering scalability in resource-limited settings.

This thesis seeks to address these challenges by developing and optimizing ultrasonic systems that integrate MEMS technology, machine learning, and ultrasonic signal transmission and reception. The research presented here focuses on designing high-accuracy ultrasonic rangefinders and fault detectors using advanced signal processing techniques. Additionally, machine learning algorithms are embedded within these systems to enhance performance across a range of applications.

Context

Ultrasonic micromachined transducers (MUTs), primarily categorized as capacitive and piezoelectric, are advancing the development of compact and cost-efficient sensing solutions. These transducers offer several advantages, including seamless integration with electronic systems, reduced manufacturing costs, and enhanced coupling performance. According to the Market Research and Strategy Center (Yole Group, 2023), the global market for MUT-based

ultrasonic modules, valued at $2.1 billion in 2017, is projected to grow to $6.2 billion by 2025. Figure 0.1 illustrates this forecast across various sectors. Although the market saw a decline in 2020, dropping from $4.6 billion in 2019 to $3.8 billion, a steady recovery is expected, with a CAGR of 5.1% driving growth towards the $6.2 billion mark by 2025. Key application areas include automotive ADAS, industrial automation, consumer fingerprint sensors, and medical technologies, underscoring MUTs' wide-ranging industrial applicability and versatility.

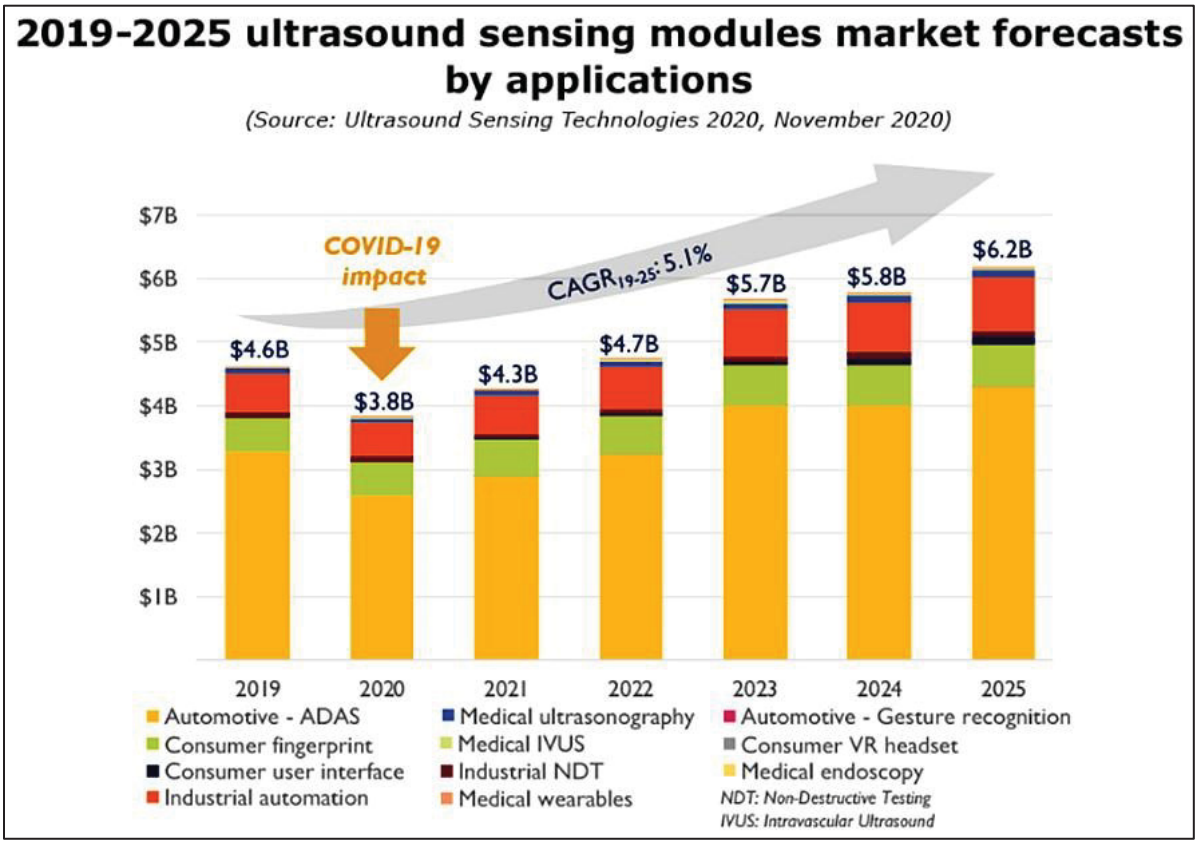

Figure 0.1 Forecasts of ultrasound sensing modules market
Taken from Yole Group (2023)

As illustrated in Figure 0.2, the top section of MUTs is coated with a metal layer. When an electrical voltage is applied to this metal, it induces mechanical vibrations in the underlying material. Similarly, applying a mechanical force to the piezoelectric crystal generates an electrical voltage. The resonant frequency of the transducer is typically governed by its thickness. To enhance wave transmission efficiency, a matching layer is positioned in front of

the transducer to optimize the power transfer of the emitted waves (Maadi, M., 2020). The device operates in two primary modes:

Transmission Mode (Figure 0.2a): In this mode, an electrical signal (voltage) is applied to the piezoelectric material, causing it to deform and produce ultrasound waves, which are then emitted from the transducer. The metal layers surrounding the piezoelectric element facilitate the efficient transmission of these waves.

Reception Mode (Figure 0.2b): In reception mode, the transducer operates in reverse. When ultrasound waves strike the piezoelectric material, they induce vibrations that generate a corresponding electrical signal. This signal can subsequently be processed and analyzed. The metal layers assist in capturing and transferring the ultrasound energy effectively to the piezoelectric element, enhancing signal quality.

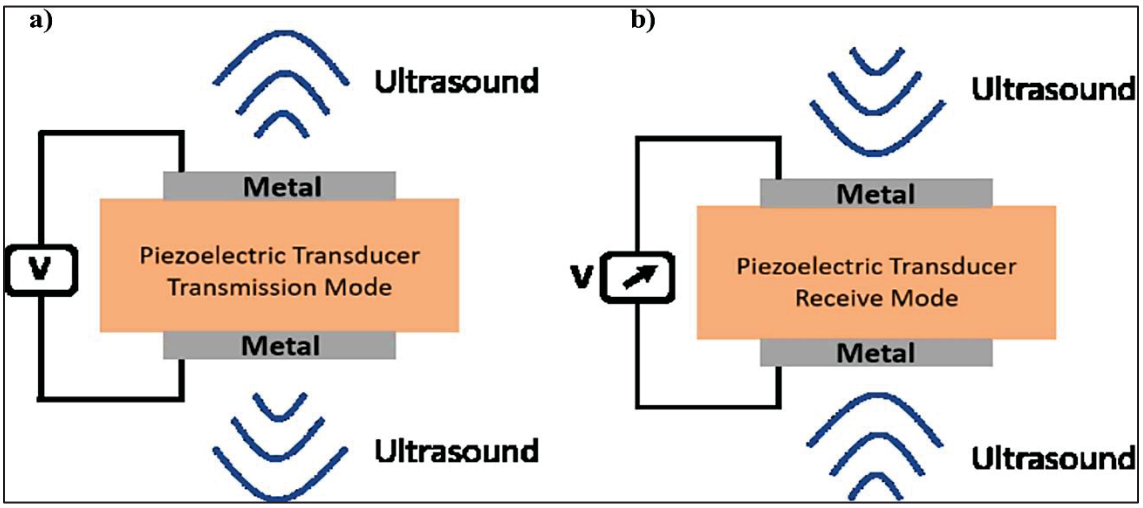

Figure 0.2 Piezoelectric Transducers in transmit and receive operation modes
Taken from Maadi, M. (2020)

Piezoelectric micro-machined ultrasonic transducers (PMUTs) leverage a piezoelectric structure that facilitates the design of compact, thin devices well-suited for modern applications. They are compatible with integrated circuits, provide high bandwidth, and are capable of effective coupling in water. The small size of PMUTs supports high operational frequencies and reduces production costs. One of their unique advantages is the flexibility in adjusting frequency modes by varying the thickness of the piezoelectric and polymer layers.

PMUTs can operate in both transmitting and receiving modes for ultrasound waves, with their behavior defined by the following fundamental equations:

$$D = dT + \varepsilon^{T}E \tag{0.1}$$

$$S = s^{E}T + d^{t}E \tag{0.2}$$

where D is the electrical displacement, T is the mechanical stress, E is the electrical field, S is the strain, ε^{T} is the dielectric constant measured at a constant stress, s^{E} is the elastic compliance measured at a constant electrical field, and d and d^{t} are the piezoelectric coefficients for the direct and converse piezoelectric effects, respectively. Finally, by simplifying these equations, it can be seen that the two piezoelectric constants d_{33} and d_{31} determine the characteristics and response of the transducer. The PMUTs are usually divided into two categories; Thickness Extension Mode (TEM) and Flexural Vibration Mode (FVM) that have piezoelectric constants of d_{31} and d_{33} respectively (Wang, H., et.al. (2020)).

Thickness Extension Mode: As shown in Figure 0.3, this structure consists of a piezoelectric material, two electrodes, a backing layer, and a matching layer. The resonance frequency, f, is determined by the speed of sound, C_P, within the piezoelectric material and its thickness, t, and can be expressed as:

$$f = \frac{nC_{p}}{2t} \tag{0.3}$$

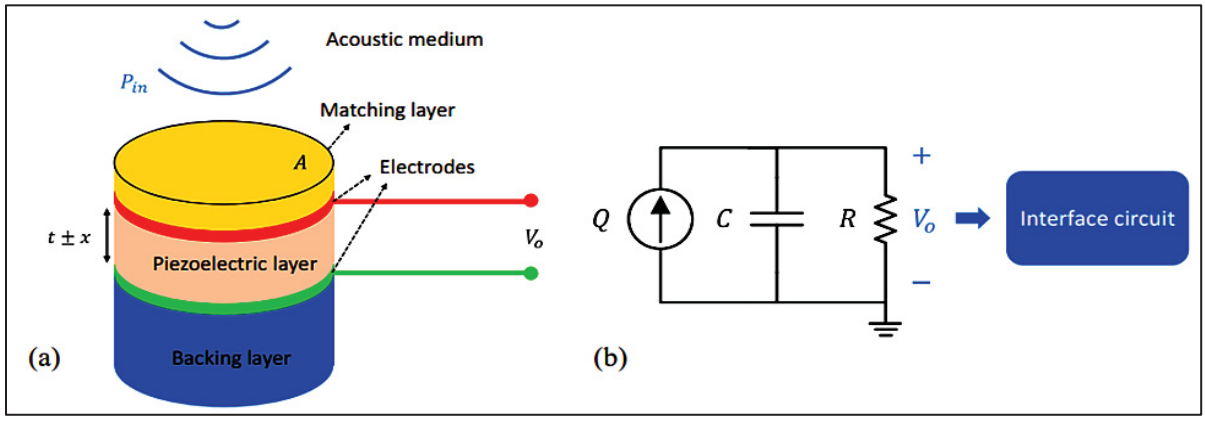

Figure 0.3 TEM Piezoelectric Transducer a) structure b) equivalent circuit
Taken from Wang, H., et.al. (2020)

where n is the number of the mode.

Flexural Vibration Mode: This structure, which is shown in Figure 0.4, includes a thin membrane and a cavity. The membrane contains a piezoelectric material, two electrodes and one elastic layer which is excited by the d_{31} coefficient to achieve vibration.

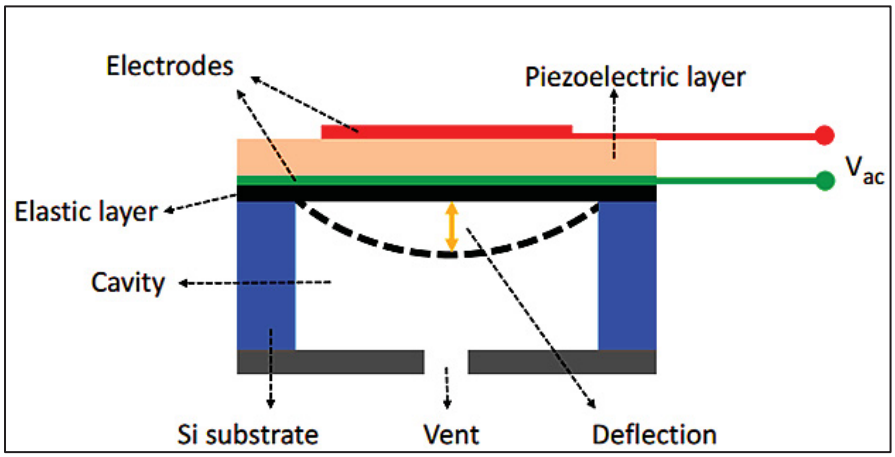

Figure 0.4 Schematic of FVM piezoelectric transducer
Taken from Wang, H., et.al. (2020)

Common piezoelectric materials used in this structure include ZnO, AlN, and PZT. While ZnO offers suitable piezoelectric properties, it is vulnerable in liquid environments (e.g., in medical applications) and is therefore not recommended for such uses. AlN, on the other hand, provides superior thermal and chemical stability compared to ZnO, making it a more practical choice for a wider range of applications. Both sputtered-PZT and sol-gel PZT exhibit high coupling coefficients and strong piezoelectric constants, enhancing the efficiency and sensitivity of the transducer.

Wireless transmission enables information exchange between devices without physical connections like cables or wires. With the rise of digital communication, wireless transmission has become integral to numerous applications, ranging from everyday devices like smartphones and laptops to industrial systems, medical devices, and Internet of Things (IoT) solutions. A variety of wireless technologies has emerged to meet specific requirements, each with distinct advantages and limitations based on the transmission medium and operational environment.

Wireless transmission can be achieved through various methods, including radio frequency (RF), infrared (IR), optical, and ultrasonic techniques, each with unique characteristics. For instance, RF transmission is prevalent due to its extended range and high signal rates, though it can be prone to interference and requires regulatory compliance. Infrared transmission, while secure and power-efficient, relies on a clear line-of-sight and is vulnerable to obstacles, such as furniture or walls, which can disrupt IR signals. Additionally, IR can be affected by ambient light sources like sunlight or artificial lighting, which may degrade signal quality. Optical methods, using visible or laser light, provide high bandwidth and efficiency but face challenges from environmental conditions such as fog or reflective surfaces, requiring an unobstructed line of sight.

Ultrasonic transmission, relying on sound waves in the ultrasonic frequency range, offers distinct advantages over these traditional methods, particularly when implemented using MEMS technology. Ultrasonic waves are less susceptible to electromagnetic interference, making them ideal for environments where RF signals are prone to disruption. Unlike IR, ultrasonic signals are less affected by light or minor obstacles, giving them a clear advantage in specific applications. MEMS-based ultrasonic transducers are compact, cost-effective, and can be easily integrated into small devices, making them well-suited for applications like medical devices, where space and power constraints are critical.

Moreover, ultrasonic communication can propagate through liquids, a capability that RF and optical signals lack. This makes ultrasonic transmission particularly useful in underwater environments or fluid-based applications, such as in industrial and medical settings. Additionally, the shorter range of ultrasonic signals enhances security by reducing the risk of interception. Through MEMS technology, ultrasonic transducers can be seamlessly integrated with other electronic components on a single chip, enabling the development of compact, reliable systems for healthcare, consumer electronics, and industrial IoT applications (Mazzilli & Dehollain, 2020).

Despite these advantages, MEMS-based wireless transmission faces challenges such as limited bandwidth, signal attenuation, and noise susceptibility, which can degrade signal quality and limit communication range. MEMS devices also have limited output power and must operate energy-efficiently, which can restrict their ability to handle high-frequency or continuous

signals. AI and advanced algorithms can help address these challenges by enabling adaptive signal processing to reduce noise, optimizing signal compression to manage bandwidth limitations, and using error correction to ensure signal integrity. Additionally, AI can manage power consumption, select efficient transmission paths, and support real-time signal analysis, significantly enhancing the performance and reliability of MEMS-based communication systems (Faudzi, Sabzehmeidani, & Suzumori, 2020).

Machine Learning: Importance and Advantages in MEMS Ultrasonic Applications

The contemporary technological landscape places significant emphasis on the development of highly accurate, scalable, and cost-effective diagnostic and monitoring solutions. Sectors such as healthcare, manufacturing, and infrastructure require robust tools capable of delivering real-time insights under harsh and variable conditions. Ultrasonic technology, renowned for its non-invasive probing and high spatial resolution, has emerged as a crucial modality for addressing these demands. When augmented by machine learning (ML) algorithms and wireless communication, ultrasonic systems become even more transformative, offering sophisticated approaches for fault detection, range measurement, and flow monitoring (Luijten, B., (2023)). ML-driven strategies have proven exceptionally powerful for boosting both performance and functionality in MEMS-based ultrasonic devices. Traditional ultrasonic sensing relies heavily on complex algorithms and threshold-based rules, which often suffer from reduced reliability in the presence of noise, signal attenuation, or unpredictable environmental fluctuations. In contrast, ML models excel by learning directly from data, adapting to changing operational scenarios, and refining their predictive capabilities over time. These data-driven techniques enable the creation of next-generation ultrasonic platforms that are markedly more flexible, accurate, and efficient than their conventional counterparts.

A key advantage of ML within MEMS ultrasonic applications lies in its ability to distill essential features from complex waveform data. Traditional signal processing methods may overlook minute yet significant signal variations, resulting in suboptimal performance in applications such as imaging, fault detection, or distance measurement. By leveraging deep learning architectures, ultrasonic systems can automatically learn to emphasize critical signal characteristics, thus enhancing detection accuracy and overall system resilience.

Moreover, machine learning techniques enable real-time classification and anomaly detection, pivotal for industrial and biomedical use cases. In industrial environments, advanced ML-empowered ultrasonic sensors can promptly identify early-stage mechanical wear or pipeline defects, minimizing downtime and operational expenses. In medical diagnostics, ML-enhanced ultrasonic imaging facilitates higher resolution and more reliable detection of pathologies, thereby improving patient outcomes. Ensemble learning methods, including gradient boosting and random forests, further bolster decision-making by amalgamating multiple predictive models, which improves reliability and diminishes the likelihood of false positives (Veroniki, A. A., et. al. (2025))

Another compelling benefit of incorporating ML into MEMS ultrasonic applications is the feasibility of energy-efficient data processing. MEMS devices often function in power-constrained settings, typical of IoT-based sensor networks, where resource optimization is critical. ML algorithms tailored for embedded systems, including lightweight neural networks and feature-selection techniques, reduce computational overhead without compromising accuracy. This combination of intelligence and efficiency renders ML especially attractive for real-world deployments that demand robust, low-power, and high-performing ultrasonic solutions.

In sum, the fusion of machine learning and MEMS-based ultrasonic technology paves the way for a new generation of intelligent, adaptive sensing systems. By harnessing sophisticated data-driven algorithms, these systems can operate reliably across diverse scenarios, deliver improved diagnostic capabilities, and open pathways to novel applications within and beyond traditional industrial and biomedical domains (Pyle. R, et. al. (2023); Gandomzadeh, D., et. al. (2023)).

This study thoroughly explores two ultrasonic applications: range-finding and fault detection. As the problem statement, it can be concluded that conventional ultrasonic rangefinders struggle to maintain accuracy over long distances, making them less reliable for extended-range applications. Existing fault detection methods primarily rely on vibration and acoustic emission analysis, which may not always be effective for early detection. Additionally, traditional approaches face challenges in capturing complex signal characteristics, limiting

their ability to extract meaningful features. Moreover, many fault detection systems are costly, making them less accessible for widespread industrial use.

Research Objectives

This thesis aims to advance the methodologies and performance of ultrasonic transmission through the design, fabrication, and optimization of novel MEMS-based devices. The research approach begins with the development of a specialized device, followed by the integration of data processing and pre-processing techniques to improve performance. A tailored model is then be formulated to address key parameters of interest, including latency, accuracy, and power consumption. The primary objectives of this research are as follows:

- To demonstrate the potential applications of MEMS-based ultrasonic communication systems.
- To identify and address the technical challenges inherent in implementing MEMS-based ultrasonic communication systems.
- To review and assess existing techniques and solutions developed for ultrasonic communication.
- To elucidate the operational principles of MEMS-based ultrasonic transducers and their integration with electronic systems.
- To evaluate the scalability and integration of ultrasonic communication systems in IoT and embedded devices.
- To investigate the application of ultrasonic communication as a framework for secure, short-range transmission.
- To design efficient, real-time embedded systems utilizing ultrasonic transmission, with applications spanning industrial automation, healthcare, and consumer electronics.

Thesis Contributions

This thesis makes the following original contributions:

1. **High-Accuracy Airborne Rangefinder via Deep Learning:** Designed and implemented an ultrasonic rangefinder based on piezoelectric transducers and deep

learning, achieving 100% accuracy. This rangefinder outperforms traditional models and is highly robust under diverse environmental conditions, making it suitable for advanced driver assistance systems (ADAS).

2. **Sensitive and Accurate Piezoelectric Sensor Design:** Developed a highly sensitive piezoelectric beam sensor, enhancing detection capabilities across ultrasonic applications, with significant improvements in diagnostic precision and operational reliability.
3. **Industrial Fault Detection Using Ultrasonic Signals:** Created a system that combines ultrasonic signal processing with machine learning models for fault detection in motors and pipelines, achieving high accuracy and enabling real-time deployment on microcontrollers.
4. **Integration of Machine Learning for Fault Diagnosis:** Utilized recursive feature elimination (RFE) and ensemble learning to refine feature sets and improve classification accuracy, producing robust and scalable fault detection systems for various industrial components.
5. **Innovative Real-Time Monitoring Embedded System:** Demonstrated the use of advanced machine learning models on an ARM Cortex M4 microcontroller, achieving real-time monitoring with optimized processing efficiency and minimized memory usage.
6. **Ultrasonic Flow Meter Design (Appendix II):** Designed a non-intrusive ultrasonic flow meter using microcantilevers to measure flow velocity based on time delay, showcasing accurate flow rate measurements in industrial settings.
7. **Low-Quality Factor CMUT for Medical Imaging (Appendix III):** Designed and optimized a capacitive micromachined ultrasonic transducer (CMUT) with a low-quality factor, reducing noise and artifacts and enhancing image clarity and resolution in medical ultrasound diagnostics through detailed simulations and experimental validation.

These contributions have been documented in four journal papers (three published and one in writing) and five conference papers. Chapters 2 through 4 and based on the three published papers.

Thesis Organization

This thesis is organized as follows:

- Chapter 1 presents an overview of ultrasonic MEMS transducers, detailing their applications, existing commercial products, and associated limitations.
- Chapter 2 discusses challenges in achieving range-finding accuracy and outlines the solutions developed to address these issues.
- Chapter 3 introduces a machine learning model for industrial fault detection using ultrasonic signals, achieving high classification accuracy for motor and pipeline faults, and demonstrating efficient real-time monitoring on microcontrollers.
- Chapter 4 examines the application of classification models, including gradient boosting, stacking, and bagging, for identifying faults in pipelines and motors. This chapter highlights the real-time implementation of the model on an ARM Cortex-M4F microcontroller and explores the role of dimensionality reduction techniques in enhancing accuracy and efficiency.
- Chapter 5 concludes with a summary of the research contributions, a discussion on the research outlook, and suggestions for potential improvements and future directions.

Additionally, three appendices present supplementary projects on ultrasonic MEMS, covering a fault detection system, an ultrasonic flow meter, and a low-QF optimized CMUT array for imaging applications.

CHAPTER 1

LITERATURE REVIEW

This chapter provides a concise overview of Ultrasonic MEMS transducers, highlighting their applications and available commercial products.

1.1 MEMS transducers and their applications

In recent advancements in ultrasonic sensing and fault detection, various innovative approaches have demonstrated the versatility and precision of MEMS-based ultrasonic technologies across different applications.

High-resolution data processing in ultrasonic applications has seen substantial advancements through innovations in micromachined ultrasonic transducers. Wang et al. (2020) demonstrated the design, fabrication, and testing of a compact 4×4 piezoelectric micromachined ultrasonic transducer (PMUT) array optimized for endoscopic photoacoustic imaging. Utilizing a 4 μm-thick ceramic PZT layer, this array achieves higher piezoelectric coefficients and lower stress, enhancing performance in miniaturized devices. Measuring only 1.8×1.6 mm^2, the array operates at a resonance frequency of approximately 1.2 MHz, making it suitable for clinical applications. Complementing this, Gerardo et al. (2018) developed a polymer-based capacitive micromachined ultrasonic transducer (CMUT) array for medical imaging, offering a cost-effective alternative to traditional piezoelectric transducers. Their novel fabrication process with photopolymer SU-8 and Omnicoat simplifies production, reduces costs, and enables high sensitivity at low operational voltages. The resulting 64-element linear array, capable of generating ultrasound images in a liquid medium, achieves wide bandwidth and good sensitivity due to pre-biasing of the membrane. However, a consistent challenge in the literature remains the inability of most transducers to achieve a low-quality factor (QF) of less than 10, crucial for high-resolution data acquisition.

In the domain of range detection, Mingze Gao et al. (2023) presented an ultrasonic target identification system employing PMUTs to enhance industrial productivity. This system accurately identifies targets of various shapes—such as squares, circles, frames, and rings—

through a grid-based detection method. Using 3x3 PMUT arrays as transmitters and receivers, the system operates on a 3D mobile platform, enhancing stability and efficiency. However, limitations were noted in shorter detection ranges, with a 4% margin of error. Chen et al. (2023) further contributed by measuring instantaneous acoustic power in ultrasound devices using heuristic-based methods (i.e., phase shift and magnitude detection), offering improved accuracy over traditional techniques. Yet, phase cycle tracking issues restricted the measurable velocity range, thus limiting the system's application scope.

Another notable development in ultrasonic range detection is the compact PMUT-based rangefinder using AlN, as discussed by Przybyla et al. (2011). This device leverages a pulse-echo technique to provide accurate distance measurements between 30 and 450 mm. Featuring a circular AlN membrane compatible with CMOS technology, the rangefinder achieves seamless on-chip integration and improved air coupling without requiring high voltages, making it ideal for mobile applications. The design effectively mitigates issues such as signal attenuation and noise, achieving millimeter-level accuracy and low power consumption. The authors highlight this device's superior integration, power efficiency, and accuracy compared to other micromechanical and bulk transducer-based rangefinders. However, accuracy deteriorates at higher ranges (>200 mm) due to increased random noise, resulting in significant errors.

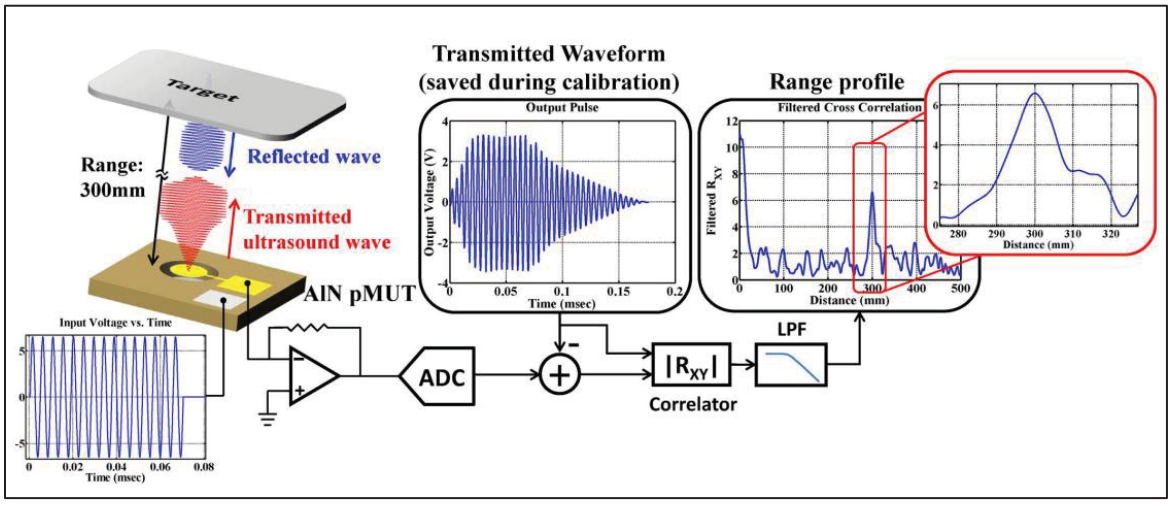

Figure 1.1 Proposed algorithm for range finding
Taken from R. J. Przybyla et al. (2011)

Guoxi Luo et al. (2023) introduced a high-accuracy ultrasonic rangefinder, depicted in Figure 1.1, that integrates six resonant cell types with varying frequencies to achieve a broad operational bandwidth. This innovative design minimizes the blind area to approximately 5 mm, enabling precise short-distance measurements up to 250 mm. The PMUT array benefits from improved bandwidth, reduced excitation cycles, and optimized signal processing, making it highly suitable for non-contact, accurate measurement applications. The study employs a cross-correlation (CC) method, wherein received ultrasonic signals are compared to a reference signal to calculate the time-of-flight (ToF). By identifying the peak of the cross-correlation function, the method measures distances based on the time delay between transmitted and received echoes. This approach enhances measurement accuracy even under conditions of weak or slightly overlapping signals, significantly improving the rangefinder's performance across various environments.

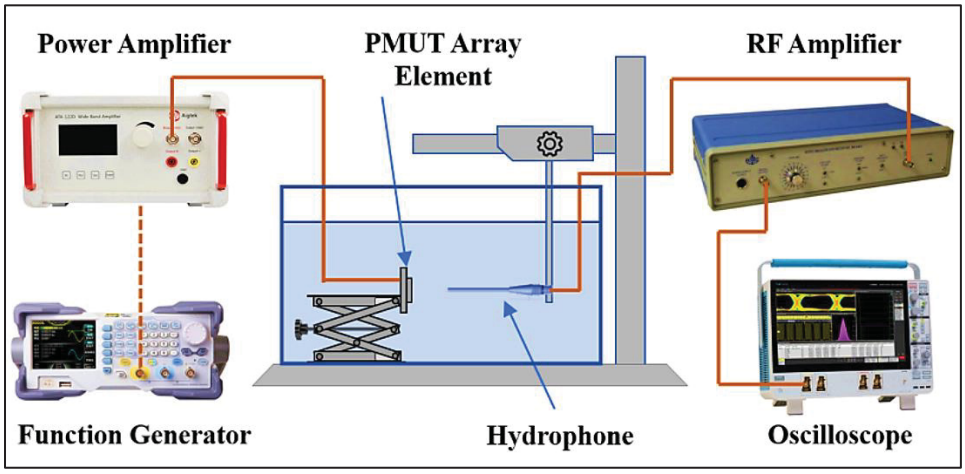

Figure 1.2 Experimental setup for ultrasonic range finding
Taken from Guoxi Luo et al. (2023)

For wind speed measurement, Bui et al. (2016) employed a single capacitive micromachined ultrasonic transducer (CMUT) with a reflector, utilizing either the TOF method or signal amplitude to measure wind speed. Experimental results showed that the TOF approach provided superior accuracy for wind speeds between 1 m/s and 10 m/s, with an error margin of less than 0.2 m/s. The study found that the full transmission/full reception mode offered the highest sensitivity, while a minority transmission/majority reception mode provided better energy efficiency. Both designs were compact, cost-effective, and well-suited for portable

wind measurement, highlighting potential for further development in low-power, miniaturized systems. In flow rate measurement, Zhang et al. (2010) introduced a self-bended microcantilever flow sensor tailored for low flow rate measurements. The sensor utilizes the differential residual stress between silicon and silicon dioxide layers to curve the microcantilever upwards, enabling the conversion of fluidic momentum into a measurable drag force. Embedded piezoelectric material within the microcantilever provides a resistance change with bending, allowing high sensitivity to flow changes. Calibrated for flow rates from 0 to 20 cm/s (equivalent to 0–1.2 L/min in a 100 μm-wide microchannel), the sensor demonstrated good repeatability and minimal zero drift. For multiphase flow measurement, Meribout et al. (2020) developed a non-radioactive ultrasonic-based flow meter for measuring gas-void fraction (GVF) and water-cut in oil field applications. A flow conditioner uses a swirl separator to create annular flow, separating gas and liquid phases to enable accurate measurement by an ultrasonic array probe. Laboratory experiments on a multiphase flow loop demonstrated the device's accuracy, with a maximum percentage error of 2% for water-cut and 3.5% for GVF. The flow meter effectively measured water-cut from 0 to 95% and GVF between 10% and 60%, with tested water and oil flow rates ranging from 50 to 500 L/min and gas flow rates from 33 to 50 L/min.

In ultrasonic fault detection, Wei, Miao, and Jiang (2024) proposed an advanced feature extraction method, FRFT-VMD, which combines fractional Fourier transform (FRFT) and variational modal decomposition (VMD) to detect pipeline defects. This method optimizes signal analysis parameters using the fourth-order central moment and envelope entropy, improving feature capture in both time and frequency domains. Experimental validation using finite element simulations and real measurements demonstrated that FRFT-VMD achieved a classification accuracy of 89.1%, outperforming other methods such as empirical mode decomposition (EMD) and traditional VMD, thus showing promise for more effective ultrasonic signal analysis in industrial settings. Patil (2022) focused on fault identification in nonlinear rotating systems, investigating the effects of bearing clearance and external defects on vibration behavior. The study employed Dimensional Analysis (DA) and Central Composite Rotatable Design (CCRD) to develop a mathematical model, assessing interactions among parameters like speed, load, and unbalance. Experimental validation showed strong

agreement with theoretical predictions, with an error margin of less than 9%. The results highlight the significant impact of factors such as shaft speed and bearing clearance on vibration amplitude, suggesting the model's effectiveness for diagnosing faults in rotor-bearing systems.

Complementary to these studies, industrial documents and commercial products related to leakage and motor bearing fault detection were examined, as summarized in Table 1.1. The methods utilized in these cases relied on traditional energy detection within specific frequency bands, underscoring the common industrial approach to ultrasonic fault detection.

In this study, ten ultrasonic fault categories investigated. Ultrasonic faults in machinery arise from various mechanical and operational issues, each with distinct causes. Low lubrication, caused by insufficient grease or oil, increases friction between moving parts, leading to irregular high-frequency vibrations, while over-lubrication, resulting from excessive grease or oil, dampens normal vibrations and creates pressure turbulence. Slow-speed faults, often due to misalignment, bearing damage, or mechanical looseness in slow-moving components, produce low-energy periodic impulses. Steam leaks, typically caused by valve malfunctions or pipeline defects, generate high-frequency turbulence as pressurized steam escapes. Cavitation, a result of rapid pressure drops in pumps or hydraulic systems, leads to vapor bubble formation and collapse, producing strong ultrasonic noise. Motor boating, triggered by motor imbalance, loose components, or electrical issues like phase imbalance, causes fluctuating frequencies. Reciprocating faults, stemming from worn pistons, valves, or cylinders in reciprocating engines, create bursts of ultrasonic energy. Thermostatic valve faults, caused by stuck or malfunctioning valves, appear as irregular bursts due to improper valve operation. In contrast, healthy pipes, free from structural issues or leaks, and healthy motors, operating without significant wear or electrical faults, display stable ultrasonic patterns. Identifying these faults through ultrasonic analysis is crucial for predictive maintenance and industrial fault diagnosis.

1.2 Conclusion

This chapter provided an overview of MEMS transducers and their diverse applications as discussed throughout this thesis. While MEMS-based ultrasonic transducers have shown promise across multiple fields, many studies have reported challenges with limited bandwidth. In range-finding applications, MEMS transducers can enhance signal-to-noise ratios (SNRs) and improve energy transmission; however, they also face constraints related to restricted detection ranges, low efficiency, high costs, environmental sensitivity, and complex circuitry that inflates production expenses. Although advanced algorithms can significantly improve measurement accuracy, reliability, and control over extended ranges, the computational complexity and power demands of these techniques can limit their practicality in cost-sensitive scenarios. Furthermore, issues such as increased noise at longer ranges and phase cycle tracking inaccuracies present additional hurdles.

For fault detection, while vibration sensors have traditionally been employed, ultrasonic sensors offer the advantage of earlier fault detection, potentially reducing downtime and maintenance costs. Despite these benefits, ultrasonic fault detection systems encounter limitations due to environmental influences, computational time, and accuracy, especially when microcontroller units (MCUs) are not utilized. Addressing these challenges through continued research and optimization is essential to unlock the full potential of MEMS-based ultrasonic technology, enabling it to meet the demanding requirements of both industrial and consumer applications.

Table 1.1 The available products for Ultrasonic Leakage and Motor Fault Detections

Part_Number	Manufacturer	F1	F2	Sensitivity dB	Battery (V)	Battery (mAh)	Contact	Contact-less	Price $
0028-8000	Bacharach	34k	42k	80	9	550	No	Yes	1,249.00
SKF TKSU 10	SKF	35k	42k	83	1.5	2250	Yes	Yes	3,126.89
LKS1000-V3	Synergys	30k	50k	80	1.4	2700	No	Yes	4,267.00
ULD-300	Amprobe	35k	45k	NA	9	550	No	Yes	753
ULCD	Megger	35k	45k	NA	9	650	No	Yes	4,845.00
LEAK	SDT	35k	42k	83	1.5	2250	No	Yes	1,995.00
TRAP	SDT	35k	42k	83	1.5	2250	No	Yes	2,295.00
HATCH	SDT	39.6k	40.1k	83	1.5	2250	No	Yes	4,995.00
TIGHT	SDT	35k	42k	83	1.5	2500	No	Yes	2,995.00
ULTRA	SDT	35k	42k	83	1.5	2500	Yes	Yes	2,995.00
711-202-G1	Whisper	40k	43k	83	9	550	No	Yes	589
ULD-405	Amprobe	20k	90k	NA	1.5	2250	No	Yes	909
UP100KT	UE Systems	36k	44k	NA	9	550	No	Yes	1,595.00
VPE-GN	AccuTrak	36k	42k	80	9	550	No	Yes	1,208
UL101	CTRL	38.5k	41.5k	NA	9	550	Yes	Yes	1,999.00
ANS-112	Ansonics Son-Tector 112	35k	45k	NA	9	550	Yes	Yes	1,050.00
UP3000KT/UP3000SL	UE Systems	35k	45k	NA	NA	NA	No	Yes	3,795.00
MDE-2000NC	Marksman	36k	44k	NA	1.5	2250	No	Yes	850.00
BS10/BS30	Sonotec	20k	100k	NA	3.7	4050	No	Yes	NA
LDT-1	ABQIndustrial	NA	NA	NA	9	550	No	Yes	925
TUD-1 / TG-1	Sonel	39k	41k	NA	9	550	No	Yes	283.92
90061-FlexUS	SDT	36.4k	40.4k	NA	1.5	2500	Yes	Yes	1,350.00
16455	Robinair	NA	NA	NA	9	550	No	Yes	1,618.83
ULD586	LandTek	20k	100k	NA	1.5	2250	No	Yes	217.99
569001	Biddle	35k	45k	NA	9	NA	No	Yes	650
R9100	REED	38k	42k	Ajustable	9	550	No	Yes	145.77
HHLT-1	OMEGA	36k	44k	NA	9	550	No	Yes	143.09
ULD-400	Amprobe	20k	90k	NA	1.5	2250	No	Yes	1,408
ULD-420	Amprobe	20k	90k	NA	1.5	2250	No	Yes	2,056.84
E+A25:N25M2268	Allsun	36k	44k	NA	9	550	No	Yes	134.99
EM2280	UTG	36k	44k	NA	9	550	No	Yes	302.78
DFX-7	Dakota	1.8M	19M	NA	1.5	2250	No	Yes	3,650.00
UTD9600	UFD	0.4M	20M	NA	9	550	No	Yes	2,377.11
LUBE	SDT	35k	42k	83	1.5	2250	Yes	No	2,495.00
ANS-112	Ansonics Son-Tector 112	35k	45k	NA	9	550	Yes	Yes	1,050.00
SKF TKSU 10	SKF	35k	42k	83	1.5	2250	Yes	Yes	3,126.89
UL101	CTRL	38.5k	41.5k	NA	9	550	Yes	Yes	1,999.00
UP3000SC	UE Systems	35k	45k	NA	NA	NA	Yes	No	3,595.00
BS20/BS40	Sonotec	20k	100k	NA	3.7	4050	Yes	No	NA
LUBE	SDT	35k	42k	83	1.5	2250	Yes	No	2,495.00

CHAPTER 2

HIGH-ACCURACY AIRBORNE RANGEFINDER VIA DEEP LEARNING BASED ON PIEZOELECTRIC MICROMACHINED ULTRASONIC CANTILEVERS

Amirhossein Moshrefi, Abid Ali, Suaid Tariq Balghari, and Frederic Nabki

Departement of Electrical Engineering, École de Technologie Supérieure,
1100 Notre-Dame Ouest, Montréal, Québec, Canada H3C 1K3

Paper published in: IEEE Transactions on Ultrasonics, Ferroelectrics, and Frequency Control, July 2024.

Abstract —This article presents a high-accuracy air- coupled acoustic rangefinder based on piezoelectric microcantilever beam array using continuous waves. Cantilevers are used to create a functional ultrasonic rangefinder with a range of 0–1 m. This is achieved through a design of custom arrays. This research investigates various classification techniques to identify airborne ranges using ultrasonic signals. The initial approach involves implementing individual models such as support vector machine (SVM), Gaussian Naive Bayes (GNB), logistic regression (LR), k-nearest neighbors (KNNs), and decision tree (DT). To potentially achieve better performance, the study introduces a deep learning (DL) architecture based on convolutional neural networks (CNNs) to categorize different ranges. The CNN model combines the strengths of multiple classification models, aiming for more accurate range detection. To ensure the model generalizes well to unseen data, a technique called k-fold cross-validation (CV), which provides the reliability assessment, is used. The proposed framework demonstrates a significant improvement in accuracy (100%), and area under the curve (AUC) (1.0) over other approaches.

Index Terms— Acoustic signal processing, airborne ultrasonic range finding, machine learning (ML), piezoelectric micromachined ultrasound cantilever, time-of-flight (ToF) measurement.

2.1 Introduction

An ultrasonic rangefinder measures distance based on the time-of-flight (ToF) principle, where it calculates the time taken for ultrasonic sound waves to travel from the transmitter (T_x) to the receiver (R_x). This travel time, combined with the known speed of sound in air, allows the device to accurately determine the distance to the object. Range finding technology, crucial in various sectors, enhances functionality and safety across numerous applications: robotics rely on it for obstacle-free navigation; augmented reality systems leverage it for improved user interaction with virtual elements; security systems use it for motion detection near critical areas; vehicle parking assist systems and warehouse automated guided vehicles benefit from short-range range sensors to avoid collisions; interactive museum exhibits use short-range finding to activate engaging learning experiences; and medical devices depend on precise distance measurements for accurate instrument placement (Nihtianov, S., & Luque, A. (2018); Li, J., et.al. (2022); Dunbabin, M., & Marques, L. (2012)). Ultrasonic rangefinders offer significant advantages over laser systems, including relatively low-power consumption and low-cost, making them ideal for budget-sensitive applications related to the Internet of Things (IoTs). They reliably operate in environments with smoke, steam, or fog, where optical sensors fail. In addition, ultrasonic sensors can detect transparent obstacles, such as glass or clear fluids, which lasers might not recognize, broadening their applicability in various industrial and consumer settings (Ranjan Laha, S., Pattanayak, B. K., & Pattnaik, S. (2022); Hosur, P., Shettar, R. B., & Potdar, M. (2016); Toa, M., & Whitehead, A. (2020); Iniewski, K. (Ed.). (2017)). Several studies have been conducted in this field, focusing on different aspects of ultrasonic range finding technology. Gao, M., et. al. (2023) introduced an envelope-based ultrasonic detection system using piezoelectric micromachined ultrasonic transducers (PMUTs) that offered improved accuracy over traditional laser sensors, particularly in handling transparent targets. The system performed well in diverse environments, detecting various colors and transparencies. However, it faced limitations with shorter detection ranges with a 4% error. Chen, X., et. al. (2019) used a multifrequency continuous-wave (MFCW) technique to optimize for short ranges (i.e., under 100 mm). However, the high-frequency-dependent attenuation limited its effectiveness to shorter distances, potentially restricting broader application. He, Q., et. al. (2014) demonstrated successful energy transmission in

water and tissue, with a peak power transfer of 35 W at a reception distance of 20 mm. However, some drawbacks of this work included low-efficiency levels (i.e., 0.026% in water and 0.096% in tissue) and sensitivity to the reception angle and lateral distance, highlighting the need for further optimization in T_x design to improve overall performance and efficiency. Gaal, M., et. al. (2019) presented an air-coupled ultrasonic transducer using charged cellular polypropylene to enhance sensitivity through an additional bias voltage. This approach improved the signal-to-noise ratio (SNR), aiding in nondestructive testing. However, its need for complex circuitry to handle high voltages, potential variability in sensor performance, and higher production costs may limit its widespread adoption.

In addition to device improvements, several advanced algorithms have been developed to enhance ultrasonic rangefinder performance. Ghahramani, A., (2019) introduced algorithms based on the phase differences in ultrasonic signals for measuring airspeed using microelectromechanical systems (MEMS) ultrasonic anemometers, extending operational range under varying temperatures and velocities. However, the complexity of the model may restrict practical application in simpler, cost-sensitive environments. Robichaud, A., et. al. (2020) developed a method for dynamic control of the transducer's quality factor, improving both the axial and depth resolutions of PMUTs using electrostatically controlled mechanical dampers. This innovation faced challenges with the actuators' response times and the nonlinear effects of the damping system, which impacted precision. Jackson, J. C., (2013) provided an overview of various methods for measuring the ToF of acoustic pulses in through-air applications, noting that cross correlation (CC) and phase-based methods, despite their higher computational demands, offer significant accuracy improvements over traditional threshold methods. Przybyla, R. J., Horsley, D. A., & Boser, B. E. (2011) discussed an ultrasound rangefinder system based on the CC method that leveraged a piezoelectric aluminum nitride (AlN) mem- brane to improve micromechanical rangefinder performance, demonstrating enhanced accuracy and reduced noise within a range of 30–450 mm. However, increased random noise at higher ranges posed a challenge. Chen, Y., et. al. (2023) measured the instantaneous acoustic power of ultrasound devices based on heuristic-based methods (i.e., phase shift and magnitude detection) more accurately than traditional methods, but faced

limitations due to phase cycle tracking issues, restricting measurable velocities to a small range.

Device improvements enhance accuracy and sensitivity in diverse environments, handling various targets, including transparent objects. They also improve SNRs and energy transmission. However, they face challenges such as limited detection ranges, low efficiency, cost, environmental sensitivity, and complex circuitry, raising production costs. Advanced algorithms boost measurement accuracy and reliability, extending operational ranges and providing precise control. Yet, their complexity and computational demands limit practicality in cost-sensitive environments. They also suffer from increased noise at higher ranges and phase cycle tracking issues. Continued research and optimization are necessary to address these challenges and fully realize the potential of ultrasonic range finding technologies in various industrial and consumer applications.

While PMUTs excel in miniaturization and integration with other MEMS devices, it is pertinent to consider for range finding the piezoelectric microcantilever beam array structure as an alternative micromachined ultrasonic transducer. Piezo- electric cantilever beams provide significant benefits in terms of sensitivity, fabrication simplicity, displacement amplitude, cost, and mechanical robustness. These attributes make them a preferred choice for certain range finding applications. Accordingly, these structures have been considered as the micromachined ultrasonic transducers in this study.

This work aims to leverage piezoelectric microcantilever and deep learning (DL) algorithms to achieve a high-accuracy ultrasonic rangefinder that aims to provide enhanced accuracy differentiated performance metrics. An array designed and fabricated based on the PiezoMUMPs microfabrication process is used. The dataset for modeling contains 1000 ultrasonic waves, each one including 10 000 samples. Preprocessing and scaler approaches are used to denoise and scale the data. To enhance the visualization of the data, several dimensionality reduction techniques are used, including principal component analysis (PCA), t-distributed stochastic neighbor embedding (t-SNE), linear discriminant analysis (LDA), and bottleneck features derived from a convolutional neural network (CNN). A DL model, featuring a specialized architecture, is proposed to facilitate robust analysis. The performance of this model is rigorously validated using a diverse subset of the dataset through k-fold cross-

validation (CV). In addition, the Rx operating characteristic (ROC) curve is used to compare and validate the effectiveness of the model in distinguishing between classes. The structure of this study is outlined as follows. Section II presents the theoretical underpinnings, materials, and method- ologies used in the overall framework, including a detailed introduction to our model and an explanation of the k-fold CV process. In Section III, the aforementioned algorithms are applied and assessed using practical datasets to demonstrate their effectiveness. Finally, Section IV provides a conclusion of the research, summarizing key findings and implications.

2.2 Methods and Materials

In this section, the proposed piezoelectric microcantilever structure is introduced and then components of the proposed framework are explained. Due to the advanced capabilities of DL models, we have engineered a robust framework that integrates CNN and dense layers. This model leverages the strengths of both the architectures to enhance the performance.

2.2.1 Airborne Transceiver

Figure. 2.1 illustrates the design of our proposed devices, which comprise an array of cantilevers. Each cantilever is constructed from a stack of piezoelectric-on-silicon with top metal electrodes. The extracted signal is represented in terms of either current or voltage, depending on whether the device functions as an R_x or T_x, respectively. This work encompasses three arrays of cantilever design variants. In piezoelectric transduction, when subjected to physical deformation via pressure, vibration, or force, the piezoelectric materials elicit an induced electrical field. Conversely, when electrical energy is applied, mechanical deformation is engendered, as detailed in (Ali, A., & Lee, J. E.-Y. (2019)). The resultant electrical charge density stemming from the piezo-electric cantilever can be quantified using the piezoelectric constitutive equations outlined below

$$S_1 = s^{\epsilon}\, T_1 + d_{31} E_3 \tag{2.1}$$

$$D_3 = d_{31} T_1 + \epsilon^{T}\, E_3 \tag{2.2}$$

where S_1 and T_1 are the strain and stress in the longitudinal direction of the piezoelectric layer, respectively, D_3 is the electrical charge density, d_{31} is the piezoelectric strain constant, $s\epsilon$ is the elastic compliance in a constant electric field, ϵ_T is the dielectric constant of the piezoelectric material under constant stress conditions, and E_3 is the electric field developed in the out of plane direction (Roy, K., Lee, J. E.-Y., & Lee, C. (2023); Uddin, M. N., et. al. (2016)). From (2.2), it is clear that the charge density is proportional to the developed stress. The total charge in a read-out capacitor can be derived by integrating D_3 over the electrode area and incorporating the piezoelectric constitutive equations. The charge (Q) produced on the electrodes is given by the following equation (Sonmezoglu, S., Arslan, Y., & Erkan, H. (2017); Park, J. H. (2010)):

$$Q = \iint_A D_3 dA \tag{2.3}$$

where A is the surface area of the electrode.

However, enhancing the quantity of charge generated by the cantilevers under applied force or pressure can effectively improve the SNR of the piezoelectric MEMS cantilever. It is well-known that a fundamental noise source in piezoelectric sensors is thermal–electrical noise generated by dielectric leakage in the piezoelectric film Levinzon, F. A. (2004); Yao, D., & Xu, J. (2022). This leakage may be represented with a resistance R_l in series with C_{piezo} with value $R_l = (\tan \delta/\omega \times C_{piezo})$, where $\tan \delta$ is the loss tangent of the material. The resistance generates a voltage noise $v_n = \text{sqrt}(4kbT\ R_l)$ (V/(Hz)1/2) in series with C_{piezo}. Alternatively, and equivalently through source transformation, vn may be represented as a charge source $Q_n = C_{piezo} \times vn$ (C/(Hz)1/2) in parallel with C_{piezo}. For a dielectric-loss noise- limited sensor, it is clear that the ratio of signal power to noise power SNR^2 in a 1-Hz noise bandwidth is given by the following equation:

$$SNR^2 = \frac{Q_{piezo}^2}{Q_n^2} = \frac{Q_{piezo}^2}{C_{piezo}} \cdot \frac{\omega}{4k_b T \tan \delta} \tag{2.4}$$

where C_{piezo} is the capacitance value of the top electrode region, ω is the excitation frequency, kb is Boltzmann's constant, T is the temperature, and tan δ is the dielectric loss angle of the piezoelectric material, here AlN. Herein, (ω/4kbT tan δ) is strongly dependent on thermal noise and mechanical structure of the piezoelectric transducer. This relationship clearly shows that the charge Q_{piezo} out- putted from Devices A–C are such that the overall SNR of device C is improved. There is a positive correlation between the cantilever SNR and Q_{piezo}. Furthermore, Q_{piezo} can be increased to enhance the SNR of the cantilever. The corresponding voltages or currents are obtained from the piezoelectric cantilever such that

$$V_0 = \frac{Q_{piezo}}{C_{piezo}} = \frac{d.Q_{piezo}}{\varepsilon A_0} \tag{2.5}$$

Herein, Q_{piezo} is the quantity of charges generated in the stress region under the action of the external signal, C_{piezo} is the capacitance value of the stress region, and d is the thickness. Herein, ϵ is the dielectric constant of the piezoelectric material, and different subregions correspond to the same value of ϵ. A_0 is an area of the stress region. Q_{piezo} is given by the following equation:

$$Q_{piezo} = A_0 d_{31} \sigma_0 \tag{2.6}$$

where σ_0 is the stress exerted under the action of the external signal.

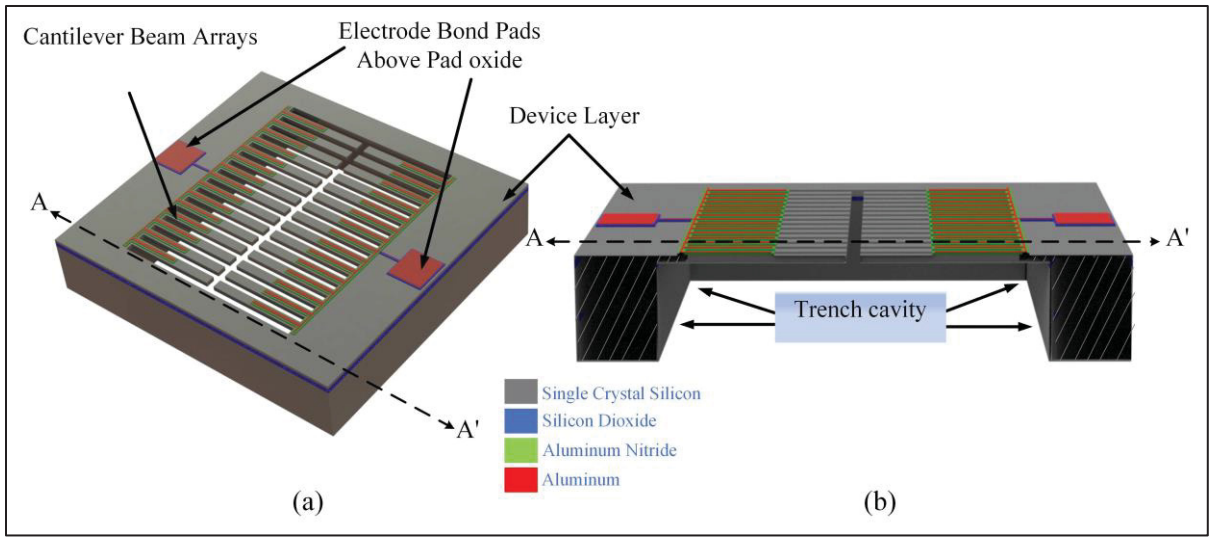

Figure 2.1 (a) Three-dimensional schematic of the piezoelectric cantilever beam arrays, with the material stacks color-coded for clear differentiation. (b) Cross-sectional view of the device along the A–A' axis, illustrating the trench cavity beneath the device

2.2.2 Design and Simulation of MEMS Transceiver

The received signal of the MEMS cantilever is extracted in terms of current or voltage depending on the device being used as the R_x or T_x, respectively. The cantilever beam structure consisted of four stacked materials: silicon as the movable substrate, silicon dioxide as the electrical insulator of the silicon, 1-µm-thick aluminum for the top electrode, and pads and AlN as the piezoelectric layer. The silicon also acts as the electrical ground with a thickness of 10 µm. Three different design variants were fabricated, as shown in Figure. 2.2(a)–(c). The dimension of Design A (length × width) is 650 × 1500 µm, whereas Devices B and C have a different number of cantilever beams; each single cantilever has the same length as Design A, with each cantilever having a width of 100 µm. To analyze the mode shape and eigen-frequency of the proposed device, the device model was built in COMSOL Multiphysics as shown in Figure. 2.2(d)–(f). The laser Doppler vibrometer (LDV)-measured quality fac- tor for Device C is 359.3, significantly better than that of Device A, 260.4, and slightly better than that of Device B, 353.3. The FEM-simulated eigenfrequencies of the proposed Devices A–C are 28.28, 29.34, and 28.45 kHz, respectively. The measured resonant frequencies agree well with the FEM eigenfrequency simulations to within 0.5%. The SNR is a critical acoustic parameter for piezoelectric cantilevers. To enhance the SNR, the devices have been designed

specifically for this purpose. The mode shape was measured for them using an LDV system by applying a 20-Vpp sine wave and is shown for the three structures illustrated in Figure. 2.2(g)–(i). The measured mode shape of each design type is presented in Figure. 2.3(a), outlining the increased displacement achieved by Design C. Furthermore, the resulting normalized displacement over frequency achieved is shown in Figure. 2.3(b), outlining the differences in the frequency response and dis- placement level of each design. The applied voltage was also swept from 0 to 20 Vpp, and the resulting normalized dis- placement is shown in Figure. 2.3(c). Design C exhibits improved performance in terms of displacement and sensitivity compared with the others. In addition, incorporating an array of multiple piezoelectric microcantilever and designing trenches between adjacent cantilevers has proven effective in further improving the signal level (and thus the SNR). As such, Design C was selected for the focus of the DL model presented in this work. For a more detailed analysis that shows why Design C is superior to Designs A and B, refer to the Supplementary Materials linked to the paper.

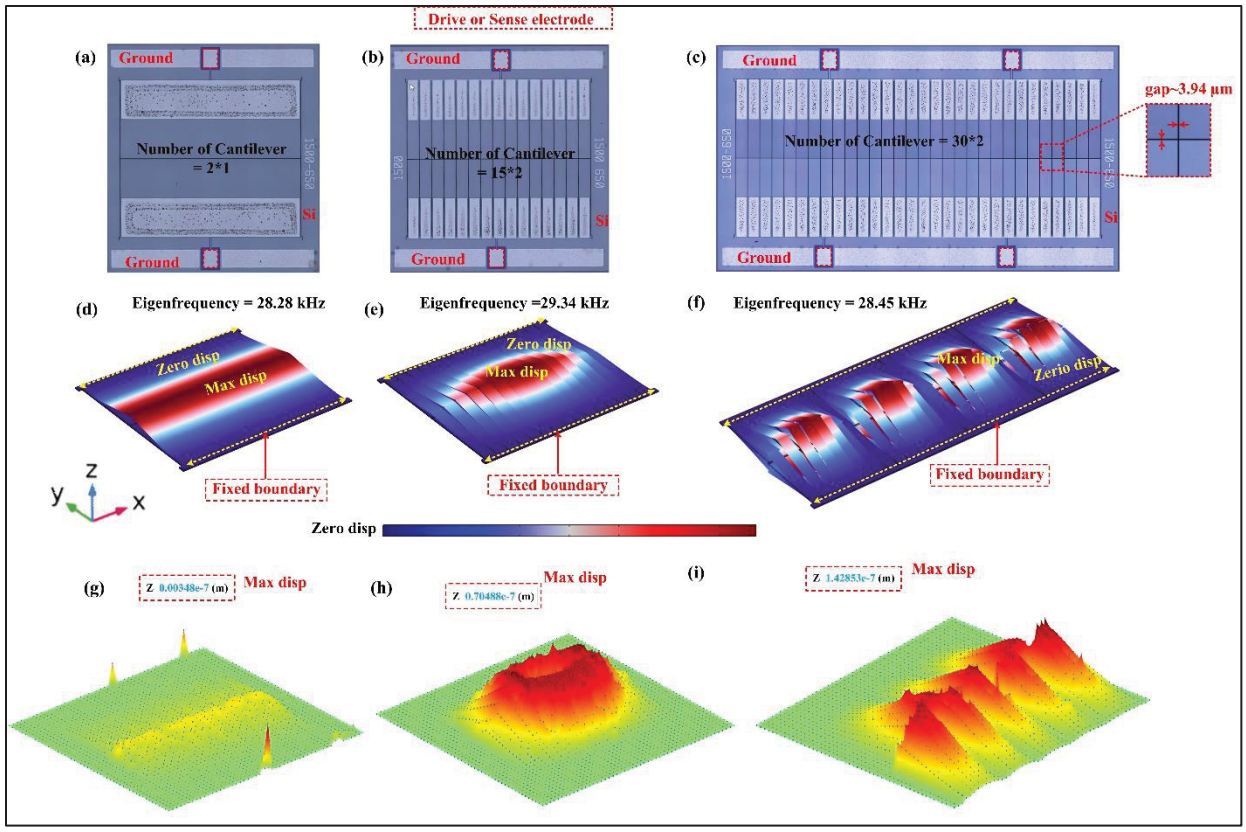

Figure 2.2 Piezoelectric MEMS cantilever variants presented from multiple perspectives. (a) Cantilever Design A features dimensions of 1500 µm in length and 650 µm in width. (b) Design B which is an array of cantilevers, arranged in a 15 × 2 configuration, maintains the same length as Design A, with each cantilever having a width of 100 µm. (c) Cantilever Design C mirrors the dimensions of Design B but doubles the number of cantilevers to 30 × 2, enhancing the signal level of the cantilever. This section also includes a micrograph of the fabricated devices, with an inset highlighting the gaps between adjacent cantilevers. (d)–(f) Finite element method (FEM) eigenfrequency simulations confirm the mode shape of the presented designs. (g)–(i) Visualization of the mode shapes of the cantilevers, as measured through LDV scanning results

2.2.3 Fabrication of the MEMS Range Meter

The devices in this work were fabricated using a low-cost commercial technology, PiezoMUMPs from Science Inc., Santa Monica, CA, USA, (Cowen, A., et. al. (2014)). The five-mask process begins with a 150-mm-thick silicon on-insulator (SOI) wafer as shown in Figure. 2.4(a) with a 10-µm device layer which has been n-doped through phosphosilicate glass (PSG) for improving electrical conduction. In the next step, oxide is thermally grown and subsequently deposited and patterned as shown in Figure. 2.4(b) to prevent electrical shorting

in areas without AlN. RF sputtering is used in the next step to deposit AlN followed by deposition, patterning, and etching steps depicted in Figure. 2.4(c). A top conducting layer is required to act as the top electrode for which a metal stack of 20-nm chrome and 1-µm aluminum is layered through a lift-off process to form the top electrodes, electrical pathways, and bond pads in Figure. 2.4(d). Silicon is thereafter etched using deep-reactive ion etching (DRIE) to form the structural components of the device in Figure. 2.4(e). The next step is the bottom-side DRIE etching of the structure performed with a protective coating on the front side of the substrate shown in Figure. 2.4(f). The final step is to dry plasma etch the protective coatings forming the final released structure.

2.2.4 Data Preprocessing

In this study, two piezoelectric micro-cantilever beam arrays are considered, one fixed as a T_x and one movable as R_x. As mentioned in Section II-B, Design C was selected. During measurement of the received data, different noises could interfere with the ultrasonic data for range finding. In addition, preparing the raw data is necessary before training a machine learning (ML) process to scale the input data; otherwise, the training phase may not be effective. The pass-band's flat frequency response allows for the noise to be eliminated using a Butterworth filter (Mello, R. G. T., Oliveira, L. F., & Nadal, J. (2007)). Furthermore, the scalability of the training data is a key factor when working with neural networks. To improve the training efficiency, the data are typically scaled in ranges like [1; 1] or [0; 1], depending on the activation functions used in the models. Scalers preserve the relationships among the original data points while ensuring that each feature contributes equally to model training. This can improve the performance of algorithms that are sensitive to the scale of input data by providing a consistent scale for all features, thereby speeding up the learning process (Patro, S. G. K., & Sahu, K. K. (2015)).

1. Noise Reduction and DC Offset Removal: To mitigate dc offset, eliminate unwanted spikes, trends, and outliers from the ultrasonic signal, noise reduction is performed using a Butterworth filter in the time domain. This type of filter is favored in control systems due to its lack of peaking in the frequency response, which ensures minimal signal distortion. The

passband frequency response of a Butterworth filter is designed to be as flat as possible, providing a smooth out-put without fluctuations in the signal's amplitude within the passband (Dastres, R., & Soori, M. (2021)).

2. Scaling the Input Data: In preparation for training the DL model, it is essential to preprocess the ultrasonic signals by scaling the input signals (features) to a uniform range. This preprocessing step, known as standardization, accelerates computational efficiency during model training. Given that ultrasonic data exhibit features at various scales, scaling ensures each feature contributes equally, preventing those with larger magnitudes from disproportionately influencing the model. Popular scaling techniques include the Standard scaler and Minmax scaler (Thara, D. K., PremaSudha, B. G., & Xiong, F. (2019)). The Standard scaler normalizes the features as follows:

$$Z = \frac{X - \mu}{\sigma} \tag{2.7}$$

where X is the original vector, μ is the mean, Z is the normalized vector, and σ is the standard deviation of the input vector.

2.2.5 Data Augmentation

Data augmentation artificially expands the existing ultra- sonic data to train ML models. By making minor adjustments to the original data, this technique enhances the diversity and robustness of the models, preventing over-fitting. It is particularly useful when the initial dataset is small or to improve ML model performance. DL models require extensive and varied data for accurate predictions, but acquiring such data can be challenging. Analyzing the existing dataset, including the size and distribution of ultrasonic signals, is crucial for effective augmentation. One technique used is flipping input signals, which mirrors them along a central axis to create additional, varied data points.

2.2.6 Dimensionality Reduction and Visualization

In ML, especially when working with complex data like ultrasonic signals, it is beneficial to reduce the complexity of the data. This process is called dimensionality reduction, and it involves transforming high-dimensional data into a more manageable and informative form with fewer features. PCA is one of the prominent methods for linear dimensionality reduction. It identifies orthogonal directions that capture the maximum variance, making it a valuable second-order statistical method (Van Der Maaten, L., Postma, E. O., & Van Den Herik, H. J. (2009)). PCA is used to analyze the acoustic data to find the most important information. While PCA is effective in reducing dimensionality, t-SNE excels at revealing hidden structures. Unlike PCA which focuses on overall spread, t-SNE shows how data points are connected, making it ideal for visualizing complex data (Agis, D., & Pozo, F. (2019); Devassy, B. M., George, S., & Nussbaum, P. (2020)).

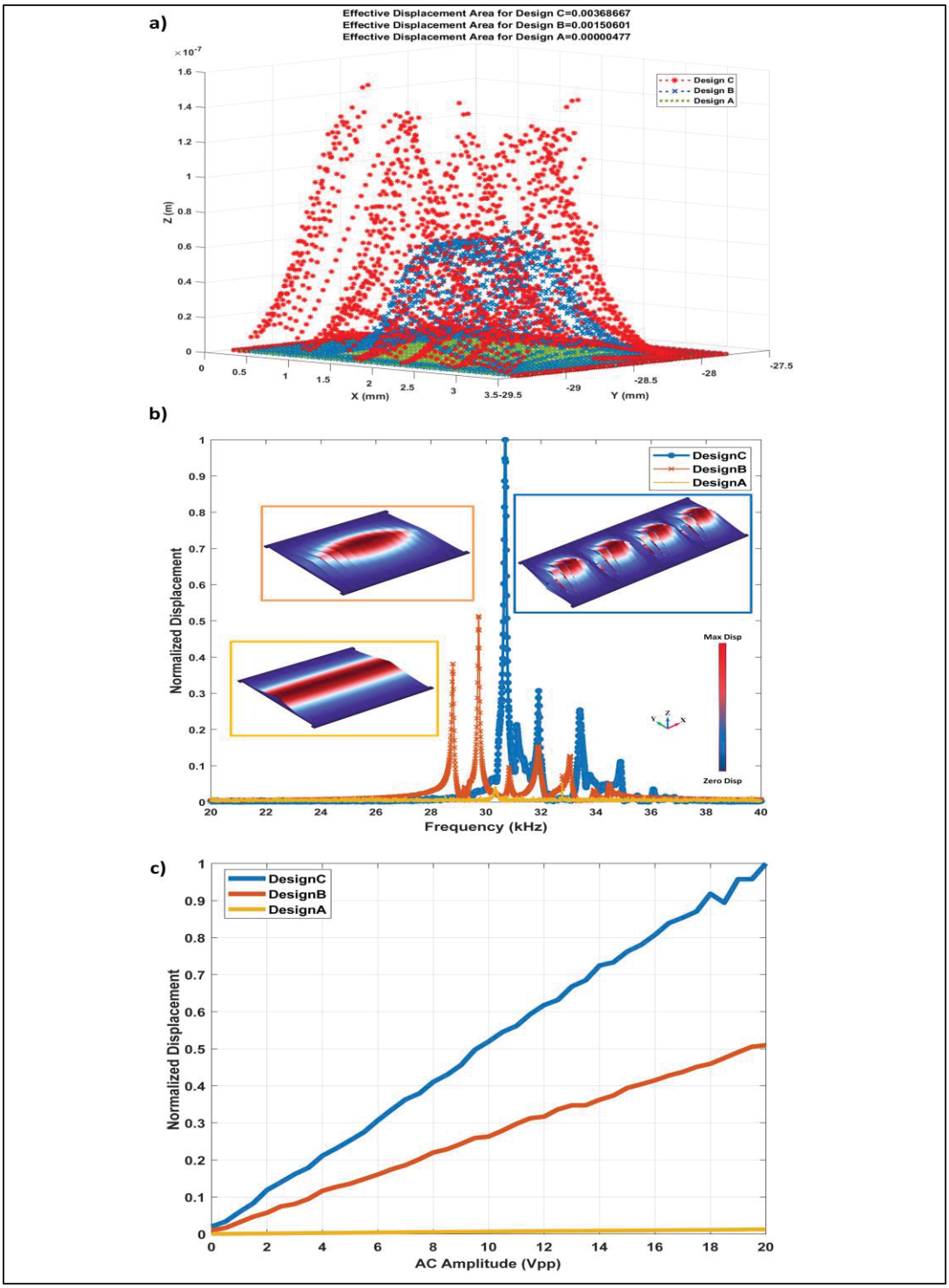

Figure 2.3 (a) Measured comparative mode shape graph. (b) Normalized displacement versus frequency for a constant ac actuation voltage of 20 V_{pp}. (c) normalized displacement versus ac actuation voltage amplitude

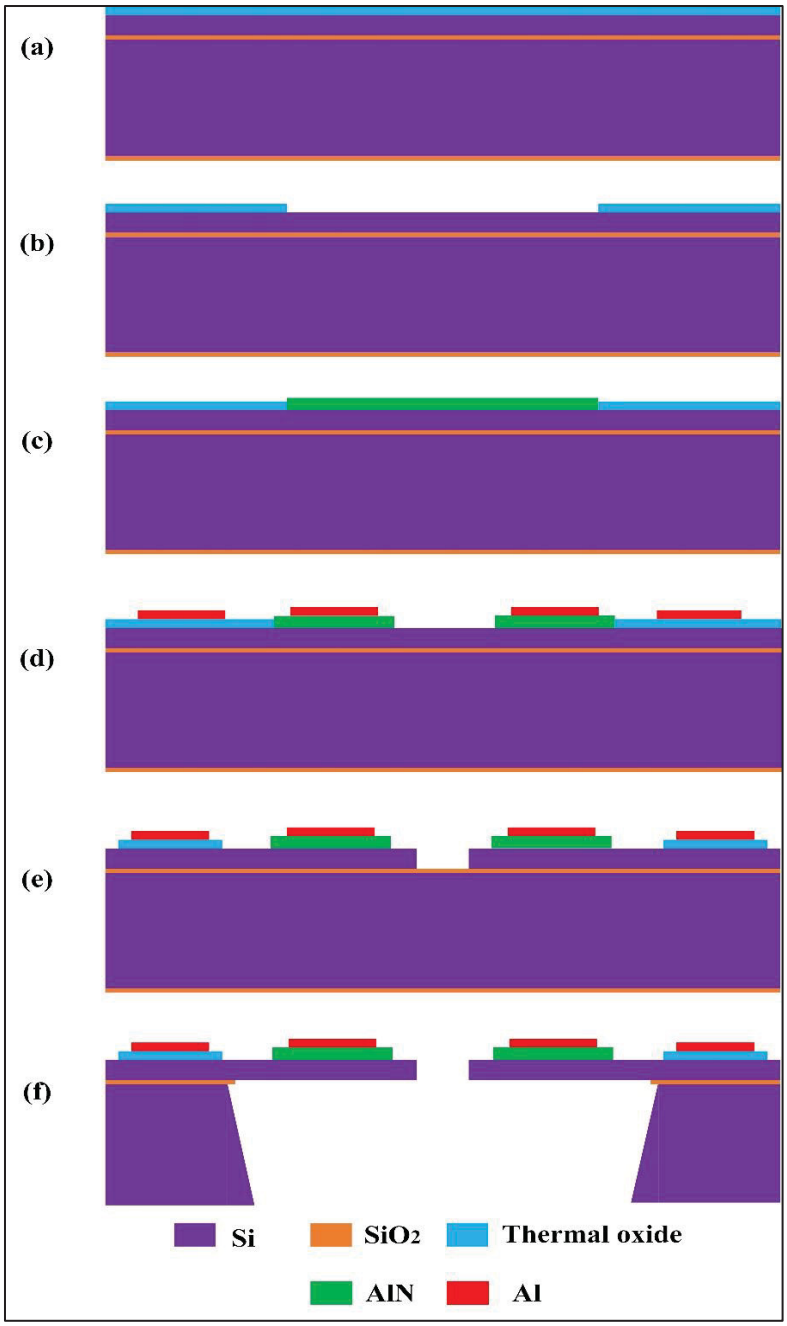

Figure 2.4 PiezoMUMPs' fabrication process overview. (a) Begins with a silicon (Si) wafer, which includes a 10-µm device layer. (b) Patterning of thermally grown oxide is executed using RIE. (c) 0.5-µm layer of AlN is deposited and patterned through RF sputtering followed by RIE, to serve as the piezoelectric material. (d) Metal stack consisting of 20-nm chromium (Cr) and 1-µm aluminum (Al) is deposited and patterned to form the top electrodes, pads, and interconnect pathways. (e) Device structures are then formed via DRIE down to the buried oxide layer, shaping the functional elements of the device. (f) Cantilevers are released through bottom-side DRIE, with a front-side protective layer subsequently removed by plasma etching

To create a clearer comparison and visualize the data with class labels, LDA may be used. Unlike PCA and t-SNE that preserve the local data structure, LDA prioritizes separating different categories (ranges) in the ultrasonic data. It achieves this by optimizing the ratio of class-variances that highlights these class differences (Adebiyi, M. O., et. al. (2022)). LDA is a useful tool for analyzing ultrasonic data with class labels. It simplifies the data while keeping separation between these classes clear. This is helpful for small datasets but can be affected by outliers. In addition, bottle neck features as a part of the proposed model will be investigated.

2.2.7 Featuring Process

This study analyzes ultrasonic data to identify different classes. To achieve this, 30 features were extracted from the data, covering various aspects such as time, frequency, and power distribution. These features included basic statistics such as maximum, average, standard deviation, skewness, and kurtosis along with more specific measures such as peak information, zero crossing, crest factor, and shape factor. To distinguish between the classes with the most discernment, the independent and more important features were selected.

2.2.8 Proposed DL Architecture for Range Finding

The task of detecting range can be approached as a supervised classification problem. Our proposed model is specifically designed to categorize ultrasonic signals from a piezoelectric cantilever into 11 distinct classes, spanning distances from 10 to 1000 mm. The details of this model's architecture are outlined and elaborated upon in this section, with visual illustrations provided in Figure 2.5. This structural breakdown clarifies how the model processes and classifies the ultrasonic data into the specified range classes.

The process begins by capturing ultrasonic data, which is subsequently preprocessed to refine the raw signals for analysis. This involves normalizing the data and configuring it into a format suitable for neural network processing by defining its input shape.

Following this, a CNN is used to analyze the data, detecting spatial hierarchies and uncovering hidden patterns within the ultrasonic signals (Khan, A., et. al. (2020), Shahrivari, S. (2014)). The data then progress through a sequence of fully connected (FC) layers, known as a multilayer perceptron (MLP) network. This network uses a softmax function at the output layer

to classify the data into predefined ranges. The softmax function predicts a probability distribution across different classes, identifying the most likely category for each input. Table 2.1 details the architecture's layers, including their functions, output shapes, and the adjustable parameters during training, providing insight into the network's learning capacity.

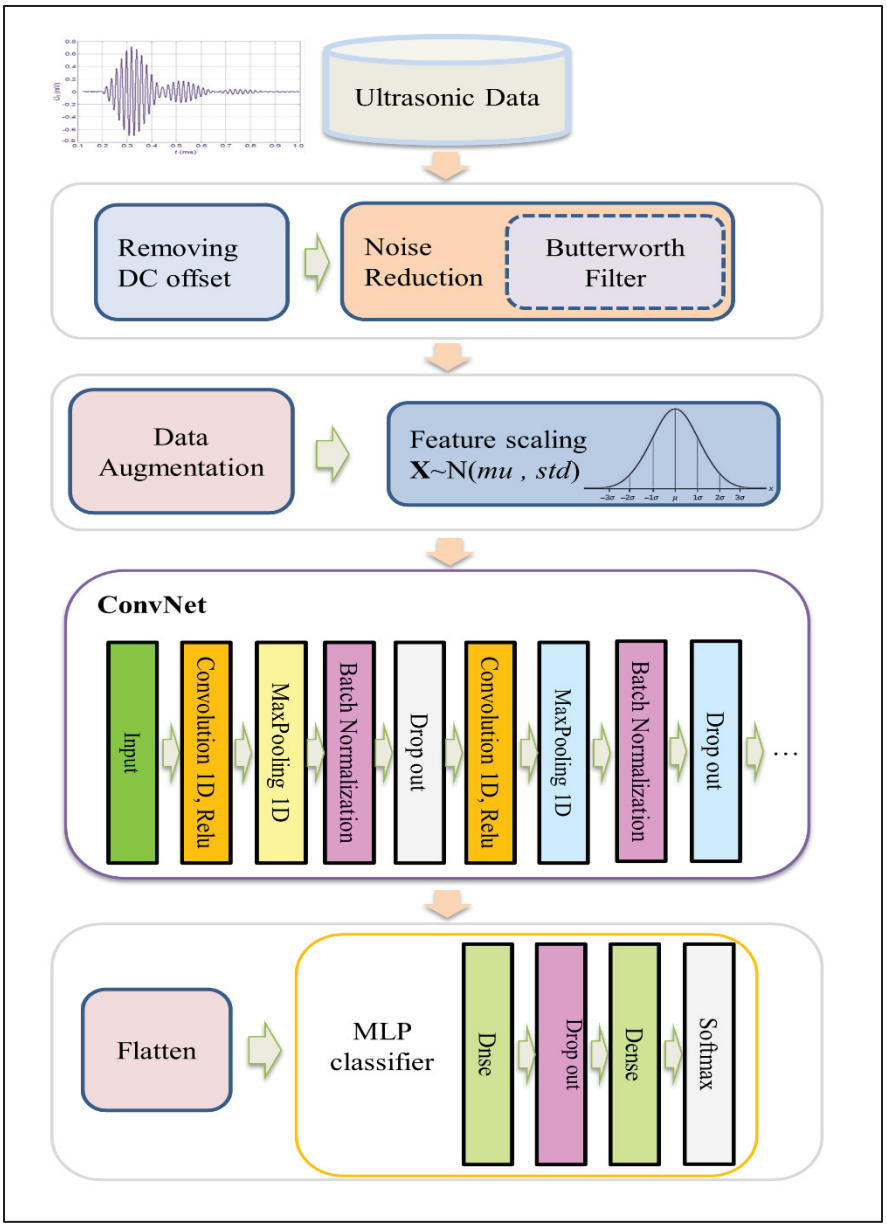

Figure 2.5 Overview of the DL model architecture

Table 2.1 Proposed model architecture and parameters

Layer (type)	**Output Shape**	**# of Parameters**
Conv1d_1	(None, 9994, 4)	32
Max_pooling_1	(None, 4997, 4)	0
Batch_normalization_1	(None, 4997, 4)	16
Dropout_1	(None, 4997, 4)	0
Conv1d_2	(None, 4997, 4)	84
Max_pooling_2	(None, 2496, 4)	0
Batch_normalization_2	(None, 2496, 4)	16
Dropout_2	(None, 2496, 4)	0
Flatten_1	(None, 9984)	0
FC_1	(None, 256)	2556160
Output	(None, 11)	2827
Total parameters: 2559135		
Trainable parameters: 2559119		
Non- trainable parameters: 16		

1) Input and Reshape Layers: The 1-D data were reshaped into arrays as a tensor for further processing in a DL model. This process is known as data batch processing (Shahrivari, S. (2014)). A “Reshape” layer was used to alter the dimensions of the input data without any loss of information.

2) Convolutional Neural Network: For automatic feature extraction from ultrasonic signals, we used a CNN designed to detect and classify ranges from 10 to 1000 mm. Unlike traditional neural networks, CNNs use layers of filters, known as kernels, to scan the data. These kernels enable the CNN to recognize patterns across the data, even when these patterns are shifted or slightly altered in position. This capability distinguishes CNNs from classic neural networks, as they apply convolutional operations to the input. This allowed for robust feature detection, essential for accurate range classification, as CNNs are adept at discerning complex patterns in data such as ultrasonic waves. The convolution layer is the core component of the CNN model, where the data undergo initial processing. In this layer, multiple filters— each designed

to detect specific patterns—are applied to the data. These filters act like sliding windows, moving across the data to capture and extract various conceptual patterns from different locations within the dataset. This operation allows the CNN to identify and emphasize features that are critical for understanding and classifying the input signals effectively. The below equation represents convolution operation of each convolution layer (Lamothe-Fernández, P., et. al. (2020)).

$$L_f^s(y) = \left(\sum_{c=1}^{n} \sum_{i=1}^{i=t} W_f^s(i) \times L_c^{s-1}(x-i) \right) + b_f^s \tag{2.8}$$

Here, $L_f^s(y)$ refers to the sample at location y in the s^{th} convolutional layer for the f^{th} filter. L_f^{s-1} is the sample for the layer preceding the s^{th} convolutional layer for the c^{th} channel, and n being the total number of channels. $w_f^s(i)$ denotes the value at location i of the f^{th} filter in the s^{th} convolutional layer, t represents the total elements of the filter w_f^s, and b_f is the bias term for the f^{th} filter.

3) FC Layer and Activation Function: After the convolutional layers, the network uses an FC (dense layer) to combine the extracted features and make a final decision. To give probabilities for each class, the output layer uses a special function called softmax that acts like a voting system, assigning scores to how likely the data belong to each class (Laredo, D., et. al. (2020); Yates, L. A., et. al. (2023)). For working with m classes, the softmax layer is composed of m nodes and expressed by $\sum_{i=1}^{m} P_i$ where i =1, . . ., 11; p_i specifies a discrete probability distribution. The softmax function converts logits into probabilities as follows:

$$a_i = \sum_{k=1}^{m} h_k W_{ki} \tag{2.9}$$

$$p_i = \frac{\exp(a_i)}{\sum_{j=1}^{m} \exp(a_j)} \tag{2.10}$$

where h is the activation of the penultimate layer nodes, W is the weight linked by the penultimate layer to the softmax function, and ai is the total input into a softmax function. Finally, the predicted class would be derived as follows:

$$\text{Predicted\_class} = \arg\max(p_i) \tag{2.11}$$

Other network operators and layers contain the following parts.

1) Flatten Operator: Takes a multidimensional array and stretches it into a single long list.

2) Dense Layer: Combines information from all previous neurons to produce a single output value. This layer acts as a final decision-maker based on all the evidence it receives.

3) Max-Pooling Layer: Shrinks the size of the data by keeping only the most important elements (the maximum values) in a specific region.

4) Normalization Layer: Adjusts the values of all neurons in a layer to have a similar range. It standardizes the value of different input levels.

5) Dropout Layer: During training, randomly turns off a certain percentage of neurons to prevent the model from relying too heavily on any specific features.

2.2.9 k-Fold CV

To evaluate the generalization capabilities of our model on a new data, we used k-fold CV. This technique divides the dataset into multiple segments and systematically trains the model on all the segments except one, which is reserved for testing. The model's performance is then assessed on this withheld segment. By cyclically rotating the segment that I left out and repeating this process for each fold, we gain a comprehensive understanding of how the model performs across different subsets of the data. This iterative testing approach provides a robust measure of the model's ability to generalize to unseen data (Yates, L. A., et. al. (2023); Wong, T.-T., & Yeh, P.-Y. (2020)).

2.2.10 Evaluation Metrics

To see how well the system identified different ranges from ultrasonic signals, four key metrics are tracked.

1) Correct Detections (True Positives; TP): When the system correctly identifies the range.

2) Missed Detections (False Negatives; FN): When the system misses the correct range.
3) False Alarms (False Positives; FP): When the system identifies a range that is not actually there.
4) Correct Rejections (True Negatives; TN): When the system correctly rejects an out-of-range signal.
These numbers are then used to calculate more comprehensive performance measures such as accuracy as follows (Reddy, B. H., & P, K. (2022)):

$$\text{Accuracy} = \frac{\text{TP} + \text{TN}}{\text{TP} + \text{FN} + \text{TN} + \text{FP}} \tag{2.12}$$

The loss function compares the similarity between the predicted probabilities and the true one-hot encoded labels such that

$$\text{Loss} = \sum_{i=1}^{N} y_i . \log \hat{y}_i \tag{2.13}$$

where N is the number of outputs, y_i is the true probability, and $\hat{y}_i$ is the predicted probability.

2.3 RESULTS AND DISCUSSION

Our experimental results confirm that the model design is functioning effectively. The measurement setup comprises a Tektronix MD0405403 oscilloscope, a WA301 wideband amplifier capable of handling up to 30 V, and a Keysight 33600A function generator. A Torlab micro-positioner facilitates the movement required to evaluate the performance of the prototype rangefinder. The schematic of setup is shown in Figure. 2.6(a). In addition, visualization detailed of experimental arrangement is provided in Figure. 2.6(b). However, it is crucial to note that preprocessing the data is essential to achieve the highest accuracy in range detection. Our ultrasonic rangefinder demonstrates the capability to accurately identify objects within a range of 10–1000 mm. Due to the significant attenuation of acoustic waves at

higher frequencies, ToF-based ultrasonic rangefinders typically operate at lower frequencies, which is around 30 kHz in this study, to achieve extended measurement ranges (Gaal, M., (2019)). As depicted in Figure. 2.6(c), first, a burst sine wave is applied to the T_x. On the receiving side, the R_x chip captures the data, which is then amplified and transferred to an oscilloscope for display and storage. The oscilloscope is configured to average eight signals. The random noise within the system escalates as the distance to the Rx increases.

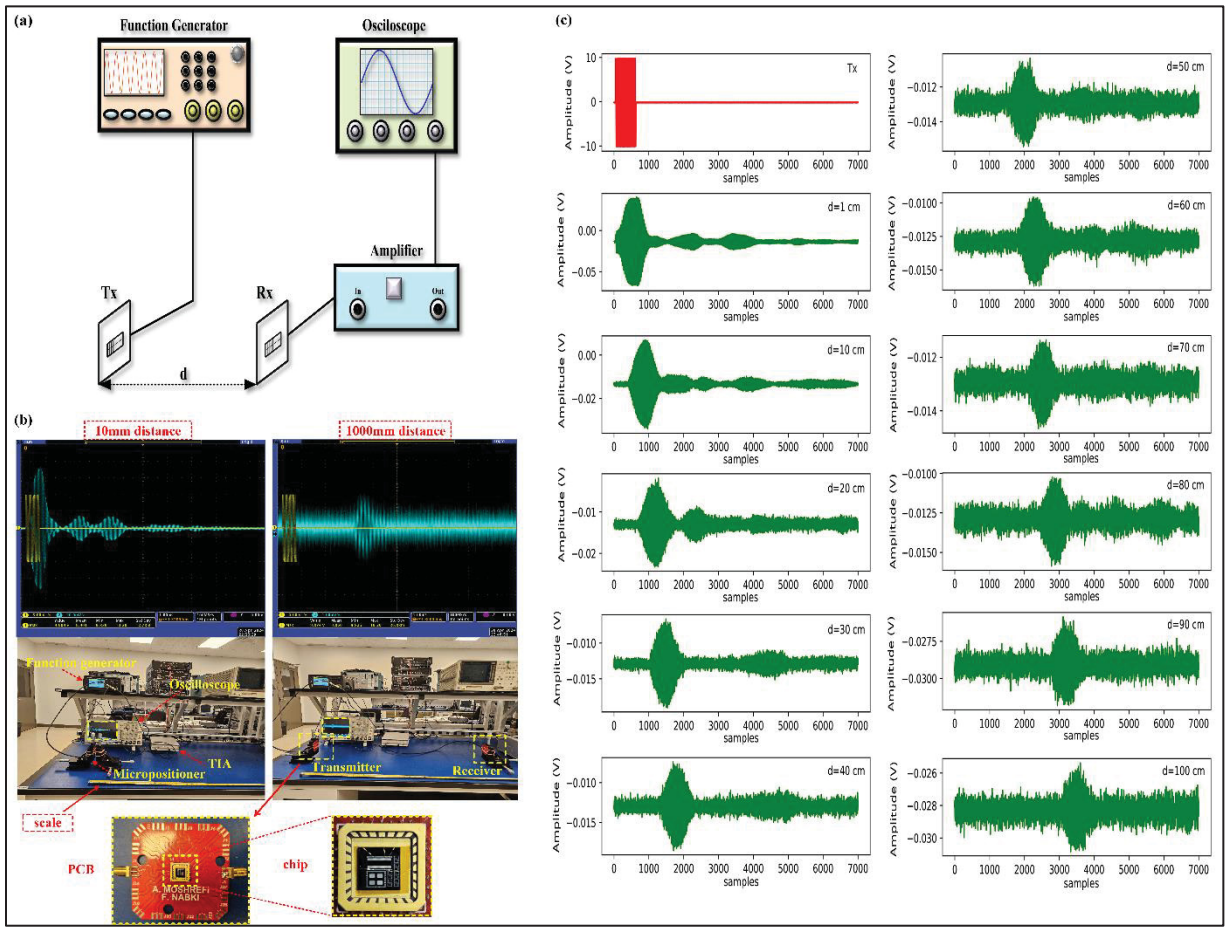

Figure 2.6 (a) Schematic of the test setup. (b) Picture of the rangefinder practical test setup. (c) Transmitted signal and the resulting received signals at different ranges. The red curve shows the input Tx signal, whereas the green curves show the received averaged data from the Rx cantilever at different ranges

This phenomenon is primarily attributed to signal attenuation during transmission. At greater distances, this attenuation intensifies, thereby degrading the SNR, which poses challenges in maintaining signal clarity and accuracy.

2.3.1 Data Visualization

To better understand the features within the ultrasonic data, especially when analyzing rangefinders, we can use dimensionality reduction techniques. These techniques take complex, high-dimensional data and transform it into a more manageable and visually interpretable format with fewer dimensions. Using these dimensionality reduction techniques, we can gain valuable insights from complex ultrasonic data and improve our understanding of the underlying patterns and relationships. Figure. 2.7 shows these visualization results, where Figure. 2.7(a) uses PCA and captures variance in the data but results in overlap- ping clusters, showing limited class separation. Figure. 2.7(b) uses t-SNE and provides better separation than PCA by capturing local structure well, but it can struggle with global structure and scalability. Figure. 2.7(c), which uses LDA, maximizes class separability linearly, enhancing distinction but still exhibits overlap and may not capture complex relationships. Figure.2.7(d) demonstrates superior performance in feature selection due to the use of bottleneck features from a neural network, which effectively capture complex and high-level abstractions, resulting in distinct and well-separated clusters. Bottleneck features benefit from nonlinear transformations and are optimized through supervised training, making them more robust and discriminative.

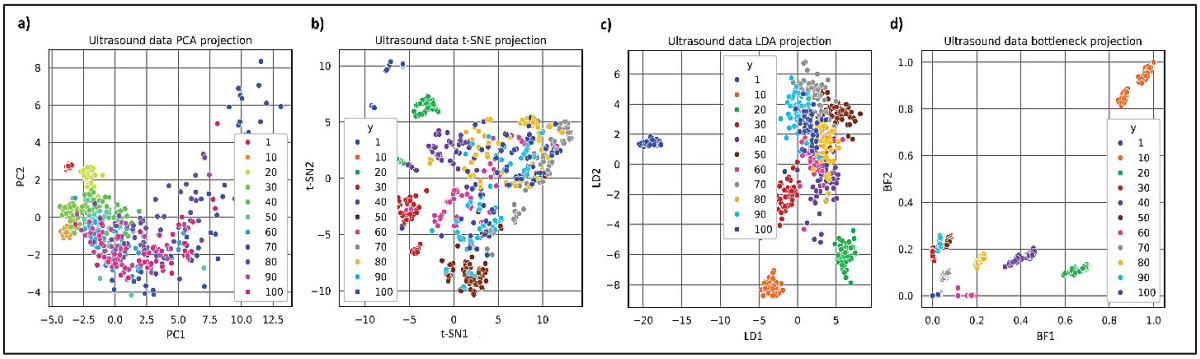

Figure 2.7 Visualization of ultrasonic signals using the dimensionality reduction approaches including (a) PCA, (b) t-SNE, (c) LDA, and (d) bottleneck features from the proposed architecture

This leads to clear class distinction with minimal overlap, demonstrating their effectiveness in capturing the most relevant features for class separation. Overall, bottleneck features offer a

more accurate and efficient method for distinguishing between different classes within this dataset.

2.3.2 Conventional Classifier

As discussed before, first the proposed framework obtains the raw signals, and it preprocesses and Standard scales the time series acoustic signals. Consequently, a variety of time and frequency-domain features are extracted from the data, which serve as input to the classifier. Then, five classifiers including support vector machine (SVM) (Chandra, M. A., & Bedi, S. S. (2021)), Gaussian Naive Bayes (GNB) (Ontivero-Ortega, M., et. al. (2017)), logistic regression (LR) (Ohsaki, M., et. al. (2017))., k-nearest neighbor (KNN) (Nti, I. K., Nyarko-Boateng, O., & Aning, J. (2021)), and decision tree (DT) (Kamiski, B., Jakubczyk, M., & Szufel, P. (2018)) are used to distinguish the airborne ranges. For SVM (cost = 0.510 and Gaussian kernel), GNB (smoothing = 0.005), KNN (K = 7), LR (sklearn = 0.90), and DT (orientation: “Gini,” min split sample: 5) are considered. Afterward, a CNN DL structure based on k-fold CV is designed to detect and classify the air coupled ranges by the ultrasonic signals.

2.3.3 DL Model

To comprehend how well an artificial intelligence model is learning and getting better over time, both accuracy and loss curves as the validation tools are applied. Accuracy curve tracks the model’s correct predictions as a percentage over the training process. A continuously increasing accuracy curve indicates the model is learning and performing better at classifying data points correctly. On the other hand, the loss curve measures the difference between the model’s predictions and the actual values. Lower loss signifies the model’s predictions are closer to true values. Ideally, the loss curve should steadily decrease during training while the prediction is improving. As depicted in Figure 2.8, by analyzing both the curves together, we can gain valuable insights into the model’s training progress. A high and stable accuracy curve coupled with a steadily decreasing loss curve suggests the model is effectively learning and performing well.

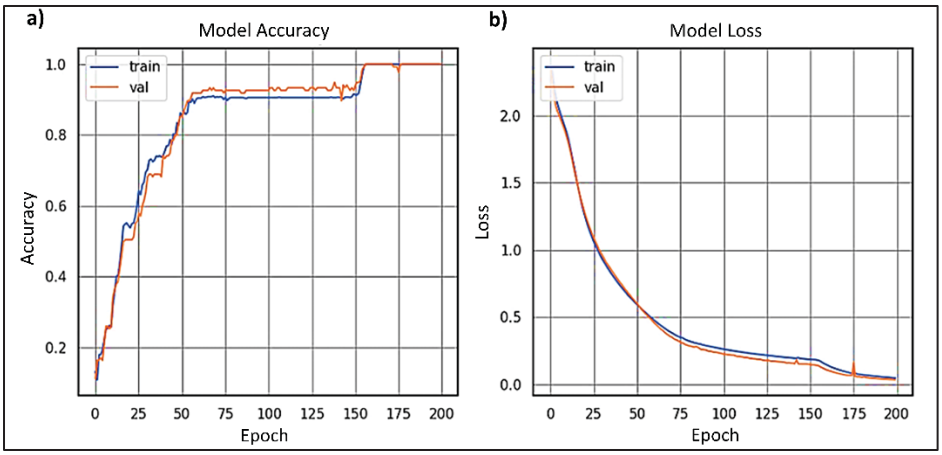

Figure 2.8 (a) Accuracy and (b) loss curves during the training process of airborne range finding by the proposed DL model

To ensure our findings are reliable and generalizable to new unseen data, we used stratified k-fold CV with rotation estimation in this ultrasonic airborne range finding research.

Table 2.2 shows comparison of the classification accuracy of different methods on the dataset. It showcases the proposed architecture's high performance across all the evaluated scores within the tested ranges. The proposed model does not exhibit variation and yet yields higher accuracy during a fivefold CV. In addition, the bar plot for the fivefold CV analysis is shown in Figure 2.9, outlying the DL model's accuracy.

Another metric to evaluate the models is the area under the curve (AUC) of the R_x ROC, as shown in Figure 2.10. The ROC curve plots the true positive rate against the false positive rate at various threshold settings. The AUC represents the likelihood that the model will correctly classify. A higher AUC value (the more vertical ROC) indicates better model performance. The ROC of the models in Figure 3.10 demonstrates the high performance of the proposed DL model.

To benchmark our model against the CC method, which is widely used in conventional range finding as detailed in Jackson, J. C., et. al. (2013) and Luo, G., et. al. (2023), we applied 50 signals from the test dataset, spanning distances from 10 to 1000 mm.

Table 2.2 Performance of different approaches including SVM, GNB, LR, KNN, DT, and Deep model, respectively, through the k-fold CV

Model Fold_#	SVM	GNB	LR	KNN	DT	Proposed (DL)
Fold_1	88.39	72.76	88.39	79.01	91.96	1.00
Fold_2	88.83	78.12	86.16	76.33	96.42	1.00
Fold_3	88.33	74.55	87.5	81.25	93.30	1.00
Fold_4	87.94	74.41	85.71	81.69	93.31	1.00
Fold_5	92.85	73.66	89.28	80.35	94.19	1.00
Average	89.37	74.73	87.41	79.73	93.83	1.00
Std. Dev.	1.981	2.036	2.034	1.493	1.651	0.00

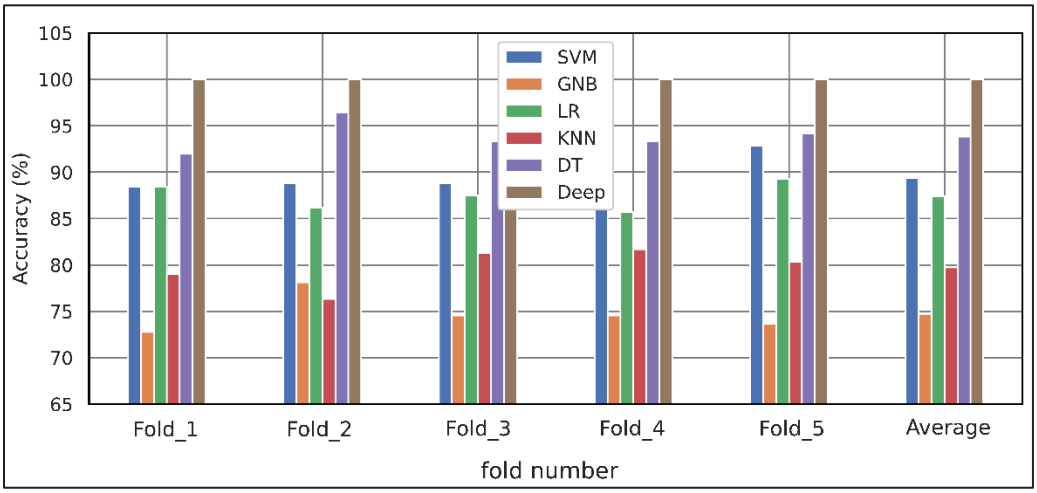

Figure 2.9 Bar plot for the six classification models using fivefold CV

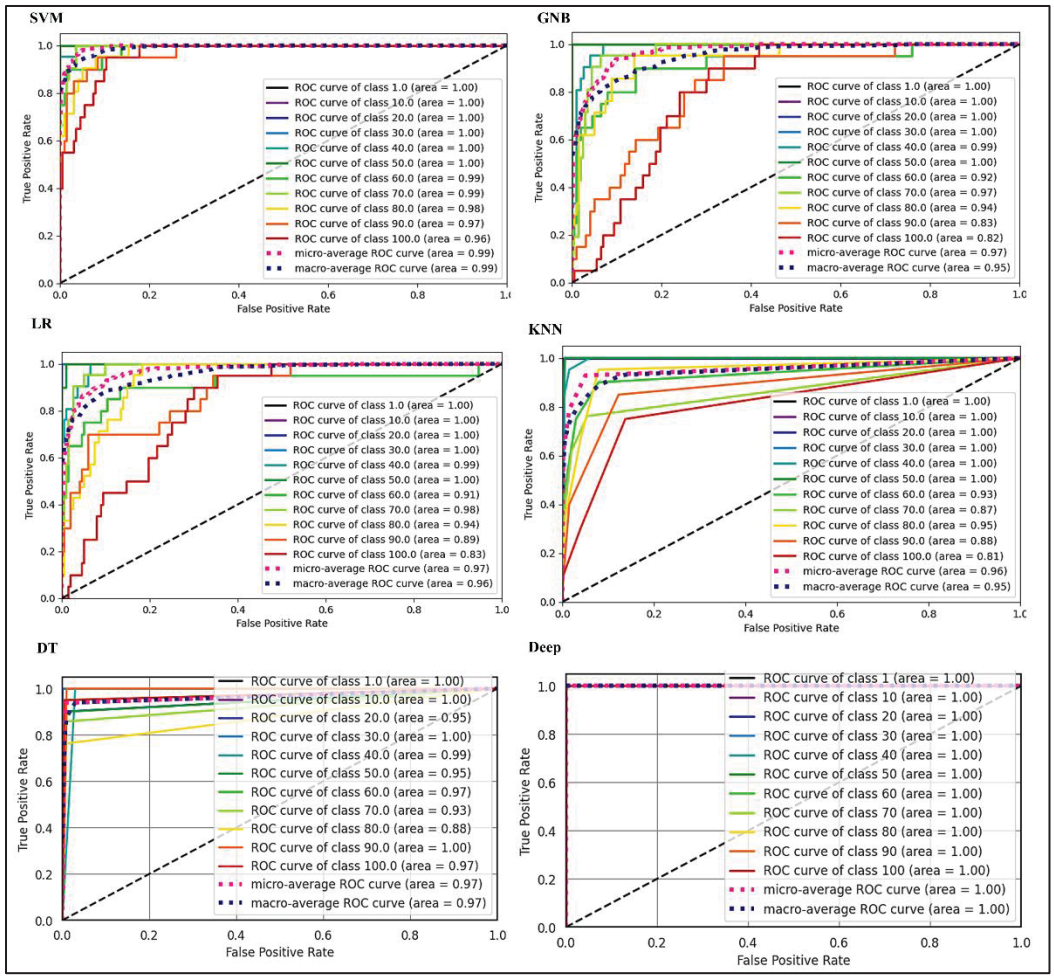

Figure 2.10 Model performance based on ROC curve for ultrasonic airborne rangefinder models

The results, displayed in Figure 2.11, reveal that as distance and noise levels increase, the CC method not only introduces a bias error at lower ranges but also fails to accurately track the correct distance at higher ranges.

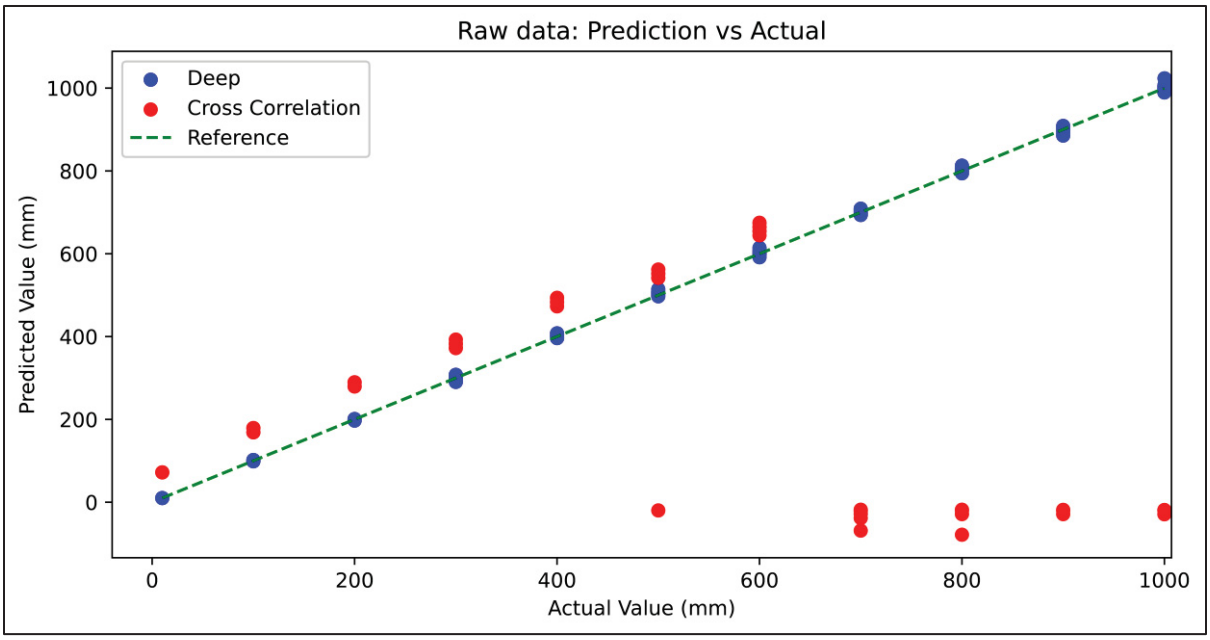

Figure 2.11 Output range result for CC and proposed DL model for the actual range values of 10–1000 mm

Figure 2.12 further illustrates the variation in results for each data point, underscoring the better performance and accuracy of our proposed model. In future work, we aim to extend our analysis by comparing various regression models to our current approach. This will allow us to explore different methodologies for enhancing precision and resolution for higher ranges.

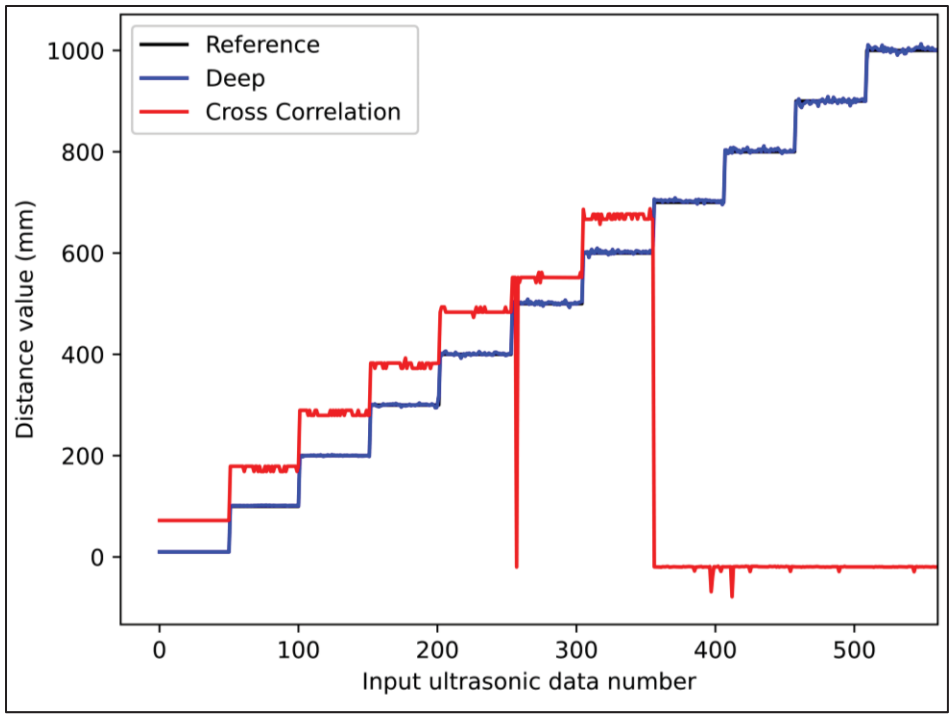

Figure 2.12 Data variations for CC and proposed model for the range of 10–1000 mm

2.4 CONCLUSION

This research presented a novel design for an ultrasonic rangefinder using piezoelectric microcantilever beam arrays, involving three structures that were developed and fabricated. Then, it demonstrated a comprehensive approach for enhancing range detection accuracy from 10 to 1000 mm, leveraging both traditional ML algorithms and advanced DL techniques. The proposed DL model is characterized by its integration of CNNs and FCs' layers. Classification algorithms such as SVM, GNB, RF, KNN, DT, and the proposed DL model were applied to distinguish the different ranges and compute performance metrics. The proposed DL model distinctly outperforms traditional methods in terms of accuracy, as confirmed by rigorous k-fold CV and AUC metrics. It also makes reliable predictions (i.e., no variations) in comparison to other approaches.

CHAPTER 3

INDUSTRIAL FAULT DETECTION EMPLOYING META ENSEMBLE MODEL BASED ON CONTACT SENSOR ULTRASONIC SIGNAL

Amirhossein Moshrefi[1], Hani H. Tawfik [2], Mohannad Y. Elsayed [2] and Frederic Nabki[1]

[1] Department of Electrical Engineering, Ecole de Technologie Supérieure, ETS, Montreal, QC H3C 1K3, Canada

[2] MEMS-Vision International Inc., Montreal, QC H4P 2R9, Canada

Paper published in: Sensors, MDPI, March 2024.

3.1 Introduction

In today's industry, rapid growth has led to more widespread automated processes, as well as an increased demand for advanced equipment and machines. Motor and pipeline spare parts have been increasingly used in machine maintenance due to the advent of industrial automation. Meanwhile, preventing the breakdown of these types of equipment would be beneficial to reduce the cost and time of maintenance. There are some methods to detect industrial faults which have different characteristics. Industrial equipment fault monitoring with technologies like vibration analysis and temperature sensing has been available for many years. However, as demonstrated by the installation potential failure (IPF) curve in Figure 3.1, ultrasound is alternatively an efficient technology to sense certain mechanical and electrical faults in order to predict failures much earlier than other monitoring technologies (Messer, A. (2015)).

In this study, common faults of pipes and motors are investigated. In order to transport fluids from one place to another, pipes are widely used. Numerous pipe segments connected with joints make up the pipeline networks that extend for several kilometers. Various factors, including traffic and surface loads, may cause the pipes and joints in these pipelines to be overstressed, resulting in leaks and pipe bursts. On the other hand, due to pipeline defects (Yu, Y., et. al. (2021)) such as cracks, cavitation, corrosion, and other mechanical damage, the

problem of pipeline operation safety can become very difficult to manage (Quy, T. B., & Kim, J. M. (2021); Zhang, M., et. al. (2022)).

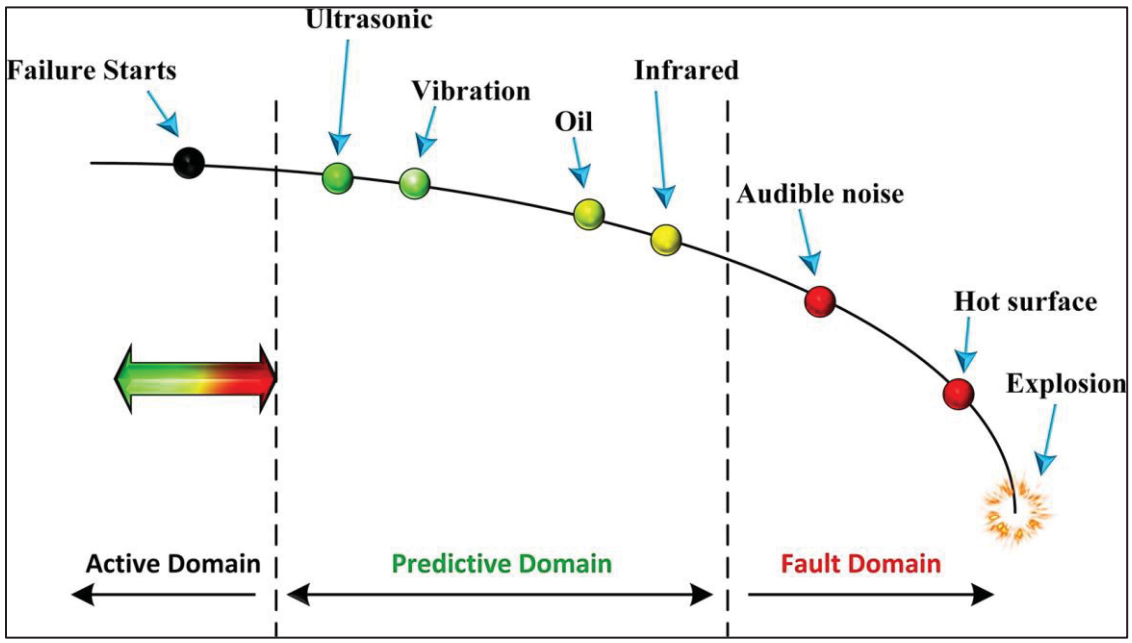

Figure 3.1 IPF curve for industrial fault prediction delay
Taken from Messer, A. (2015)

Moreover, bearings need to be considered for diagnosing rotating machinery faults or diagnosing shaft failures in industrial processes. Bearings are among the most important peripheral mechanisms in most developing countries and have to operate under high loads and speeds. Their failure, mostly due to incorrect lubricant selection, contamination, loss of lubricant, or over-greasing, causes malfunctioning of the machinery and shutdown, which in turn affects the quality and cost of the products (Toma, R. N., Piltan, F., & Kim, J. M. (2021)). Highlighting the symbiotic relationship between motors and pipelines in industrial settings is crucial for understanding their collective impact on system efficiency and safety. These components frequently operate as part of a unified system across numerous industrial applications. For instance, in the chemical processing sector, motors power pumps that facilitate the movement of fluids through pipelines. A malfunction in the motor could result in reduced pressure or flow within the pipelines, compromising the efficiency and safety of the process. Moreover, simultaneous fault detection in both motors and pipelines fosters an all-encompassing approach to predictive maintenance. Through diligent monitoring of these

components, industries can avert unplanned downtime, refine maintenance schedules, and bolster system reliability. This strategy is particularly vital in sectors such as oil and gas, where the failure of any component might induce substantial production setbacks and environmental risks. Additionally, the interconnected nature of motor and pipeline failures—where a fault in one could exacerbate issues in the other—underscores the importance of understanding these relationships for effective fault diagnosis and mitigation. For example, a blockage in a pipeline might overload a motor, causing it to overheat and fail, whereas motor failure could disrupt fluid flow, leading to increased pressure and strain on pipeline joints or seals. In scenarios where motors propel compressors or pumps linked to pipelines, like HVAC systems in large buildings or water treatment facilities, maintaining the faultless operation of both elements is imperative for energy conservation and cost-efficiency.

Adherence to regulatory and safety standards frequently necessitates extensive monitoring and fault detection across all crucial industrial system components. In the pharmaceutical industry, preserving the integrity of motors and pipelines is essential for ensuring product sterility and quality. Any defects in these elements could jeopardize the entire production cycle, potentially resulting in regulatory breaches and health risks. For example, in the food and beverage industry, motors drive pumps and agitators that convey ingredients, mixtures, or final products through pipelines. Failures in these systems may cause contamination, product wastage, or safety issues, highlighting the importance of unified fault detection mechanisms (Aguayo-Tapia, S., et. al. (2023)). To address the aforementioned faults, many approaches have been investigated in the literature. In addition to ultrasound and vibration, other signals such as infrared and audible noise as well as oil leakage can detect faults. As discussed before, among them, ultrasound signals have the ability to distinguish industrial faults more efficiently Soliman, M. H. A. (2020). However, in order to analyze ultrasonic signals, conventional methods like FFT (Al-Sagheer, R. H. A., et. al. (2019)), filtering, and windowing (Jaafar, N. S. M., et. al. (2019); Ting, L. L. (2017)), due to the overlapping of noise and signal, are not effective. Alternatively, intelligent methods like machine learning (ML) can detect subtle changes in the received signals from the ultrasonic sensor (Messer, A. (2015); Pandey, S., (2021)).

Based on the literature, many authors studied fault detection using artificial intelligence (AI) algorithms by focusing on various derived signals. Quy, T. B., & Kim, J. M. (2021) introduced a technique using a KNN classifier embedded in a microcontroller unit to classify the leak faults in real-time. They extracted the hybrid features from acoustic emission signals through a gas pipeline. Ding, H., et. al. (2021) introduced an algorithm for detecting faults in spacecraft, specifically focusing on four types of leaks with varying leakage conditions. Their approach utilizes acoustic signals and combines SVM with empirical mode decomposition (EMD) as the underlying technique. According to the assessment of a pipeline by Coelho, J. A., Glóri a, A., & Sebastião, P. (2020), a system based on a wireless sensor network designed to monitor distribution systems using a random forest (RF) algorithm was used to precisely locate fluid leaks. They concluded that, by employing more features, accuracy could be increased. Rai, A., & Kim, J. M. (2021) highlighted the insufficiency of historical data on pipeline failures for the existing supervised AI methods. To address this challenge, they introduced an alternative approach focused on a health index perspective. Their proposed method incorporates multi-scale analysis, the Kolmogorov–Smirnov (KS) test, and a Gaussian mixture model (GMM) to accurately determine the leakage situation in pipelines. Wang, H., et. al. (2020) proposed a method that employs Principal Component Analysis (PCA) to integrate data from multiple sensors for the accurate prediction of rolling bearing lifespan. This approach significantly enhances reliability by amalgamating various features from vibration signals, though it relies heavily on extensive lifecycle data for effective modeling. A notable limitation of their work is its dependence on complete lifecycle test data from rolling bearings to achieve precise modeling, necessitating comprehensive testing to identify optimal sample sizes. This requirement potentially limits the method's application in scenarios where extensive historical data is unavailable, likely increasing the time and cost associated with the predictive maintenance process. Additionally, this method primarily focuses on time-domain features, which may restrict the depth of data feature analysis and risk missing valuable insights from other domains, such as frequency. Saucedo-Dorantes, J. J., et. al. (2021) introduced a condition monitoring methodology for induction motors, analyzing motor stator currents and vibrations to estimate different features across multiple domains. Utilizing genetic and PCA algorithms for feature selection, followed by dimensionality reduction via the Linear Discriminant

Analysis (LDA) algorithm, this approach ultimately evaluates the refined features using a neural network classifier to achieve global and individual classification ratios. However, the complexity of this method and its intensive computational resource requirements are significant drawbacks. The process involves multiple advanced stages, including high-dimensional feature estimation, optimization with Genetic Algorithms and PCA, and dimensionality reduction through LDA, before proceeding to fault diagnosis. This complexity not only necessitates consider- able processing power but also complicates real-time application, potentially limiting its practicality in scenarios where rapid and efficient diagnostics are essential. Research on rotating machinery fault diagnosis using ensemble kernel extreme learning machines based on stacked denoising autoencoders (SDAE) was explored Pang, S., et. al. (2020). This study focused on gear, rotor, and real engine rolling bearing datasets, extracting vibration characteristics from both time and frequency domains. The PCA algorithm was used to merge two sets of SDAE features from multiple domains into essential low-dimensional features, which were then classified for fault patterns using the ensemble kernel extreme learning machine. Despite its innovative approach, this method encountered challenges such as lengthy training times, complex implementation, high computational costs, and the need for large amounts of labeled data for training the models. Our contribution builds upon these insights, utilizing ultrasonic data for early detection characterized by its minimal computational demands. This enables efficient deployment on MCUs, offering quick responsiveness with reduced memory usage, thereby addressing some of the limitations highlighted in the aforementioned studies. Maliuk, A. S., (2021) conducted research on detecting bearing faults through signal processing and proposed another approach based on the Gaussian mixture model (GMM). Their method leverages a fault-frequency-oriented GMM window series for reliable feature extraction. The classification step is performed using the weighted KNN algorithm. As discussed before, besides pipeline faults in industrial equipment, rotating machinery faults commonly occur in many different areas and manufacturing sectors. These include aerospace, power generation, oil refining, machining, automotive, railway transportation, pumping systems, etc. (Aguayo-Tapia, S., et. al. (2023); Piltan, F., & Kim, J. M. (2023); Alidadi, M., & Rahimi, A. (2023)). To prevent operational malfunctions that could potentially result in catastrophic failures, various condition monitoring

techniques have been developed for the purpose of fault detection and diagnosis in bearings. Abdelrhman, A. M., et. al. (2020) introduced a diagnosis and detection model for bearing faults in rotating machinery. Their approach involves the utilization of multivariate analysis of variance to extract parameters from acquired data sets. Time-domain features are employed, and a binary logistic regression (BLR) modeling technique is utilized for the fault diagnosis and detection. Similarly, Jiang, Q., et. al. (2022) proposed a method for weak rotating machinery fault diagnosis. They introduced a multiscale permutation entropy feature extraction approach, which involves calculating time series with equal overlapping segments. The extracted features are then used as input for classification using SVMs. To optimize the SVM parameters, the authors introduced a chaos firefly optimization algorithm as a solution to the parameter optimization problem. Another study by Da Silva Souza, J., et. al. (2021) proposed an SVM-based classifier by employing statistical data features for bearing fault recognition. They investigated the presence of different types of bearing defects and combinations of statistical attributes on SVM accuracy. In another work by Jung, W., Bae, J., & Park, Y. H. (2021), using adaptive wavelet denoising and statistical–spectral acoustic features, the authors performed a binary classification task to monitor the health conditions of a ball bearing with a microphone under noisy conditions. The authors used an adaptive wavelet method based on the kurtosis entropy index and multiple acoustic features were extracted based on expert knowledge. However, few works have investigated the use of an ensemble model in fault detection though ultrasonic monitoring. In (Moshrefi, A., et. al. (2023)), we proposed a meta model based on the majority voting of four classifiers for industrial faults. Accordingly, this study is an extension of previous work and focuses on fault diagnosis using ultrasound signals by a meta ensemble model. The research encompasses the classification of ten distinct types of faults in both pipeline and rotating machinery conditions. Statistical features from both the time and frequency domains are extracted by the PCA, LDA, and t-SNE approaches. Finally, the features are refined using RFE. Then, five widely used classification models including GNB, LR, KNN, SVM, and DT are implemented. Afterward, using an ensemble learning approach, faults are classified into ten categories. Then, the reliability of the model based on four evaluation metrics—k-fold validation, confusion matrix, ROC, and learning curve—is investigated and, ultimately, its potential for real-time application is assessed

through deployment on an MCU. Our study makes significant contributions by meticulously preparing a dataset that encapsulates 10 distinct fault types, integrating both motor and pipeline anomalies. In the initial preprocessing phase, we employ advanced techniques to effectively eliminate noise, enhancing the data's clarity. We then leverage feature reduction methods, including RFE, to meticulously select the most impactful features for subsequent analysis. During the classification phase, we introduce a novel approach by combining conventional classifiers into an innovative ensemble model. This model is rigorously evaluated through k-fold cross- validation, demonstrating its ability to accurately categorize features with 93% accuracy. The culmination of our efforts is the deployment of this framework on an MCU, where we successfully assess its capability for real-time monitoring. This comprehensive approach not only showcases the framework's high accuracy but also its practical applicability in real-world industrial settings for fault detection.

The rest of this paper is organized as follows: preprocessing, feature extraction, and methods are explained in Section 2. Then, Section 3 presents the experimental results and is followed by a conclusion.

3.2 Proposed Methodology

The proposed methodology's overview is illustrated in Figure 3.2. The entire procedure consists of five steps, each of which is explained in a separate subsection. The initial step involves acquiring ultrasonic data from a microphone array module, which is then recorded as raw data for further classification analysis. The collected data from the structure is processed to refine and prepare it for the feature extraction stage. Feature extraction is performed to transform the data into a set of numerical features known as a feature vector, which provides a concise and informative representation of the data. This study extracts a comprehensive suite of features from ultrasonic data, spanning time, power spectral density, and frequency domains. These features include minimum, maximum, mean, zero crossing times, slope change, impulse factor, shape factor, margin factor, area under curve, standard deviation, skewness, and kurtosis, offering a detailed analysis of the data's characteristics. The presence of large input vectors often poses a challenge in the predictive modeling process of machine learning models. This challenge is commonly known as the problem of high dimensionality in

raw data. To address this, a dimensionality reduction technique is employed as a solution. Finally, a machine learning classification algorithm is applied to the reduced-dimensional data for the classification task.

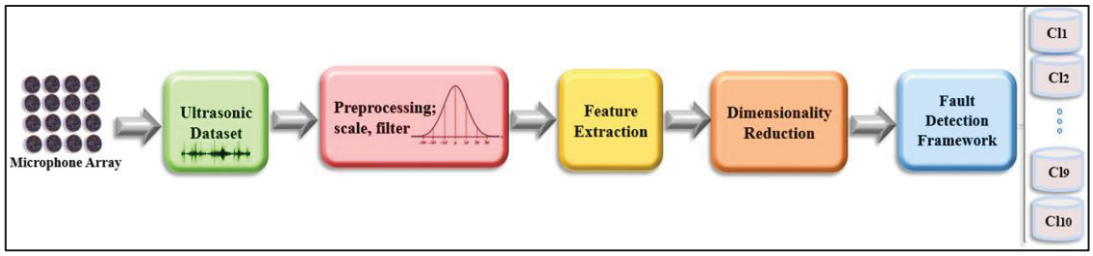

Figure 3.2 Overview of the workflow methodology

3.2.1 Preprocessing

To mitigate noise in ultrasonic signals, one technique involves utilizing a Butterworth filter in the time domain, aimed at eradicating undesired spikes, trends, and outliers. Butter- worth filters are favored in control systems for their lack of peaking, ensuring a consistent signal without unduly amplifying any frequency. These filters are crafted to sustain a flat frequency response across the passband, avoiding alterations in signal amplitude within this range Selesnick, I. W., & Burrus, C. S. (1998). This characteristic is crucial for maintaining the integrity of the ultrasonic signal's information content. The nth order Butterworth filter is mathematically described by its frequency response equation, encapsulating the filter's design to achieve the desired signal such that the following holds:

$$H(j\omega) = \frac{1}{\sqrt{1+\varepsilon^2\left(\frac{\omega}{\omega_p}\right)^{2n}}} \tag{3.1}$$

where H is the passband gain, ω is the angular frequency, ε is the maximum pass band gain, and n represents the filter order.

The data values are normalized to be comparable for the different signal sets. Among many different scalers available for feature scaling, the standard scaler in Thara, D. K., PremaSudha, B. G., & Xiong, F. (2019) is normalized as follows:

$$Z = \frac{x - \mu}{\sigma} \tag{3.2}$$

where the normalized vector, denoted as Z, is derived from the signal vector X. The normalization process involves calculating the mean (μ) and standard deviation (σ) of the input acoustic sequence X. These statistical measures are used to standardize the values in X, resulting in the normalized vector Z.

3.2.2 Feature Extraction

Firstly, to provide the characteristics of each data, some features should be considered. In this study, 30 features in time, Fourier, and power spectrum domains are extracted which are composed of maximum, average, standard deviation, skewness, kurtosis, average of peaks (peaks_mean), time of peak (peak_index), zero crossing, crest factor, and shape factor. To distinguish between the classes with the most discernment, the independent and more important features should be selected. The selected complex features are defined below:

$$\text{Skewness} = \frac{\frac{1}{N}\sum_{n=1}^{N}\left(x(n)-\bar{x}\right)^3}{\left(\sqrt{\frac{1}{N}\sum_{n=1}^{N}\left(x(n)-\bar{x}\right)^2}\right)^3} \tag{3.3}$$

$$\text{Kurtosis} = \frac{\frac{1}{N}\sum_{n=1}^{N}\left(x(n)-\bar{x}\right)^4}{\left(\sqrt{\frac{1}{N}\sum_{n=1}^{N}\left(x(n)-\bar{x}\right)^2}\right)^4} \tag{3.4}$$

$$\text{Crest\_factor} = \frac{\max\left|x(n)\right|}{\sqrt{\frac{1}{N}\sum_{n=1}^{N}x(n)^2}} \tag{3.5}$$

$$\text{Shape\_factor} = \frac{\sqrt{\frac{1}{N}\sum_{n=1}^{N} x(n)^2}}{\frac{1}{N}\sum_{n=1}^{N} |x(n)|} \tag{3.6}$$

where N is the number of samples in the input vector x(n).

3.2.3 Dimensionality Reduction

In order to enhance the accuracy and efficiency of the model, it is essential to prune every dataset. Particularly when dealing with ultrasonic signals, the dimensionality of the data should be reduced. Dimensionality reduction involves transforming high-dimensional data into a more concise and meaningful representation with reduced dimensions. One of the prominent techniques for linear dimensionality reduction is PCA which identifies orthogonal directions that capture the maximum variance, making it a valuable second- order statistical method Postma, E., & Postma, E. (2009). PCA is a highly effective approach for eliminating redundant dimensions while retaining the most informative ones. This algorithm operates by computing the eigenvalues of the covariance matrix, aiming to minimize computation costs while preserving accuracy. By extracting independent information from the acoustic data, PCA successfully reduces dimensionality while maintaining the essential aspects of the dataset. In addition to PCA, another algorithm commonly used for assessing feature distinctiveness and visualizing data separability is t-SNE, which is capable of preserving the relationships among data points in a lower-dimensional space, making it particularly useful for visualizing complex high-dimensional data. One key distinction between the PCA and t-SNE techniques is that while PCA focuses on preserving large pairwise distances to maximize variance, t-SNE primarily preserves local similarities among data points. This difference in approach makes t-SNE well-suited for visualizing intricate patterns in the data (Agis, D., & Pozo, F. (2019); Devassy, B. M., George, S., & Nussbaum, P. (2020)). For enhanced comparison and visualization, LDA, a supervised technique, is utilized. LDA seeks to generate new components that differentiate categories effectively, focusing on a class feature with the goal of identifying the projection that optimally distinguishes between faults in the ultrasonic data

(Adebiyi, M. O., et. al. (2022)). By reducing the dimensionality of the data, LDA strives to improve class separability while retaining as much information as possible. Although it offers a solution to the challenge of small sample sizes, LDA faces issues such as singularity, dependence on the assumption of Gaussian distributions, and the difficulty in determining the best dimensionality reduction.

3.2.4 Recursive Feature Elimination (RFE)

RFE selects features recursively, considering increasingly smaller sets of features at each step. By comparing different feature sets, the algorithm aims to identify the set that achieves the highest accuracy (Granitto, P. M., et. al. (2006); Ullah, S., Ahmad, Z., & Kim, J. M. (2024)). In every iteration of the RFE algorithm, the importance of each feature is measured, and the least relevant feature is subsequently removed. In other words, RFE aims to evaluate the significance of features within a dataset, given an external estimator or classifier that assigns importance weights to these features. This method systematically selects ultrasonic features from the feature set (FS) by progressively focusing on increasingly smaller subsets of ultrasonic characteristics through iterative processes. Features that are deemed less important and thus eliminated in each iteration are then placed into a ranking set (RS). With each subsequent iteration, the FS is methodically reduced to further assess the importance of the remaining features. This procedure is repeated multiple times to exhaustively analyze all possible combinations of features within the FS. Ultimately, the features are systematically organized and ranked within the RS based on their importance, as determined through the RFE algorithm. The RFE procedure is depicted in Figure 3.3.

3.2.5 Classification Using k-Fold Cross Validation

In this study, for an industrial fault detection system, we propose an effective monitoring method using ultrasonic signals based on well-known classifiers. The classification algorithm first obtains raw signals, and it then preprocesses and scales the time series ultra- sonic signals. Consequently, a variety of time- and frequency-domain features are extracted from the data, which serve as input to the classifier. Then, five classifiers including KNN, LR, DT, GNB, and SVM are employed to distinguish the fault classes. The selection of these classifiers is based

on their reduced memory requirements with lower output variations in comparison to deep learning classifiers (Yadavendra, & Chand, S. (2020)), making them well-suited for ensemble implementation. Afterwards, a meta classifier based on k-fold cross validation (CV) is designed to detect and classify the irregularities in the ultrasonic signals. The mentioned classifiers are described as follows:

SVM is a clustering algorithm specifically designed for small sample sets, demonstrating exceptional learning capabilities even when the data is limited. It also exhibits good generalization properties. The SVM algorithm, utilizing a kernel function, aims to identify the optimal hyper-plane or decision boundary (such as a point, line or plane) that effectively separates different classes of data (Chandra, M. A., & Bedi, S. S. (2021)). GNB algorithm is an extension of the Naive Bayes algorithm. Naive Bayes is a generative model that assumes the independence of features. In the case of Gaussian Naive Bayes, the algorithm assumes that the covariance matrices are diagonal, implying independence between the features. Different functions are employed to estimate the data distribution and calculate the mean and standard deviation for the training (Ontivero-Ortega, M., et. al. (2017)).

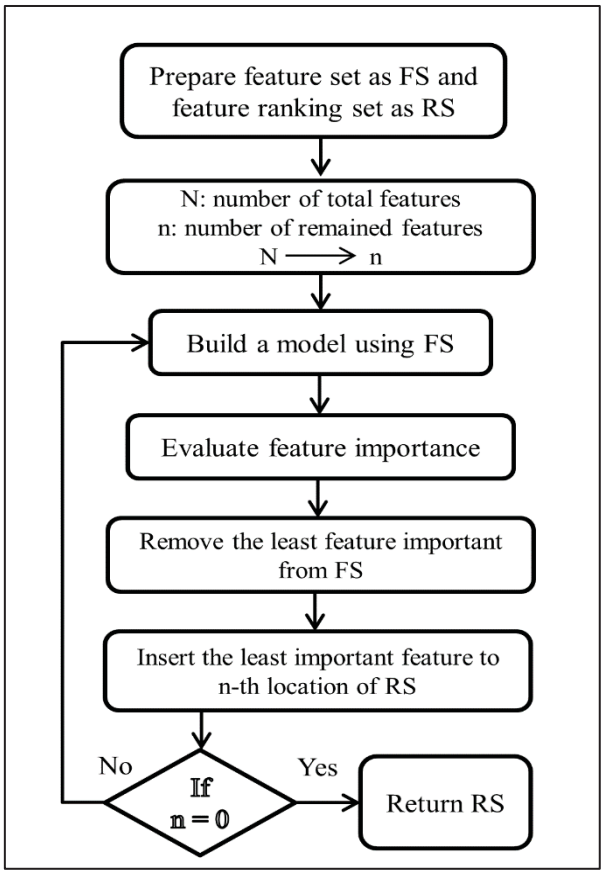

Figure 3.3 Recursive feature elimination flow diagram

LR is a machine learning classification algorithm widely used in statistical analysis. It is employed to describe data and model the relationship between a single dependent variable and two or more independent variables, which can be of ordinal, nominal, interval, or ratio level. The purpose is to determine the outcome or predict the probability of a specific event or class (Ohsaki, M., et. al. (2017)). DT is a supervised machine learning algorithm used for both regression and classification tasks. It is constructed using a directed graph technique. The decision tree follows a tree-like structure, where inner nodes represent the variables or features of a dataset, branches represent the decision rules, and each leaf node represents the output result (Kaminski, B., Jakubczyk, M., & Szufel, P. (2018)). KNN is a supervised classification approach that avoids making any assumptions about the primary data. It is a non-parametric algorithm that utilizes the similarity between new data and existing data to assign the new data to the most similar group among the available groups (Nti, I. K., Nyarko-Boateng, O., & Aning, J. (2021)). k-fold CV is employed to evaluate the generalization of industrial fault detection

analysis results on an independent dataset. By employing k-fold CV, we can assess the predictive performance of our machine learning model on unseen ultrasonic data and ensure the model's robustness (Wong, T.-T., & Yeh, P.-Y. (2019)). Using this approach, our underlying dataset is divided into k non-overlapping folds. As shown in Figure 3.4, in the test phase, the first ultrasonic signal fold is used to evaluate the model performance, while the remaining k-1 folds are used for training. Next, the second input signal fold is used for the test step and the rest of our dataset is used for the training. The procedure is repeated k times until the last ultra-sonic fold, and at last, the average value of these k experiments is used for the evaluation (Nti, I. K., Nyarko-Boateng, O., & Aning, J. (2021)). In this work, stratified k-fold CV is employed, which makes the results less susceptible to data bias and imbalance. Steps for k-fold CV are summarized as follows:

Step1: Categorize the training dataset (D_{train}) into k equal subsets such as $\{F_1, F_2, ..., F_k\}$. Here F_i will be an $m \times k$ array.

Step2: for i=1 to k:

{

Step2_1: Consider D_{train} consisting of k-1 folds, with the F_i fold designated as the testing dataset (D_{test}).

Step2_2: Using CV train the ML model and compute the accuracy, *precision*, and *recall* as presented in the evaluation metrics section.

}

Step3: Evaluate the *accuracy* using all the k instances of CV as follows:

$$Accuracy = \frac{1}{N}\sum_{i=1}^{k} Accuracy_i$$

Figure 3.4 Pseudo-code for the k-fold CV algorithm

3.2.6 Meta Classifier

In the realm of ensemble learning methodologies, stacking involves the integration of multiple learning models through a meta-classifier. As illustrated in Figure 3.5, the initial step entails training individual classification models (Ci) using the entire ultrasonic training set. Subsequently, the meta-classifier is trained using the labels from these individual machine

learning models within the ensemble (Sultana, N., & Islam, M. M. (2020)). The forecasted outputs of the classifiers (Pi) serve as meta-features, which are then combined with weights (wi). These weighted meta-features are utilized as inputs for the meta-classifier, ultimately determining the final output ($\hat{y}$), which is chosen based on the predicted class output from other classifiers. This process is defined as follows:

$$\hat{y} = \arg\max_{i} \sum_{j=1}^{m} \omega_j P_{ij} \tag{3.7}$$

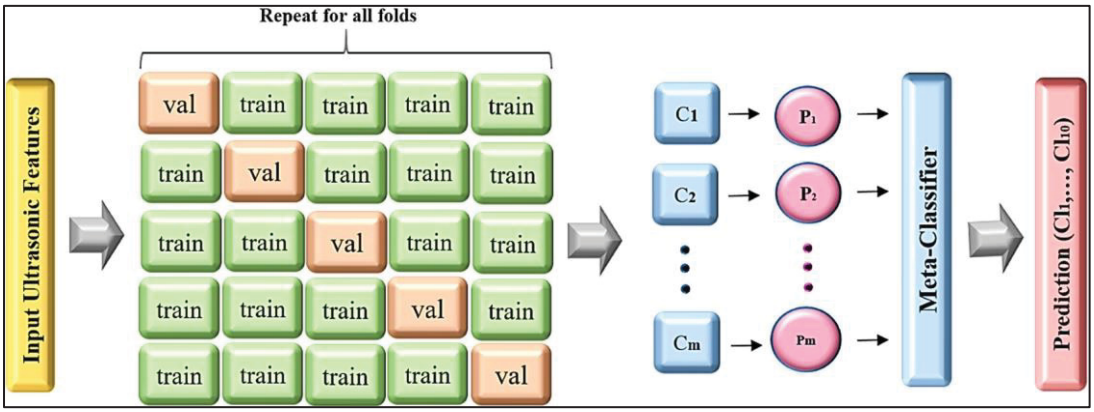

Figure 3.5 Utilization of a fault detection framework employing the k-fold CV and meta-classifier

Ensemble methods, which aggregate predictions from various base models, often enhance generalization and robustness, outperforming single-model approaches due to the diversity in the base models. In contrast, deep learning models are susceptible to over-fitting, particularly with limited datasets or excessive model capacity. Stacking meta- classifiers addresses this issue by integrating outputs from several models, each trained on different data subsets or utilizing distinct algorithms, thereby reducing the risk of over-fitting.

Stacking meta-classifiers is especially advantageous for small datasets, where they tend to outperform deep learning models that typically require vast amounts of labeled data for effective training. Moreover, deep learning models demand substantial computational power and specialized hardware like GPUs or TPUs, making them less accessible. In contrast, stacking meta-classifiers are less demanding on resources and can be trained more efficiently on conventional hardware.

Therefore, stacking meta-classifiers is often a superior choice in situations demanding high interpretability, limited data availability, constrained computational resources, simplicity in model complexity, robustness against over-fitting, reliability of results, and when domain expertise is a key factor.

3.2.7 Implementation

The “micromlgen” library, as depicted in this study, represents a critical tool for the deployment of machine learning models on microcontrollers, facilitating the conversion of such models into C code suitable for hardware environments constrained by memory, processing power, and energy consumption. Despite its utility, the practical implementation of “micromlgen” for classification tasks reveals several limitations, particularly due to the restricted computational resources of microcontrollers. The “micromlgen” library exhibits optimal performance with simpler or specifically tailored lightweight models, given its support for a finite range of ML algorithms. This includes well-known algorithms such as decision trees, support vector machines, and certain neural network types, albeit excluding support for more complex or recent models like extensive deep learning architectures.

In the realm of TinyML, which optimizes AI for low-power, compact microcontrollers, the nRF52840 microcontroller stands out for its capability to deploy AI models efficiently, leveraging TinyML libraries. This synergy is particularly conducive for embedding on- device decision-making capabilities, thus diminishing the reliance on perpetual cloud connectivity. Utilizing “micromlgen” enables the conversion of ML models into C code, rendering it compatible with the development environment of the nRF52840. This process allows for the direct integration of AI into devices, facilitating real-time data processing and decision-making. The application of TinyML libraries further enhances model execution efficiency on the nRF52840, capitalizing on the microcontroller’s functionalities while managing its limitations.

The integration of “micromlgen” for model conversion and TinyML for deployment on the nRF52840 MCU embodies a strategic methodology for embedding ML into hardware systems. This combination exploits the advantages of the aforementioned tools and the MCU’s capabilities, paving the way for the development of intelligent embedded systems proficient in

edge data processing. The implementation flowchart, illustrated in Figure 4.6, delineates this comprehensive process, underscoring the potential for developing autonomous, cloud-independent devices that prioritize privacy, speed, and reliability.

Figure 3.6 Workflow of the model implementation

3.2.8 Evaluation Metrics

In assessing the efficacy of the fault detection framework put forth, conventional quality metrics including precision, recall, F-measure, and accuracy are employed. These metrics furnish quantitative evaluations of the framework's ability to identify faults, drawing from parameters such as true positive (TP), false negative (FN), true negative (TN), and false positive (FP) (Sravani, S., & Karthikeyan, P. R. (2023)). They are defined as follows:

$$\text{Precision} = \frac{TP}{TP + FP} \tag{3.8}$$

$$\text{Recall} = \frac{TP}{TP + FN} \tag{3.9}$$

$$F_1 = \frac{2 \times \text{Precision} \times \text{Recall}}{\text{Precision} + \text{Recall}} \tag{3.10}$$

$$\text{Accuracy} = \frac{TP + TN}{TP + FN + TN + FP} \tag{3.11}$$

TP signifies the count of accurately classified samples deemed relevant, FN indicates the count of relevant samples inaccurately classified, TN denotes the count of accurately classified samples considered irrelevant, and FP represents the count of samples inaccurately classified as relevant. Precision quantifies the ratio of accurately classified relevant samples to all samples classified as relevant. Recall gauges the ratio of relevant samples accurately classified to all relevant samples within the dataset. The F1 score calculates the harmonic mean of

precision and recall, furnishing a balanced assessment of classification performance that considers both precision and recall. Accuracy determines the proportion of correctly classified samples across all classes, presenting an overall gauge of the accuracy of classification (Reddy, B. H., & Karthikeyan, P. R. (2022)). In addition, receiver operating characteristic (ROC) plots offer a comprehensive view of a classifier's performance across various levels of specificity. In this research, ROC plots are utilized to further investigate and evaluate the performance of the classifiers. The ROC plots provide insights into the trade-off between the true positive rate and the false positive rate, allowing for a more detailed analysis of the classifiers' performance.

3.3 Results and Discussion

Ultrasonic fault detection for pipes and motors is a technique to identify defects or irregularities. The process involves using a contact ultrasonic microphone sensor, also known as an ultrasonic transducer. The contact ultrasonic microphone sensor is placed in direct contact with the surface of the pipe or motor to receive the data. The profile can be due to friction, impacts, leaks, or cracks that occur naturally during operation or as a result of damage. Healthy and uniform material emits the wave in minimal disruption. Some advantages of contact measuring are that it requires no interruption of normal equipment operation, allowing for continuous monitoring. It can identify very small or early-stage faults that might not impact visible performance or be detectable through other non-destructive testing methods. Also, it eliminates the cost of an external ultrasonic transmitter and the associated operational complexities. This contact sensing is particularly suited to environments where continuous monitoring is desired without the need for frequent manual inspections or where the operational noise of the equipment itself can be leveraged to identify potential issues.

The dataset extracted from UE Systems Co. by a piezoelectric array called an "Ultra- probe" consist of 10 classes, including 4 for bearings (i.e., under-lubricated, over-lubricated, slow speed, and healthy bearing) and 6 for pipelines (i.e., steam, cavitation, motor-boating, reciprocating, thermostatic, and healthy pipe), with 20,000 samples (UE Systems. (2020)), 70% for training and 30% for testing, along with a sliding window with length of 1000 to select and augment the data. The motor rolling bearing and pipeline faults mainly consist of the main body which contains the ultrasonic signals of ten patterns: under-lubricated, over-lubricated,

slow speed, steam, cavitation, motor boating, reciprocating, thermostatic, healthy pipe, and healthy motor signals. The data samples are shown in Figure 3.7.

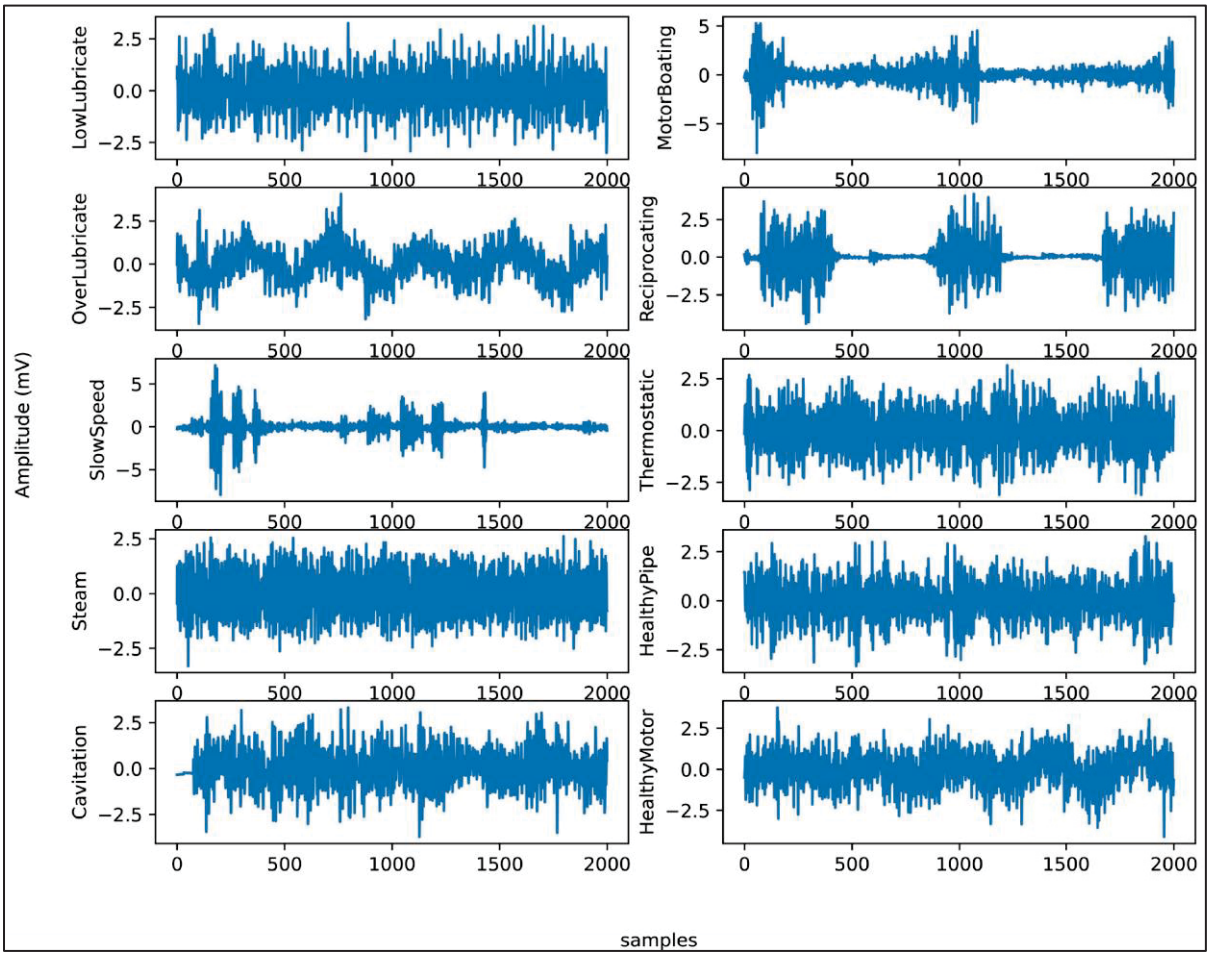

Figure 3.7 Ultrasonic signals of the ten patterns: under-lubricated, over-lubricated, slow speed, steam, cavitation, motor boating, reciprocating, thermostatic, healthy pipe, and healthy motor signals

As mentioned in the introduction, regarding the IPF curve, the rapid identification of bearing and pipe faults is a primary objective in the operation of industrial mechanisms. This study focuses on investigating the impact of features on the statistical parameters of the acquired ultrasonic datasets. The aim is to understand how different features affect the statistical properties of the collected ultrasonic data, which are crucial for the quick identification of faults in bearings and pipes. For visualization the features, other methods like PCA, LDA, and t-SNE can be considered. PCA preserves the variance in the data and is applied to the data to

reduce its dimensionality and readily visualize the faults. In addition to PCA for dimensionality reduction, t-SNE also is calculated. Figures 3.8–3.10 respectively, present the PCA, t-SNE, and LDA visualization of ultrasonic data based on two components. As mentioned in the previous section, five classifiers for our model are employed. For GNB (smoothing= 0.008), DT (orientation:"Gini", min split sample: 3), LR (sklearn = 0.98), kNN (k = 7), and SVM (cost = 0.520 and Gaussian kernel), m = 5 are considered.

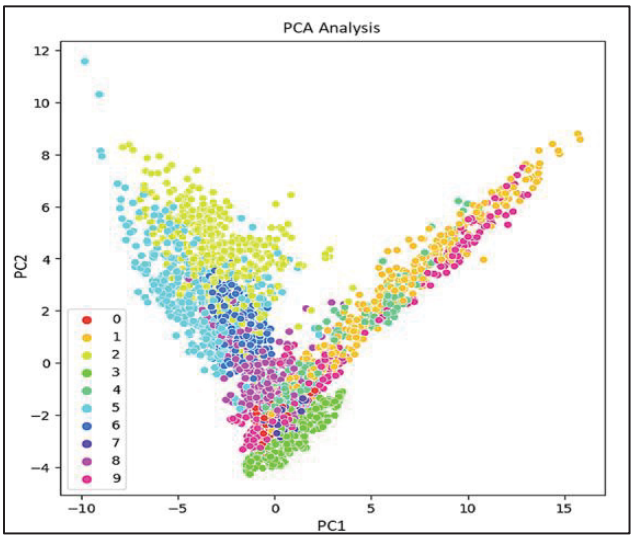

Figure 3.8 PCA representation of the ultrasonic dataset

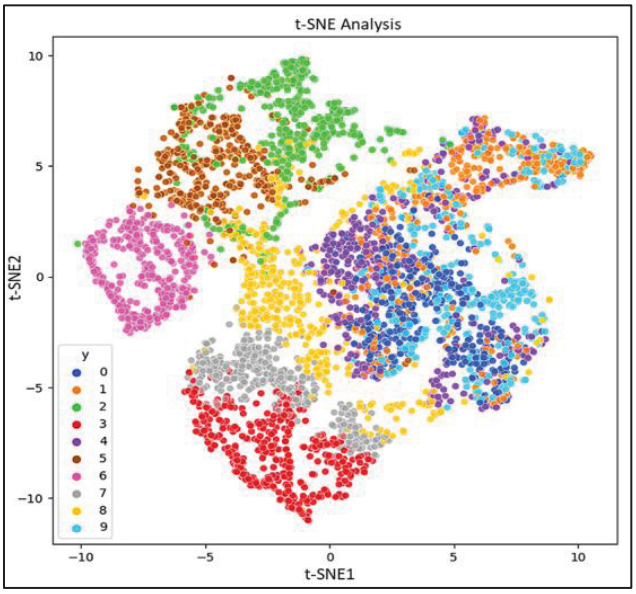

Figure 3.9 t-SNE representation of the ultrasonic dataset

Feature selection is a critical step in the classification process, aimed at identifying and eliminating irrelevant, less useful, and redundant features, while identifying the most relevant and informative inputs for a classification model. By reducing the number of input features, feature selection assists in the development of a predictive model. It plays a crucial role in enhancing the efficiency and accuracy of the classification task by focusing on the most significant features that contribute to the classification performance while eliminating noise and irrelevant information. Furthermore, feature selection is desirable to both decrease the computational cost of classification models and, in some cases, to improve the performance of the fault detection model. It enables onboard ML for MCU devices by decreasing the required memory size. However, deploying ML models on MCUs presents challenges, notably in terms of processing power consumption and limitations in flash memory, which can restrict the implementation of all available features.

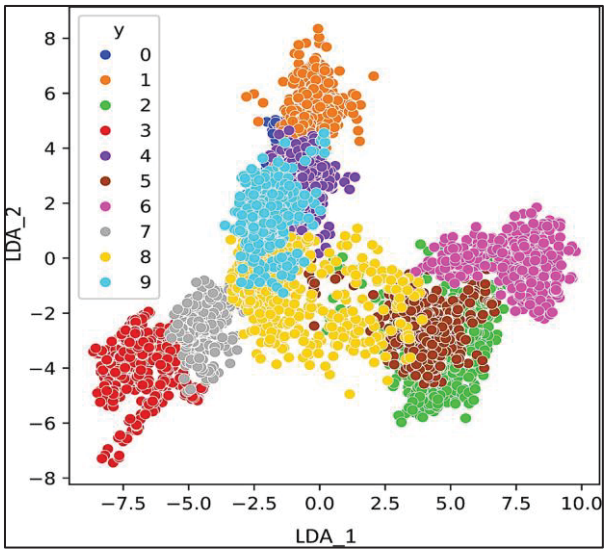

Figure 3.10 LDA representation of the ultrasonic dataset

Figure 3.11 shows the RFE method performance for our ultrasound dataset. Mostly for implementation, the RFE results can be used to deploy our desired ML models on the MCU, and the final model is used for real-time industrial monitoring.

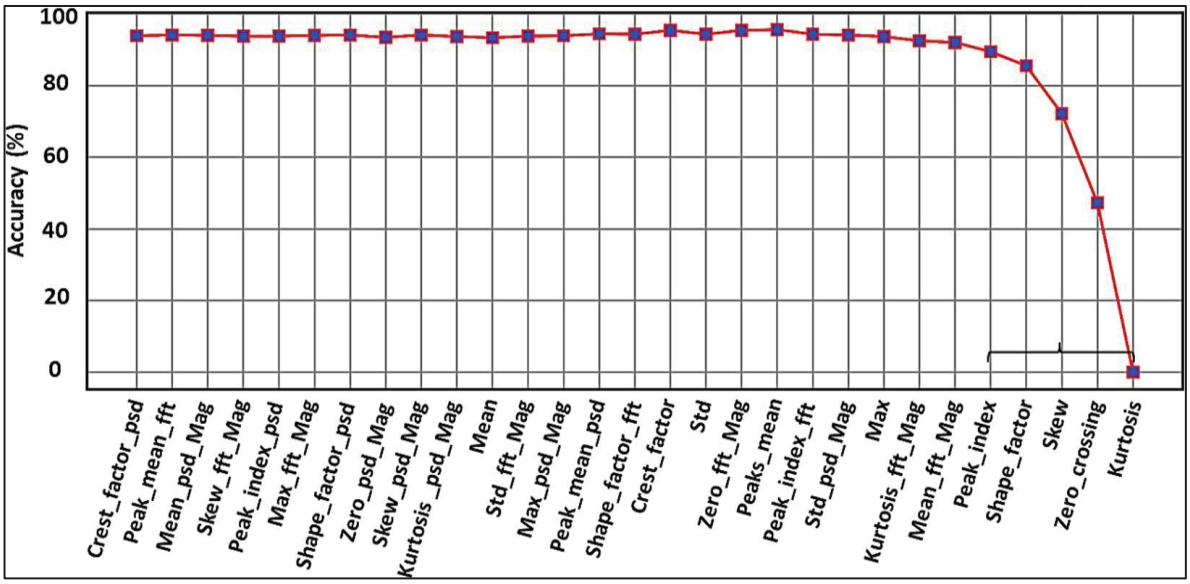

Figure 3.11 Feature selection using the RFE algorithm

In this graph, it is clear that when five features, bracketed to the right of Figure 3.11, are eliminated (i.e., kurtosis, zero crossing, skewness, shape factor, and peak index), the accuracy drops dramatically, indicating that these features play the more important role to distinguish the classes.

To validate the efficacy of the methods employed, accuracy analyses were conducted across four techniques for six classifiers. RFE distinguished itself by delivering superior accuracy in pattern classification, a claim substantiated by the results depicted in Figure 3.12.

The comparative analysis reveals that RFE achieves commendable diagnostic outcomes relative to alternative data-reduction strategies. The metric result of the six classifiers based on RFE is shown in Table 3.1.

The results in Table 3.1 show the superiority of the meta model for all the scores across the ten classes. The classification results of the selected methods, along with the utilized meta-classifier technique, are summarized using a confusion matrix, as shown in Figure 3.13. The confusion matrix provides insights into the ability of the methods to accurately classify different ultrasonic fault states. Higher values along the diagonal indicate a better model, as it correctly classifies the majority of the samples.

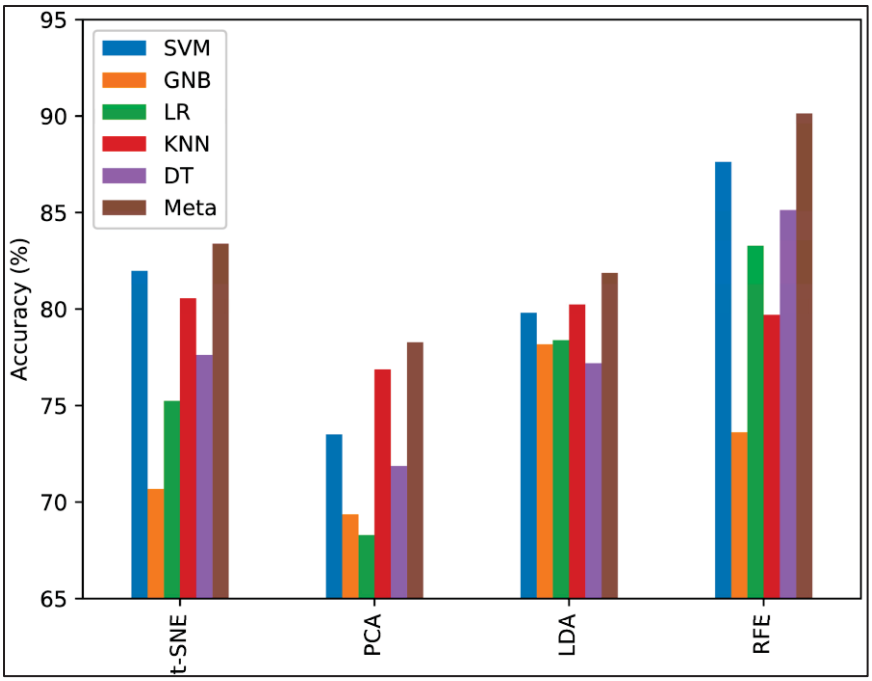

Figure 3.12 Applying multi-class classification using dimensionality reduction t-SNE, PCA, LDA, and RFE feature selection

Table 3.1 Precision, recall, F1 measure, and accuracy of fault detection that are achieved by the ML models

Classifier	Class	Precision	Recall	F1 Score	Accuracy	Classifier	Class	Precision	Recall	F1 Score	Accuracy
GNB	0	0.48	1.00	0.65	0.731	KNN	0	0.56	0.80	0.66	0.798
	1	0.57	0.45	0.50			1	0.62	0.58	0.60	
	2	0.89	0.83	0.86			2	0.86	0.84	0.85	
	3	0.97	0.93	0.95			3	0.92	0.88	0.90	
	4	0.50	0.46	0.48			4	0.68	0.71	0.69	
	5	0.82	0.92	0.87			5	0.87	0.87	0.87	
	6	1.00	0.99	1.00			6	0.98	1.00	0.99	
	7	0.88	0.95	0.91			7	0.84	0.91	0.87	
	8	0.66	0.58	0.62			8	0.82	0.70	0.75	
	9	0.91	0.22	0.35			9	0.80	0.57	0.66	
LR	0	0.58	0.95	0.72	0.817	DT	0	0.82	0.78	0.80	0.886
	1	0.76	0.63	0.69			1	0.72	0.74	0.73	
	2	0.91	0.82	0.86			2	0.93	0.91	0.92	
	3	0.92	0.90	0.91			3	0.96	0.99	0.97	
	4	0.80	0.57	0.66			4	0.79	0.85	0.82	
	5	0.85	0.93	0.89			5	0.88	0.92	0.90	
	6	0.99	1.00	0.99			6	1.00	0.99	0.99	
	7	0.76	0.95	0.84			7	0.99	0.96	0.97	

Table 3.1 Precision, recall, F1 measure, and accuracy of fault detection that are achieved by the ML models - continued

	8	0.66	0.53	0.59			8	0.89	0.85	0.87	
	9	0.84	0.66	0.74			9	0.84	0.82	0.83	
SVM	0	0.71	0.92	0.80	0.884	meta	0	0.86	0.93	0.90	0.932
	1	0.84	0.67	0.75			1	0.95	0.83	0.88	
	2	0.96	0.84	0.90			2	0.96	0.88	0.92	
	3	0.98	0.97	0.97			3	0.98	1.00	0.99	
	4	0.83	0.84	0.83			4	0.89	0.96	0.92	
	5	0.88	0.95	0.91			5	0.90	0.96	0.93	
	6	0.99	1.00	0.99			6	1.00	1.00	1.00	
	7	0.97	0.97	0.97			7	1.00	0.97	0.98	
	8	0.84	0.88	0.86			8	0.88	0.91	0.90	
	9	0.89	0.79	0.84			9	0.92	0.89	0.91	

Since the dataset used in this research includes both pipe and bearing faults, it allows us to evaluate the performance of the proposed method in handling mixed faults involving both pipes and bearings. Figure 3.14 illustrates the ROC curves of the selected models, utilizing k-fold CV.

The ROC curve serves as a measure of separability, indicating the capability of the selected models to distinguish between different fault classes. It provides a visual representation of the trade-off between the true positive rate (TPR) and false positive rate (FPR) for a predictive model across various probability thresholds. Basically, for every threshold, TPR and FPR are calculated and plotted on one chart. As can be seen, the lower FPR and the higher TPR for the given RFE thresholds demonstrate the better results. A steeper and more vertical ROC curve is desirable, as it indicates a model with better discriminative ability. The ROC curve analysis is instrumental in evaluating the performance and effectiveness of the selected models for fault classification tasks. In Figure 3.14, it can be observed that the meta model, which refers to a composite model combining predictions from multiple models, exhibits an area under the ROC curve (AUC) of 0.997 for the ultrasonic test dataset. This AUC is significantly greater than those of the other classifiers, underscoring the meta model's superior discriminative capability and predictive performance for fault classification.

Therefore, it can be concluded that the selected meta model is reliable and demonstrates strong usability in the context of ultrasonic fault detection. Its high area under the ROC curve suggests that it can effectively distinguish between different fault classes and make accurate predictions.

Furthermore, in this research on ultrasonic fault evaluation, stratified k-fold CV is utilized as a method for rotation estimation to assess the generalizability of the statistical analysis to an independent ultrasonic dataset. Our simulations provide a quantitative analysis of the classification performance across five folds and the selected ML models, as presented in Table 3.2. The average test accuracy obtained through rotation estimation for the meta-classifier is 93%. This average accuracy of the meta model surpasses that of the other models under consideration. To better provide analysis of our simulation results over the selected models through the k-fold CV method, the accuracy of each model is visualized in Figure 3.15. For more comparison, the variations in the results during the CV step for different folds are presented through a boxplot in Figure 3.16.

The distribution of the data allows for effective comparisons of accuracy across different folds within the ultrasonic dataset. The boxplot offers a graphical depiction of the five-number summary of the dataset, encompassing the minimum value, first quartile (25th percentile), median (50th percentile), third quartile (75th percentile), and maximum value. The 'box' visualizes the interquartile range (IQR), the span between the first and third quartiles, while the 'whiskers' extend to the furthest data points not considered outliers, which are plotted individually. This boxplot succinctly captures the distribution, central tendency, variability, and outliers of the ultrasonic data. It is evident from the analysis that the meta-classifier demonstrates the highest consistency in accuracy and the least variability compared to other models.

Accurately labeled data is crucial for the effectiveness of supervised learning algorithm in industrial fault diagnosis. Insufficient labeled data complicates model training and can lead to decreased accuracy. Additionally, the complexity of ultrasonic data, signal acquisition delays, and sample imbalances among faults present significant challenges in supervised diagnosis. Certain classifiers, like GNB, presuppose feature independence, which complicates the management of highly correlated data and hinders the attainment of optimal performance. Moreover, a limited dataset and uneven distribution of ultrasonic features may result in substantial predictive errors.

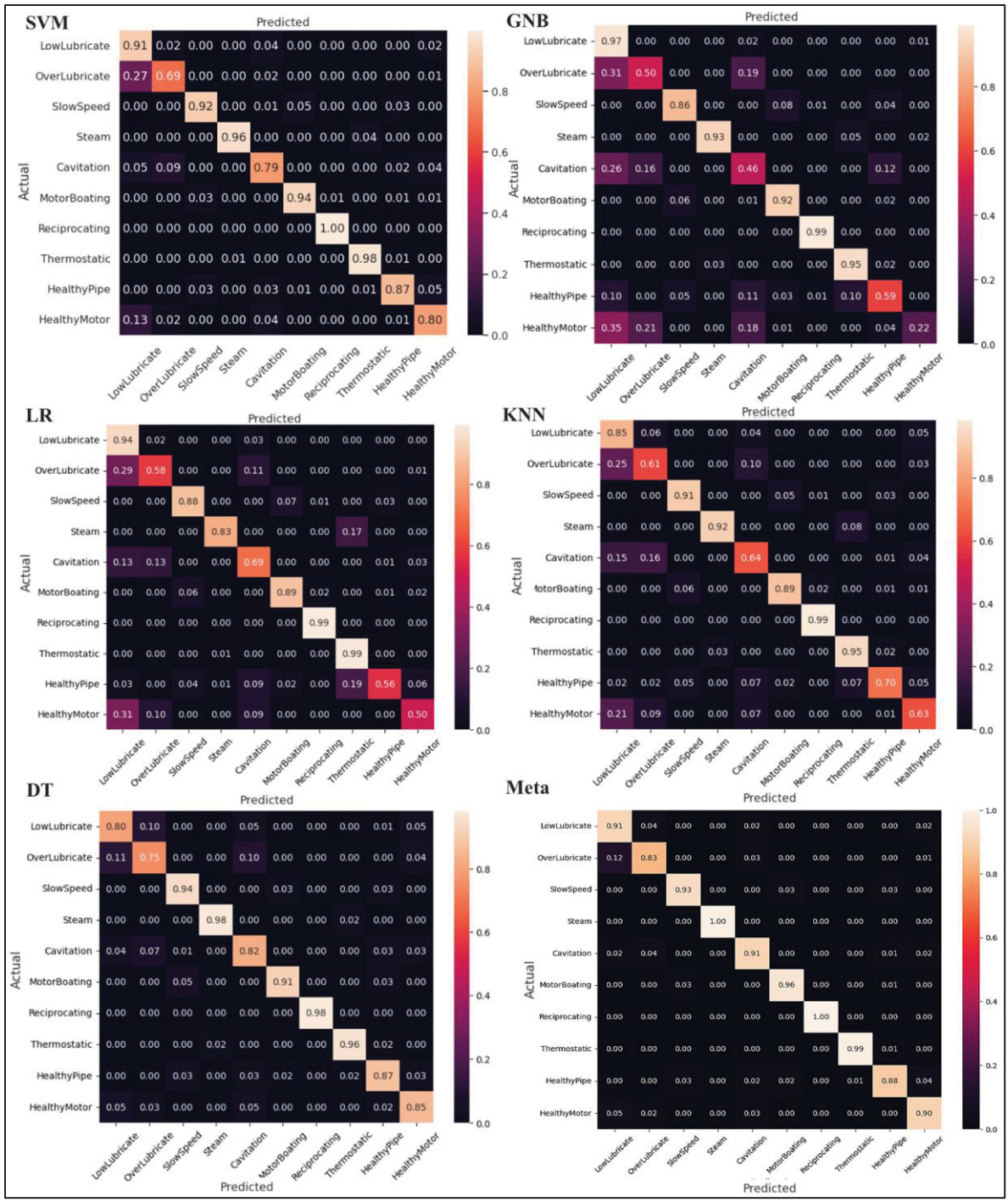

Figure 3.13 The confusion matrix based on the achieved results by the SVM, GNB, LR, KNN, DT, and meta-classifier models

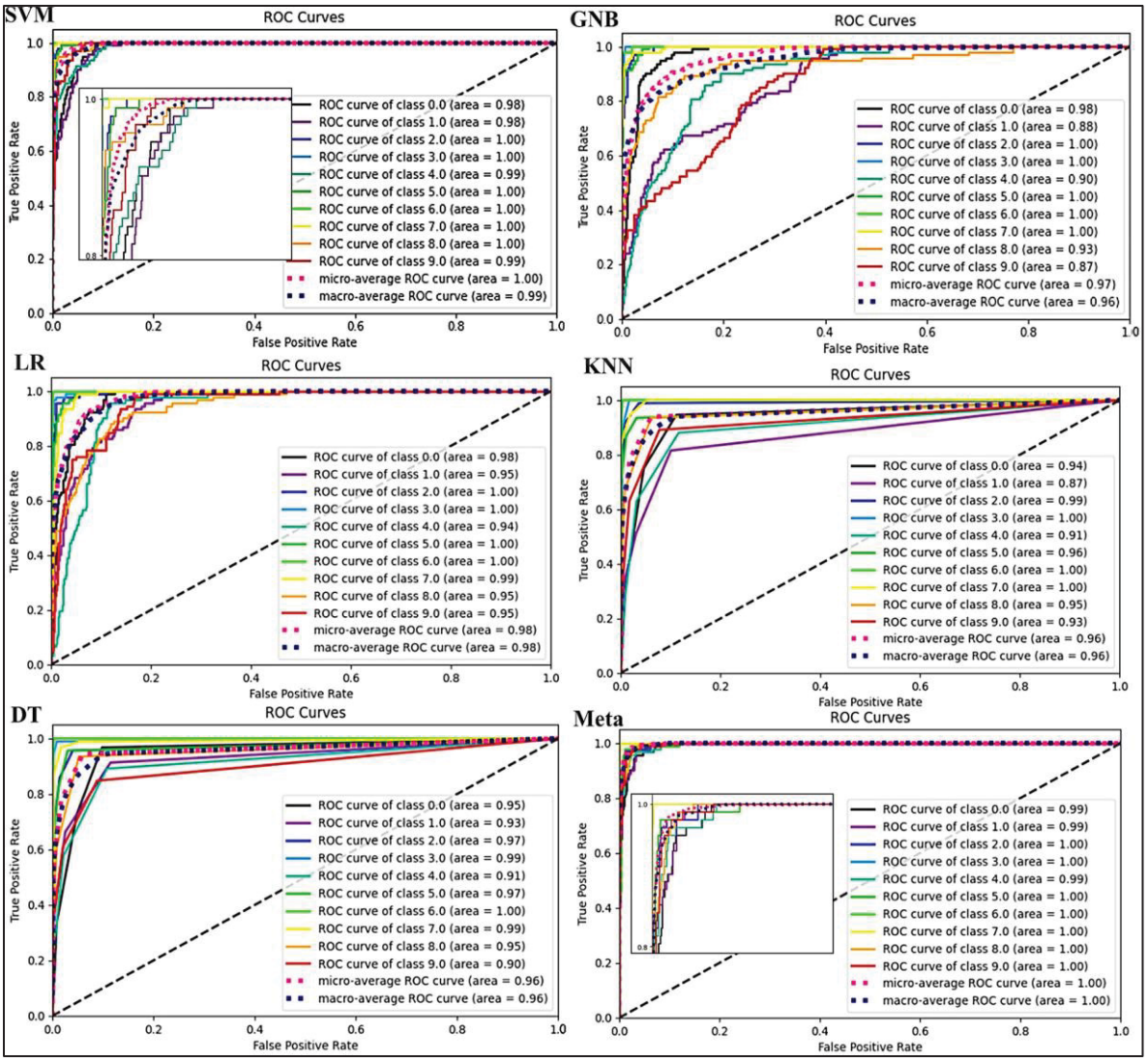

Figure 3.14 ROC curves for six classifiers

Table 3.2 Performance of SVM, GNB, LR, KNN, and meta-classifier models through 5-fold CV

k-folds	SVM	GNB	LR	KNN	DT	Meta
Fold_1	0.87717	0.71304	0.81195	0.80652	0.87826	0.92514
Fold_2	0.89347	0.74130	0.85652	0.79021	0.89021	0.93369
Fold_3	0.90217	0.73695	0.85869	0.81739	0.87173	0.93913
Fold_4	0.87934	0.73152	0.83587	0.78478	0.87608	0.92558
Fold_5	0.88587	0.74782	0.83369	0.81413	0.91630	0.93587
Average	0.88760	0.73413	0.83934	0.80260	0.88652	0.93173

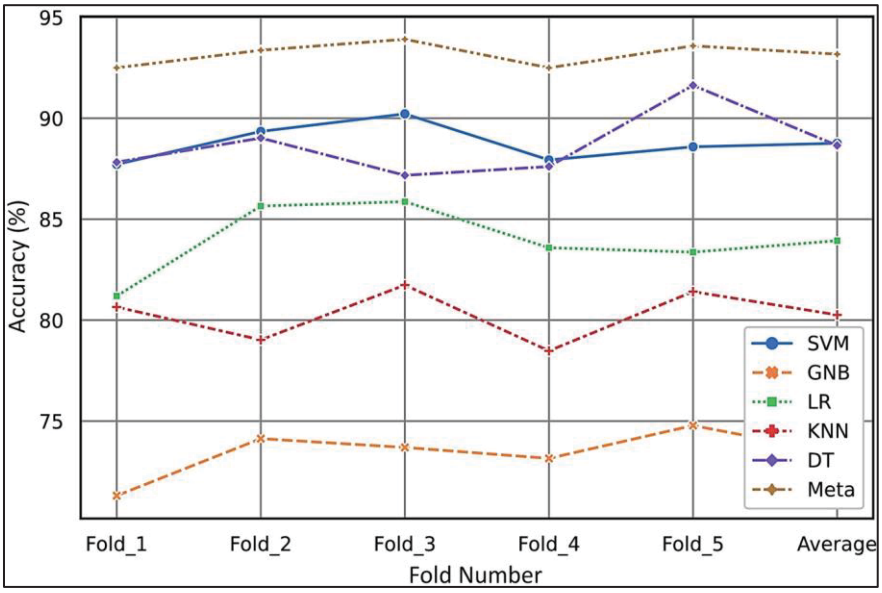

Figure 3.15 Accuracy of the six classifier models using the k-fold CV strategy

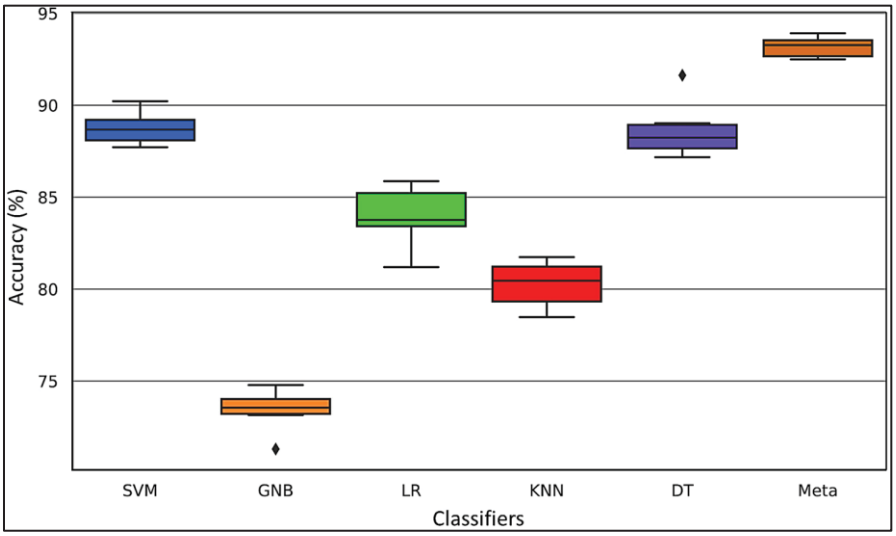

Figure 3.16 Boxplot for the six classifier models

Figure 3.17 highlights the issues arising from limited sample sizes, illustrating how insufficient data can diminish the predictive accuracy of classification models. This underscores the importance of larger and more balanced datasets for enhancing the efficacy of fault diagnosis models.

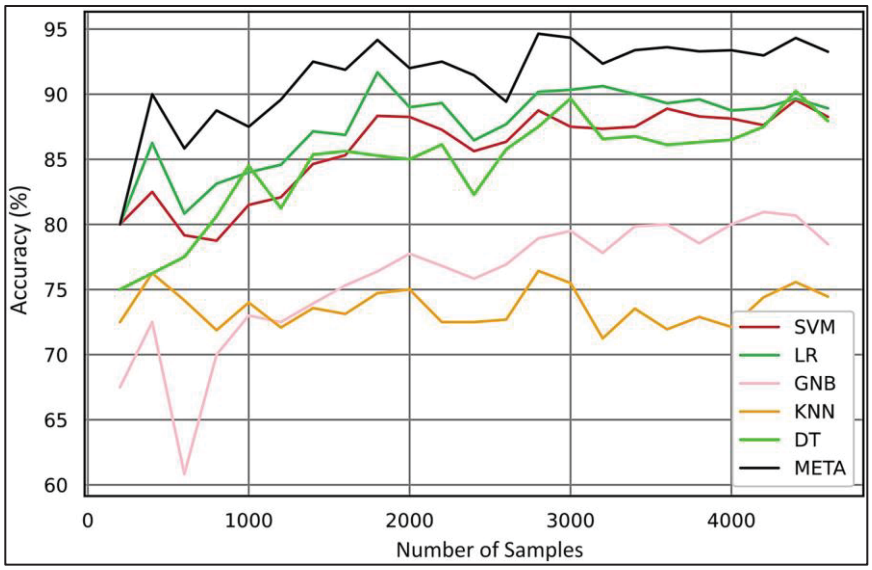

Figure 3.17 Accuracy curve vs. the number of samples (learning curve)

Figure 3.17 clearly demonstrates that the meta model can predict with high accuracy even with a limited number of samples, approximately 300. With an increase in the number of samples, the meta model consistently outperforms the other models in accuracy.

In the final step, the micromlgen library in Python is used to extract the model and deploy it onto an nRF52840 64 MHz ARM Cortex-M4F MCU.

The five optimal features, specifically kurtosis, zero crossing, skewness, shape factor, and peak index (as identified in Figure 3.11), are computed on the MCU to serve as inputs for five classifiers: GNB, LR, KNN, SVM, and DT. The outputs from these classifiers are then fed into the meta-model, which executes in a total of 11 (ms) on this MCU—this includes 6.5 (ms) for data sampling, 183 µs for feature calculation, and 4.3 (ms) for the meta model prediction. These timings were verified using a logic analyzer, as depicted in Figure 3.18, confirming that our proposed model is highly suitable for real-time condition monitoring with relatively low computational requirements.

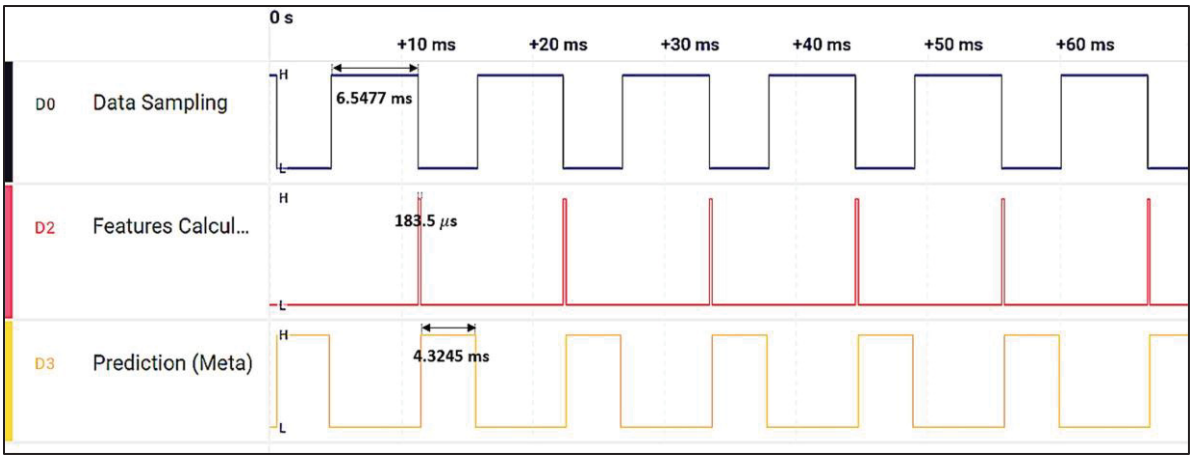

Figure 3.18 Execution timing analysis of the meta model implemented on the MCU

3.4. Conclusions

This work has introduced a precise ultrasonic industrial fault detection meta-classifier model designed for general-purpose applications, such as bearings and pipelines, utilizing contact sensors. This model is capable of determining and monitoring the health condition of industrial machinery. To assess the model's performance, a k-fold CV strategy was employed to detect and classify ten different conditions within the ultrasonic signals. The reduction methods of RFE, PCA, t-SNE, and LDA were calculated, and RFE was chosen as the input for six classification models (namely SVM, GNB, LR, KNN, DT, and the meta classifier) to discern between ten distinct classes of irregular conditions. Each model's performance was evaluated based on various metrics. The proposed meta classifier model demonstrated superiority with impressive results across multiple metrics, including ROC curves (i.e., achieving an AUC of 0.997), confusion matrices, k-fold validation (with 93% accuracy), and learning curves. Additionally, the model boasted a rapid execution time of just 11 ms on a 64 MHz Cortex-M4F MCU, confirming its suitability for real-time industrial fault monitoring applications. In future work, we aim to extend the model's deployment capabilities to a wider range of MCUs to ensure broader applicability. We plan to incorporate IoT functionalities, enabling sophisticated remote data access and control mechanisms. Efforts will also be directed towards optimizing both power consumption and memory utilization, ensuring the model's operation is both efficient and sustainable. Additionally, we will focus on the development of an

optimized PCB design, specifically engineered to enhance the reliability and performance of the monitoring system within diverse industrial environments. These targeted improvements are intended to elevate the model's practicality, adaptability, and efficiency in real-world applications.

Author Contributions: Software, A.M.; resources, H.H.T. and M.Y.E.; writing—original draft preparation, A.M.; writing—review and editing, F.N.; supervision, F.N.; funding acquisition, H.H.T. and M.Y.E. All authors have read and agreed to the published version of the manuscript.

Funding: Collaborative Research and Development Grant number CRDPJ 543712-19 from the Natural Sciences and Engineering Research Council of Canada (NSERC) with MEMS-Vision as grant industrial partner.

Institutional Review Board Statement: Not applicable.

Informed Consent Statement: Not applicable.

Data Availability Statement: Data are contained within the article.

Conflicts of Interest: Authors Hani H. Tawfik and Mohannad Y. Elsayed were employed by the MEMS-VISION company. The remaining authors declare that the research was conducted in the absence of any commercial or financial relationships that could be construed as a potential conflict of interest.

CHAPTER 4

ADVANCED INDUSTRIAL FAULT DETECTION: A COMPARATIVE ANALYSIS OF ULTRASONIC SIGNAL PROCESSING AND ENSEMBLE MACHINE LEARNING TECHNIQUES

Amirhossein Moshrefi, and Frederic Nabki

Department of Electrical Engineering, Ecole de Technologie Supérieure, ETS, Montreal, QC H3C 1K3, Canada

Paper published in: Applied Science, MDPI, July 2024.

Abstract: Modern condition monitoring and industrial fault prediction have advanced to include intelligent techniques, aiming to improve reliability, productivity, and safety. The integration of ultrasonic signal processing with various machine learning (ML) models can significantly enhance the efficiency of industrial fault diagnosis. In this paper, ultrasonic data are analyzed and applied to ensemble ML algorithms. Four methods for reducing dimensionality are employed to illustrate differences among acoustic faults. Different features in the time domain are extracted, and predictive ensemble models including a gradient boosting classifier (GB), stacking classifier (Stacking), voting classifier (Voting), Adaboost, Logit boost (Logit), and bagging classifier (Bagging) are implemented. To assess the model's performance on new data during experiments, k-fold cross-validation (CV) was employed. Based on the designed workflow, GB demonstrated the highest performance, with less variation over 5 cross-folds. Finally, the real-time capability of the model was evaluated by deployment on an ARM Cortex-M4F microcontroller (MCU).

Keywords: classification; ensemble learning; signal processing; industrial fault diagnosis; ultrasonic sensor; feature extraction; boosting.

4.1 Introduction

The current manufacturing and industrial landscapes have witnessed significant growth, fostering the pervasive adoption of automated processes and a heightened need for sophisticated equipment and machinery. With the rise of industrial automation, motors and

pipelines spare parts have become integral to machine maintenance. Condition monitoring for fault detection is essential for the safety of the environment, energy conservation, and human health (Soomro, A. A., (2022); Yang, J., (2020)). The interdependence of motors and pipelines in industrial settings is crucial for overall system efficiency and safety. In industries like chemical processing, motors drive pumps that circulate fluids through pipelines. A fault in either component can disrupt the process, affecting efficiency and safety. Identifying faults in both motors and pipelines allows for a comprehensive approach to predictive maintenance, preventing downtime, optimizing maintenance schedules, and enhancing reliability. Failures in motors and pipelines are often interconnected; for example, a pipeline blockage can increase the motor load, leading to overheating and failure. Conversely, motor failure can cause pressure build-up in pipelines. This interdependence is critical in sectors like oil and gas, where component failure can lead to significant production losses and environmental hazards. Compliance with safety standards requires monitoring all critical components, as seen in the pharmaceutical industry, where motor and pipeline integrity is vital for product quality. Examples from the food and beverage industry show that faults in these components can cause contamination and safety hazards, highlighting the need for integrated fault detection systems (Datta, S., & Sarkar, S. (2016); Becker, V., et. al. (2021)). This study explores prevalent issues in industrial pipes and motors, focusing on using ultrasonic methods to detect and assess problems like leaks, blockages, and flaws in underground pipes. Pipes are vital for fluid transport over various distances. The vast networks of pipelines stretching for kilometers consist of pipe sections connected by joints. External pressures such as traffic and surface loads can stress these pipes and joints, possibly causing leaks and bursts.

The increase in pipeline defects such as cracks, cavitation, corrosion, and various mechanical damages is a major concern for the safety and functionality of pipeline systems. These defects can compromise the integrity of pipelines, leading to potential hazards and disruptions to operations (Al-Sabaeei, A. M., et. al. (2023); Yu, Y., et. al. (2021)). Mechanical components, particularly in rotor-bearing systems, are prone to wear and failure, often due to bearing faults. These faults can lead to significant machinery downtime and require maintenance or replacement to ensure continued operation (Salunkhe, V. G., et. al. (2023)). Indeed, diagnosing faults in industrial systems is a crucial aspect of condition-based maintenance. Maintenance

engineers focus on this to prevent severe breakdowns, ensuring the systems' safety and reliability. Timely identification and re- pair of such faults can avert disastrous failures and maintain operational continuity (Zhang, M., et. al. (2022); Sharma, A. (2022)). In addition, ultrasonic fault detection offers high sensitivity for early issue identification, versatility in various applications, and non-destructive testing capabilities (Moshrefi, A., 2023)).

Various studies are conducted for the detection of industrial faults. Acoustic analysis and temperature sensing are long-standing technologies used in monitoring industrial equipment for faults. By effectively preventing equipment failures, these technologies can greatly lower maintenance expenses and reduce periods of inactivity, enhancing overall operational efficiency (Shinde, P. V., & Desavale, R. G. (2022)).

The research by Carrera-Avendaño, E., et. al. (2022) combined the dyadic Wavelet transform with the Welch–Bartlett periodogram for effective feature extraction from noisy signals. Lin, H. C., & Ye, Y. C. (2019) used FFT techniques to analyze vibration signals in unbalanced rolling bearings, revealing characteristic fault frequencies. Vishwendra, M. A., et. al. (2022) applied a K-nearest neighbor (KNN) method to detect rolling element bearing faults using kurtosis and envelope spectrum analysis. Patil, S. M., et. al. (2022) used dimensional analysis and a central composite rotatable design to identify faults in nonlinear rotating systems, focusing on the influence of bearing clearance and external defects on vibration characteristics. A comprehensive study on leak detection and localization in oil and gas pipelines was presented in Yuan, J., et. al. (2023), reviewing various methods, their benefits, limitations, and effectiveness. The authors reviewed different methods, evaluating their advantages, drawbacks, and effectiveness in detecting and pinpointing leaks within pipeline systems. Korlapati, N. V. S., et. al. (2022) evaluated multiple leak detection methods, discussing their strengths, weaknesses, and areas for future improvement. Rai, A., & Kim, J. M. (2021) tackled the issue of the limited historical pipeline failure data in AI methods by introducing a health index approach integrating the Kolmogorov–Smirnov test, multiscale analysis, and a Gaussian mixture model (GMM). In another experiment, Wang, H., et. al. (2022) classified defects in pipeline welds using the total focusing method (TFM) based on ultrasonic phased arrays, improving defect detection and characterization. They applied the HOG–Poly–SVM algorithm with ten-fold cross- validation for defect classification. In (Moshrefi, A., et. al. (2024)), we

presented a method for detecting industrial faults using ultrasonic signals by stacking an ensemble of classifiers.

Raišutis, R., T. et. al. (2023) presented a technique using ultrasonic guided waves (UGW) with helical wave modes to detect corrosion-type defects in steel pipes. They demonstrated that phase delay differences in wave signal peaks can effectively identify defects with minimal transducers and measurements. Norli, P., et. al. (2018) presented an experimental study on detecting stress corrosion cracks (SCC) in gas pipelines using guided waves and broadband ultrasound. The study successfully demonstrated the feasibility of an ART-scan-based setup for detecting SCC in a submerged pipe section, showing significant signal differences for cracks with depths of around 35% of the pipe wall thickness. Wei, M., et.al. (2024) introduced a method combining a fractional Fourier transform (FRFT) and variational modal decomposition (VMD) to detect pipeline defects using ultrasonic signals. The method significantly improved feature extraction and classification accuracy, achieving 89.1% for experimental signals. Yu, Y., et. al. (2021) presented the application of acoustic and ultrasonic methods to detect leaks, blockages, and defects in buried water and sewerage pipes. They reviewed various sensors, including accelerometers, hydrophones, and fiber optics, and explored the potential of autonomous robotics for deploying these sensors. The paper also highlighted data-driven techniques and machine learning for enhancing the accuracy and efficiency of pipe condition assessments. Cai, L., et. al. (2024) presented a method to carry out pipeline declination inspections using amplitude reduction analysis of ultrasonic echo signals. This method enhanced the detection accuracy, identifying declinations with a maximum error of 0.137° within a 2° range. However, these works faced limitations related to environmental influences, computational time, and accuracy. These limitations highlight the ongoing need for advancements in ultrasonic inspection techniques to enhance their reliability and practical applicability in diverse and real-world conditions. This work improves upon the limitations of previous studies by offering a higher accuracy, better computational efficiency, and practical real-time deployment in ultrasonic fault detection for industrial applications. This research covers ten unique fault types in both pipelines and rotating machinery. We compare dimensionality reduction techniques and ensemble classifiers to find the best model for real-time fault detection on an MCU. To address the challenge of high-dimensional data, statistical

features are extracted. Subsequently, several well-established classification models including voting, logit, GB, Adaboost, stacking, and bagging are implemented. For further investigation, dimensionality reduction techniques like principal component analysis (PCA), linear discriminant analysis (LDA), independent component analysis (ICA), and uniform manifold approximation and projection (UMAP) are analyzed. These techniques can simplify complex datasets by reducing the number of variables under consideration, while still preserving the essential structures within the data. Finally, two different approaches for MCU implementation are investigated. While previous studies have explored ultrasonic fault detection, few have integrated real-time processing on resource-constrained devices like the ARM Cortex-M4F MCU used here. The remainder of the paper is structured as follows: Section 2 provides a description of the ultrasonic fault diagnosis methodology, and details the preprocessing, feature extraction, and used methods. Sections 3 and 4 present the experimental results and the conclusions, respectively.

4.2 Ultrasonic Fault Detection Methodology

This section describes the methodologies and tools used to achieve the study's objectives. Figure 5.1 provides an overview of the proposed methodology, which consists of seven main steps. Our process starts with gathering raw ultrasonic data using a microphone array module for classification analysis. Following refinement through preprocessing steps like filtering and scaling, we then extract features to generate a concise and informative feature vector. This research uses various time-domain and static-domain features based on the mean, variance, zero crossing, envelope, crest factor, shape factor, maximum number of peaks, time of peak, skewness, and kurtosis extracted from the refined ultrasonic profile. The details of these features are illustrated in Table 4.1. To address the issue of high dimensionality in raw data, which can hinder predictive modeling for ML models, dimensionality reduction techniques are applied. Finally, an ML classification algorithm is used to categorize the data. The train–test split procedure with k-fold CV is used to evaluate the performance of ensemble learning algorithms by assessing their predictions on unseen data during model training. Finally, the model can be deployed on an MCU. High dimensionality can refer to datasets with a large number of features and classes, where numerous characteristics are derived from each signal.

By increasing the number of features, the dimensionality can increase, and the complexity of the model also increases, which may lead to longer training times and higher computational resource requirements. Furthermore, with higher dimensions, models can become more prone to overfitting, especially if the number of samples is relatively small compared to the number of features. Proper dimensionality strikes a balance between retaining sufficient information for accurate predictions and reducing complexity to enhance learning efficiency. Techniques like PCA, LDA, ICA, and UMAP are employed to achieve this balance, to effectively capture the essential structure of the ultrasonic signals while reducing dimensionality.

Table 4.1 Feature definitions and their details

Features	**Details**	**Definition**
Mean	Mean	Average of the data
	Median	The middle value of the signal
	RMS (Root Mean Square)	The square root of the mean of the squares of the signal values
Variance	Standard Deviation	The square root of the variance
	Range	The difference between the maximum and minimum values of the signal
	Interquartile Range (IQR)	The difference between the 75th and 25th percentiles of the signal
Zero Crossing	Number of Peaks	The total count of peaks in the signal
	Number of Valleys	The total count of valleys in the signal
	Peak-to-Peak Distance	The average distance between consecutive peaks
Envelope	Envelope Mean	The mean value of the signal envelope
	Envelope Variance	The variance of the signal envelope
	Envelope Energy	The sum of the squared values of the signal envelope
Crest Factor	Form Factor	The ratio of the RMS value to the mean absolute value
	Peak-to-RMS Ratio	The ratio of the maximum value to the RMS value of the signal
	Margin Factor	The ratio of the maximum value to the RMS value
	Normalized Energy	The energy normalized by the length of the signal

Table 4.1 Feature definitions and their details - continued

Shape Factor	Energy Entropy	The logarithm of the energy of the signal
	Impulse Factor	The ratio of the maximum value to the mean of the absolute values of the signal
Number of Peaks	Number of Positive Peaks	The count of positive peaks in the signal
	Number of Negative Peaks	The count of negative peaks in the signal
	Peak Amplitude	The amplitude of the highest peak in the signal
Time of Peak	Time of First Peak	The time at which the first peak occurs
	Time of Last Peak	The time at which the last peak occurs
	Time of Median	The time index of the median value
Skewness	Absolute Skewness	Skewness calculated on the absolute values of the signal
	Skewness of Positive Values	Skewness calculated only for the positive values of the signal
	Skewness of Negative Values	Skewness calculated only for the negative values of the signal
Kurtosis	Absolute Kurtosis	Kurtosis calculated on the absolute values of the signal
	Kurtosis of Positive Values	Kurtosis calculated only for the positive values of the signal
	Kurtosis of Negative Values	Kurtosis calculated only for the negative values of the signal

Ensemble learning is an ML approach aimed at improving predictive performance by aggregating predictions from multiple base models. Ensemble classifiers may be more advantageous than deep learning models in situations where factors such as interpretability, limited data, computational resources, model complexity, robustness to overfitting, result reliability, lower memory occupation, and domain expertise are crucial considerations (Yadavendra, S. (2020); Dong, X., (2020)). These fields of study have led to numerous specialized techniques including bagging, stacking, and boosting approaches.

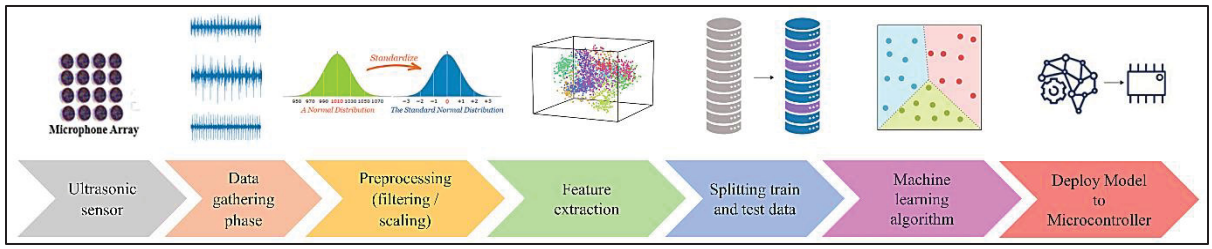

Figure 4.1 Study workflow diagram for ultrasonic fault diagnosis

4.2.1 Boosting Technique

A boosting classifier is an ensemble technique that improves model accuracy by combining multiple learners. It sequentially trains each learner to correct the errors of the previous ones (Tanha, J., et. al. (2020)). The algorithm starts by initializing a model, then iteratively computes residuals, fits new weak learners, determines optimal step sizes, and updates the model. After all iterations, the final boosted model is produced, yielding a high accuracy and robustness against overfitting. Boosting is robust to overfitting and versatile for various applications (Ju, X., & Salibián-Barrera, M. (2021)). Adaboost, GB, and Logit are investigated in this paper. Adaboost emphasizes misclassified instances by adjusting their weights. GB uses gradient descent to minimize a chosen loss function, focusing on residuals. Logit targets logistic regression, minimizing logistic loss for improved classification. The algorithm is summarized in Figure 4.2.

Inputs:

Number of observations: n

Set of m features: $F = \{f_1, \ldots, f_m\}$

Outputs:

Predicted faults: c

Code:

Initialize $G_0 x = \arg\min_{\rho} \sum_{j=1}^{N} L(y_i, \rho)$

Repeat for k in 1 to n:

{

Compute residuals $\tilde{y}_i = -[\frac{\partial L(y_i, G(x_i))}{\partial G(x_i)}]_{G(x)=G_{k-1}(x)}$, i=1,…,N

Fir a_m model $a_k = \arg\min_{\alpha,\beta} \sum_{i=1}^{N} [\tilde{y} - \beta h(x; \alpha_{k-1})]^2$

Choose a gradient step size $\rho_k = \arg\min_{\rho} \sum_{i=1}^{N} L(y_i, F_{k-1}(x_i) + \rho h(x_i; \alpha_k)])$

$G_k(x) = G_{k-1}(x) + \rho_k h(x; a_k)$

Output final regression model G_k

}

Figure 4.2 Boosting algorithm

Where n is the number of observations, m is the number of features, F is the set of m features, c is the predicted faults, y_i is the actual value for observation i, ρ is the parameter for initialization, G0(·) is the initial model which minimizes the loss function over all observations, L(·) is the loss function which measures the error between the actual value y_i and the predicted value G(·), $\tilde{y}_i(\cdot)$ the residuals computed for each observation i at step k, h(·) is the fitted model, α_k is the model parameter at step k, ρ_k is the gradient step size at step k, and $G_k(\cdot)$ is the regression model at step k.

4.2.2 Bagging Technique

A bagging (bootstrap aggregating) classifier is an ensemble learning technique de- signed to improve the accuracy and robustness of machine learning models by reducing variance and preventing overfitting. The process involves creating multiple versions of a predictor by training each on a random subset of the data, then combining their predictions to form a final

output. The bagging method addresses the bias and variance trade-off and mitigates the variance of the final prediction model, thereby reducing the risk of overfitting, particularly in the context of ultrasonic data (González, S., et. al. (2020)). The algorithm is summarized in Figure 5.3.

Inputs:
Number of observations: n
Set of m features: $\boldsymbol{F} = \{f_1. \ldots, f_m\}$

Outputs:
Predicted faults: c

Code:
Repeat for k in 1 *to* n:
{
Choose a random sample from the training dataset without repetition.
Randomly select a subset of m features to build a model.
Use the feature with the best split to divide the nodes.
Grow the tree to establish the most effective root nodes.
Combine individual classifiers' outputs for the most accurate prediction.
}

Figure 4.3 Boosting algorithm

4.2.3 Stacking Technique

A stacking classifier is an ensemble learning technique that improves predictive performance by combining multiple base models and a meta-model. Base classifiers are trained on the same dataset and their predictions are used to train a meta-classifier. This meta-classifier learns to optimally combine the base classifiers' outputs. Stacking leverages model diversity, improving the accuracy and robustness (Mohapatra, S., Maneesha, S., & Patra, P. K. (2023)). The algorithm is summarized in Figure 4.4.

Inputs:

Number of observations: n

Set of m features: $F = \{f_1, \ldots, f_m\}$

Data: $D = \{(x_i, y_i)\}_{i=1}^{n}$

Outputs:

Predicted faults: c

Ensemble classifier: H

Code:

{

Step 1: Learn base level classifiers:

for t: in 1 to T:

Learn h_t classifier based on F

Step 2: Construct new set of classifiers

Based on soft or hard outputs of h_t design a meta classifier

Step 3: Learn a meta-classifier based on new data $D' = \{(x_i', y_i')\}_{i=1}^{n}$

}

Figure 4.4 Stacking algorithm

Where D is the dataset, and T is the number of base level classifiers.

4.2.4 Evaluating Estimator Performance Using k-Fold Cross-Validation

The effectiveness of the algorithm is evaluated using k-fold cross-validation (k-fold CV), also known as rotation estimation, to verify the generalizability of the results in industrial fault detection analysis (Nti, I. K., Nyarko-Boateng, O., & Aning, J. (2021)). This method is used to assess a model's performance by splitting data into k subsets. It trains the model on k-1 subset and validates it on the remaining subsets, repeating this k times to ensure a thorough evaluation. The steps for k-fold CV are outlined in Figure 4.5.

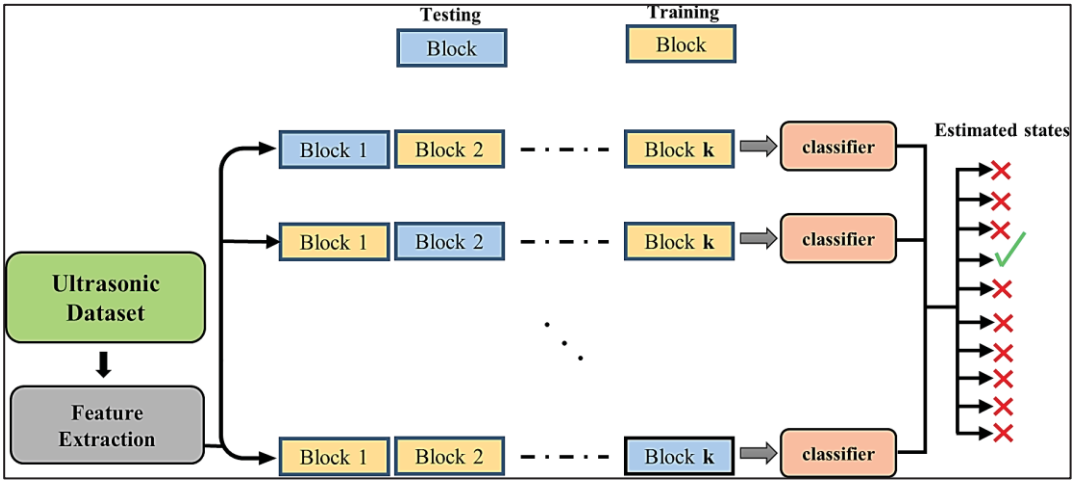

Figure 4.5 k-fold CV algorithm structure to evaluate the ultrasonic diagnosis

To determine the optimal value of k, it is important to note that reducing the value of k decreases the size of the training dataset and increases the size of the test dataset (e.g., k = 3 results in a 66% training dataset). This reduction can hinder the model's ability to learn effectively. Conversely, increasing the value of k decreases the sizes of the test sets (e.g., k = 10 results in a 10% test dataset), potentially increasing the variance of the accuracy (Marcot, B. G., & Hanea, A. M. (2021); Yadav, S., & Shukla, S. (2016)). In this study, the optimized split is considered as k = 5 for k-fold CV.

4.2.5 Ultrasonic Dimensionality Reduction and Visualization Techniques

Dimensionality reduction in ML is a technique used to reduce the number of input features or variables in a dataset. This process simplifies the dataset by transforming it into a lower-dimensional space, while preserving as much of the important information as possible. The main reasons for using dimensionality reduction includes improving model performance, reducing overfitting, and enhancing data visualization (Jia, W., Sun, M., Lian, J., & Hou, S. (2022); Toma, R. N., & Kim, J. M. (2022)). Methods include the following:

- Principal component analysis (PCA) reduces the dimensionality of a dataset by transforming it into a set of orthogonal components. These components capture the most variance from the original data (Kurita, T. (2019)).
- Independent component analysis (ICA) separates a multivariate signal into independent non-Gaussian components, assuming statistical independence. ICA excels in

identifying independent sources and handling non-Gaussian data, making it useful for noise reduction, feature extraction, and source separation (McConn, J. L., et. al. (2021)).

- Uniform manifold approximation and projection (UMAP) preserves the local and global data structure by optimizing a low-dimensional graph to reflect the high-dimensional graph. It is computationally efficient and scalable, suitable for large datasets (McInnes, L., Healy, J., & Melville, J. (2018)).
- Linear discriminant analysis (LDA): This is a statistical method used in supervised classification problems. LDA aims to find a linear combination of features that best separates industrial faults. It projects high-dimensional acoustic data onto a lower-dimensional space by maximizing the distance between the means of different classes and minimizing the variance within each class (Tharwat, A., et. al. (2017)).

By applying these algorithms, we can gain insights into the patterns and relationships within the ultrasonic signals, which can be crucial for identifying anomalies or understanding the underlying physical phenomena.

4.2.6 Evaluation Metrics

In order to measure the performance of the proposed framework in fault detection, we employ typical quality metrics of precision, recall, F-measure, and accuracy as follows (Sravani, S., & Karthikeyan, P. R. (2023)):

$$\text{Precision} = \frac{TP}{TP + FP} \tag{4.1}$$

$$\text{Recall} = \frac{TP}{TP + FN} \tag{4.2}$$

$$\text{F1\_Measure} = 2.\frac{Preciosion * Recall}{Preciosion + Recall} \tag{4.3}$$

$$\text{Accuracy} = \frac{TP+TN}{TP+TN+FP+FN} \tag{4.4}$$

where TP, FN, TN, and FP are true-positive, false-negative, true-negative, and false-positive respectively. Receiver operating characteristics (ROC) plots are visually appealing and provide an overview of a classifier's performance across a wide range of specificities. For further investigation in this research, the classifiers are also evaluated with ROC plots.

4.3 Results

As discussed in the introduction, bearing and pipe faults in industrial mechanisms are often caused by a variety of factors.

The dataset used in this study was obtained from UE Systems Co. (2020) with 10 categories: 4 bearing conditions and 6 pipeline conditions. The dataset of 20,000 samples was split into 80% for training and 20% for testing, enhanced by applying a sliding window with data augmentation including rotating, flipping, and adding noise to the original data. Ultrasonic signals, like many types of real-world data, often exist in high-dimensional spaces and can benefit greatly from dimensionality reduction. This process simplifies the data without losing significant information, making it more manageable and useful for analysis and processing. Dimensionality reduction and feature visualization are crucial for interpreting high-dimensional data. Techniques such as PCA, LDA, ICA, and UMAP offer valuable insights into the data structure by projecting it into two dimensions. PCA captures the most variance by identifying principal components in unlabeled data, making it useful for general data analysis. LDA is tailored for supervised classification, maximizing class separability. ICA excels in identifying statistically independent components, uncovering hidden patterns. UMAP preserves both the local and global data structures, making it effective for visualizing clusters or groups. Figure 4.6 shows the 2D visualizations of the ultrasonic data using PCA, LDA, ICA, and UMAP, highlighting the distinctions revealed by each method.

The outcomes were evaluated using several algorithms including voting, Logit, GB, AdaBoost, stacking, and bagging. To optimize the hyperparameters of the different classifiers, we employed a systematic method (i.e., grid search). This method involved an exhaustive search over specified parameter values to identify the best combination that enhances the model's performance. Among the hyperparameters, the "number of estimators" proved to be the most sensitive. Increasing this number generally improve accuracy but also increases the training

time. Based on our experiments, we found that using an estimator count of 100 provided a good balance between achieving high accuracy and maintaining a reasonable computation time. In addition, for Logit, regularization strength and the optimization function were selected as 0.9 and ‘lbfgs’, respectively. For voting, the ’hard’ function was used. For GB, the learning rate and depth of regression estimators were selected as 0.1, and 3, respectively. For bagging, the maximum number of samples was selected as 1000. For Adaboost, the learning rate was selected as 1.

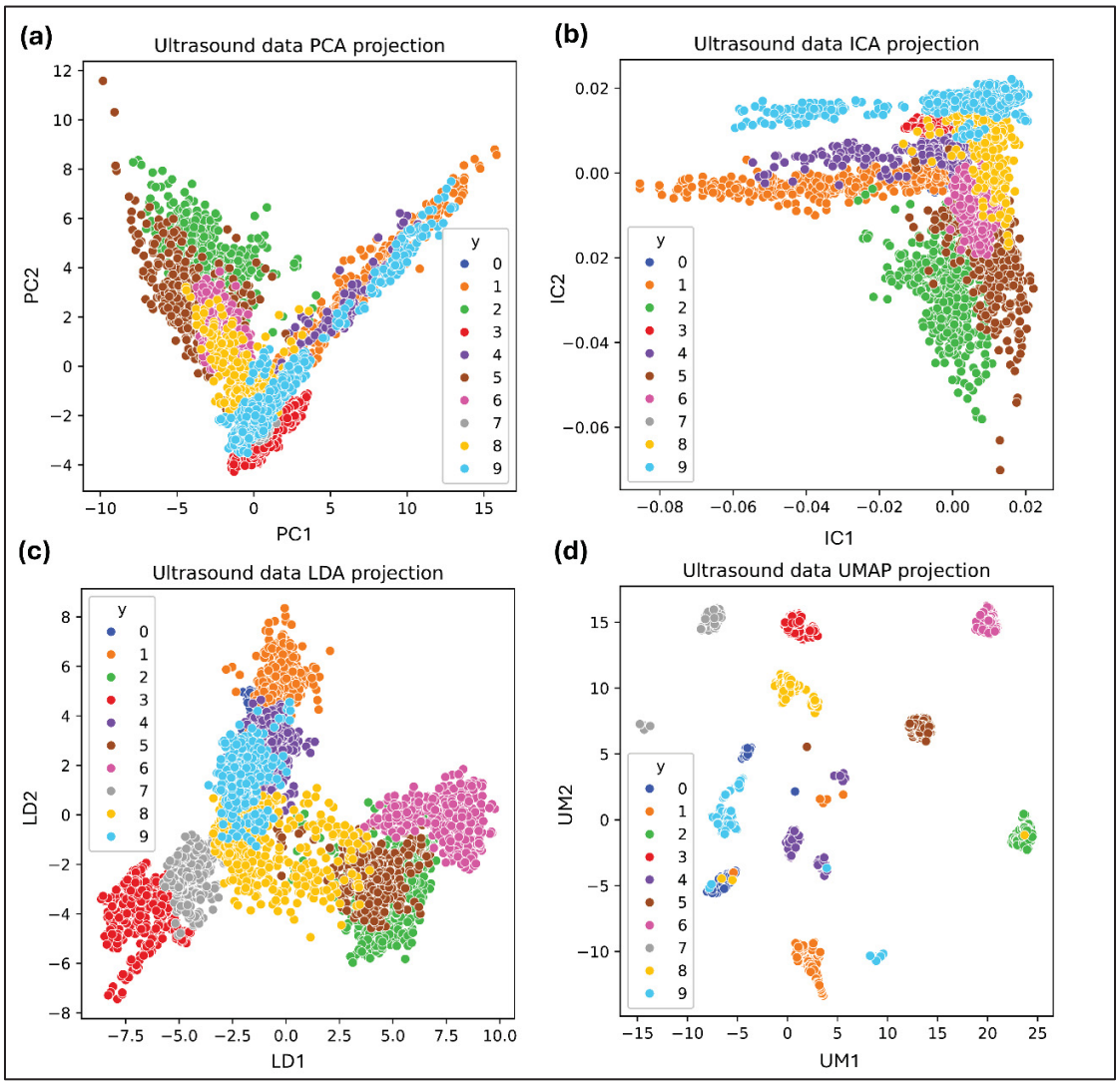

Figure 4.6 Two-dimensional representations of the ultrasonic data for the different dimensionality reduction methods evaluated: (a) PCA, (b) ICA (c) LDA, and (d) UMAP

As shown in Figure 4.7, a confusion matrix was used to assess the classification effective- ness, revealing the notably high accuracy of the GB model. The confusion matrix illustrated the algorithms' ability to classify various ultrasonic fault states such as low lubrication, over-lubrication, slow speed, steam cavitation, motor boating, reciprocating, thermostatic, healthy pipe, and healthy motor. The main diagonal of the confusion matrix consists of the TP and TN. Higher values on this diagonal indicate better model performance. This tool allowed for quick evaluation of the model's predictions and highlighted potential areas of error in the ultrasonic dataset.

In addition, in classification tasks, the ROC curve is an important tool for evaluating classifiers. It visually depicts the trade-off between the true positive rate (TPR) and the false positive rate (FPR), helping to determine a classifier's effectiveness in distinguishing between positive and negative instances. Essentially, a larger area under the ROC curve indicates a higher likelihood of correctly identifying true cases over false ones. As shown in Figure 4.8, the area under the ROC curve for each category of the dependent variable in GB consistently exceeded 0.99, demonstrating a high level of predictive precision. The ROC curve measures separability, indicating the models' ability to differentiate among fault classes. It summarizes the trade-off between TPR and FPR for a predictive model across various probability thresholds.

To thoroughly examine and qualitatively evaluate our simulated outcomes across various models, we utilized the k-fold CV technique. This method enabled us to illustrate the differences in classification effectiveness, as shown in Figure 4.9. It displays the pro- portion of correct predictions made by each model out of the total number of predictions during 5-fold data splitting. The visual representation helps highlight the comparative strengths and weaknesses of each model, ensuring a comprehensive analysis. Figure 4.9 also demonstrated that the GB model had a higher proportion of correct predictions compared to the other ensemble methods, indicating its superior efficiency.

Figure 4.10 displays a boxplot showing result variations during cross-validation across different folds. This allows for an easy comparison of the accuracy. The boxplot provides a five-number summary: minimum, first quartile, median, third quartile, and maximum. The whiskers extend to depict the rest of the distribution, excluding outliers.

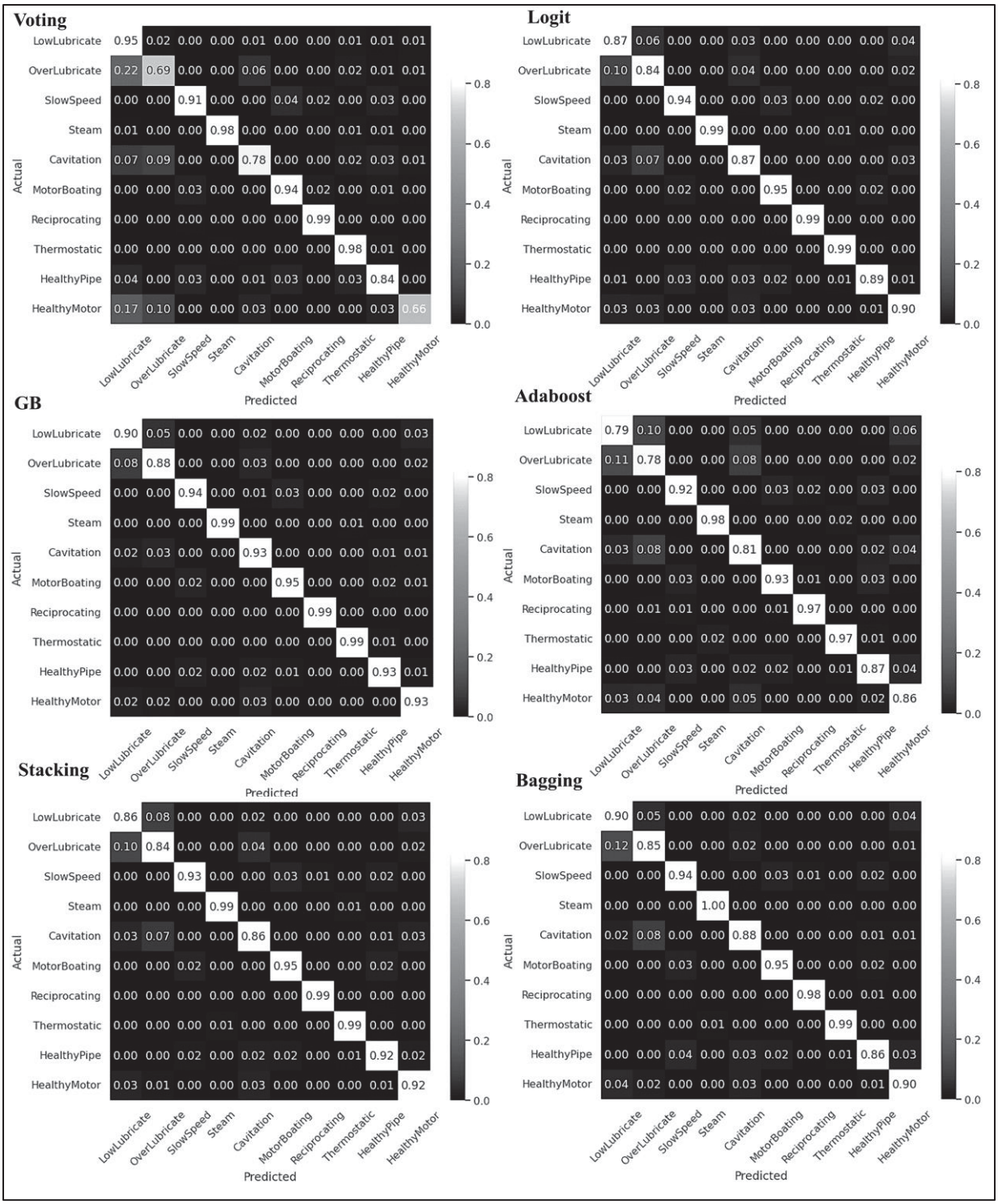

Figure 4.7 Confusion matrix for different ensemble classifiers including the voting, Logit, GB, Adaboost, stacking, and bagging algorithms

As evident, the GB model exhibited the highest accuracy and precision with the lowest distribution range. The stacking classifier indeed showed promising results, ranking second in performance after the GB classifier among the various algorithms tested.

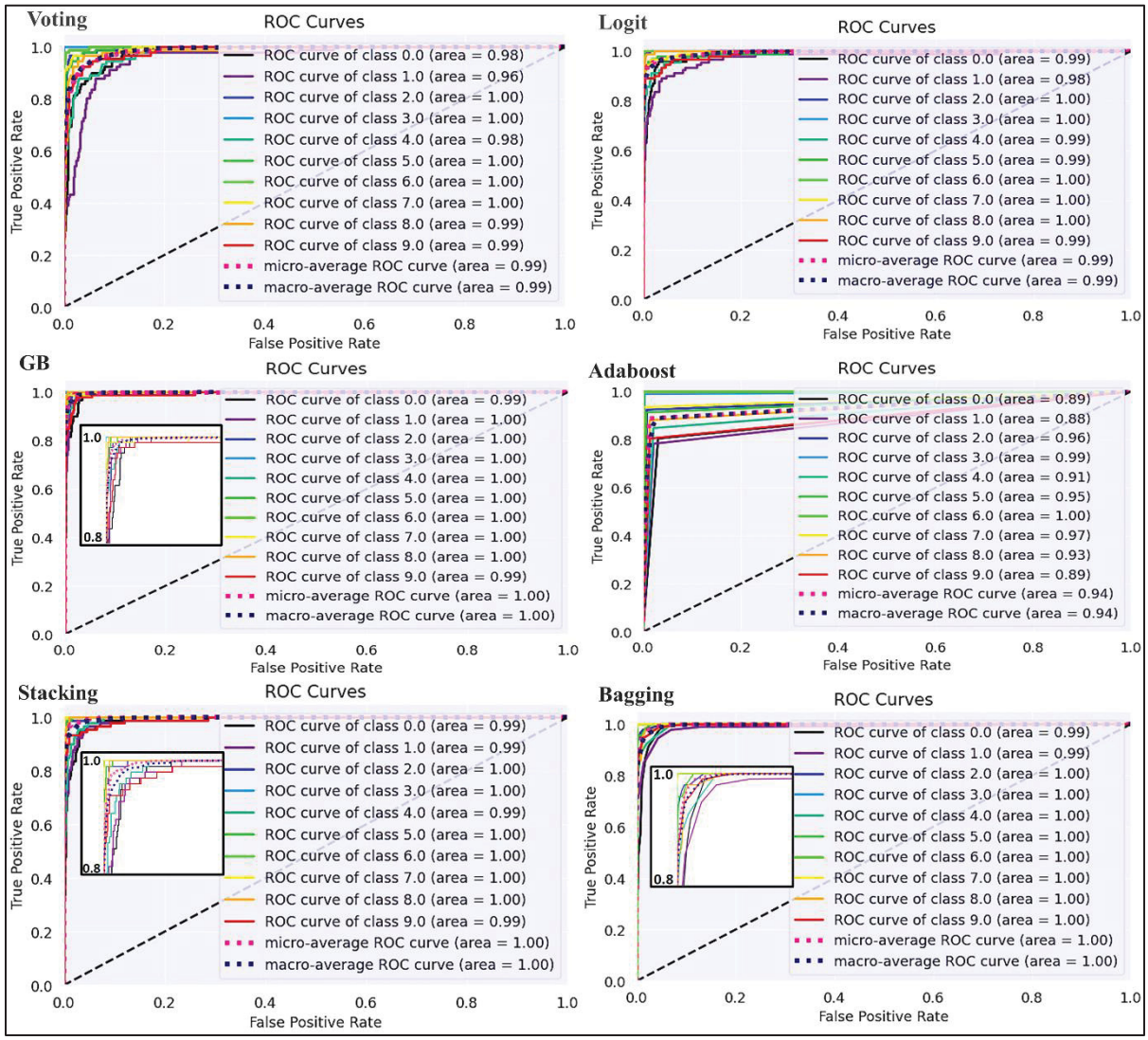

Figure 4.8 ROC curves for the voting, Logit, GB, Adaboost, stacking, and bagging algorithms

Evaluation metrics of the classifiers are shown as a bar plot in Figure 4.11 and the overall evaluation results are shown in Figure 4.12. When focusing solely on the precision metric, the bagging classifier exhibited a marginally superior average than GB.

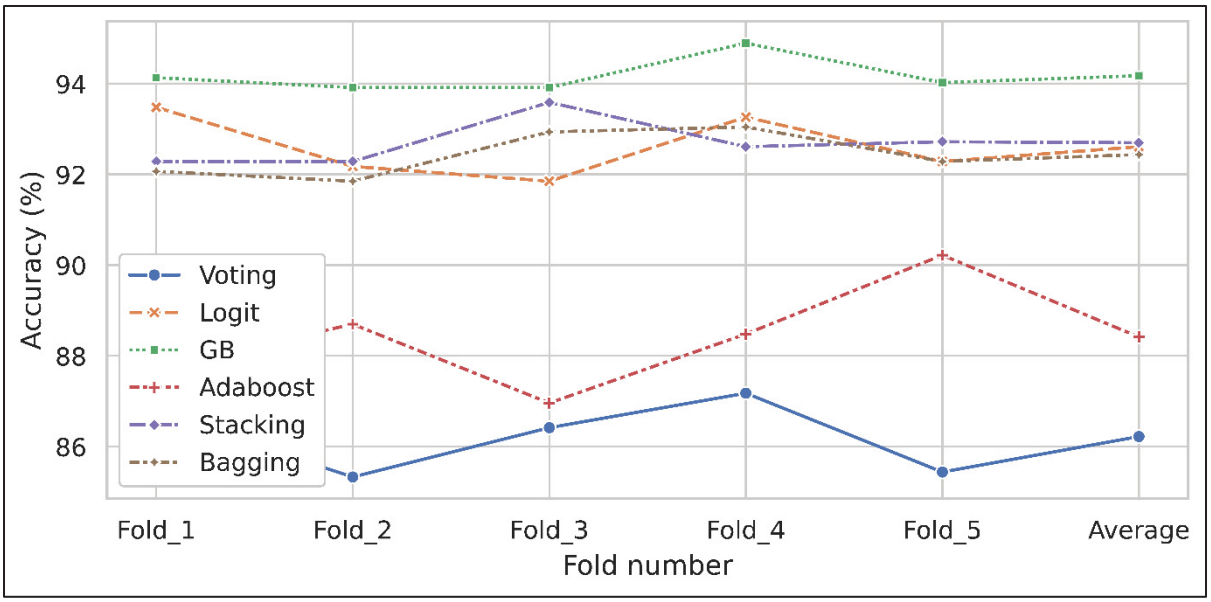

Figure 4.9 Accuracy analysis of the models using k-fold CV

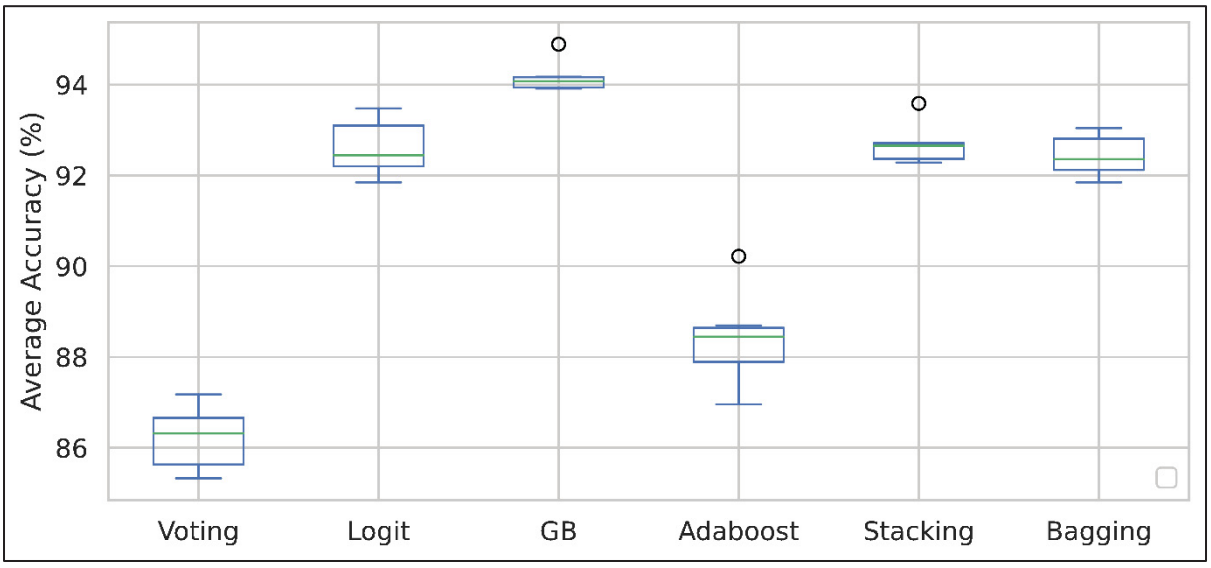

Figure 4.10 Boxplot of the accuracies for the six classifiers

Additionally, the voting classifier demonstrated commendable performance relative to the rest. Upon examining the average evaluation metrics such as accuracy, recall, precision, and F1-measure, it is evident that the GB model surpassed the other classifiers in overall performance. Among the classifiers, the GB algorithm's average accuracy (94.2%) was about 2% higher, average recall (86.5%) was about 6% higher, and average F1-measure (87.2%) was about 4% higher than the stacking classifier.

GB iteratively builds an ensemble of trees, effectively capturing complex data patterns, handling noise, and dynamically weighing features. In comparison, Adaboost struggles with noisy data and outliers, while bagging, although reducing variance, fails to capture intricate patterns as effectively. Voting aggregates multiple models but falls short when individual models differ significantly in performance, and stacking's reliance on a strong meta-classifier cannot surpass GB's individual strength. Logistic regression, being a linear model, cannot handle the non-linear complexities of ultrasonic data, making GB's non- linear approach superior (González, S., et. al. (2020)).

To further explore the effectiveness of dimensionality reduction techniques, we incorporated them as input features for the GB model. As mentioned before, the methods we examined included PCA, LDA, ICA, and UMAP. For a comprehensive understanding, Tables 4.2–4.5 provide an in-depth presentation of the respective results, including accuracy, recall, precision, and F1-measure metrics. The experimental data indicate that ICA was superior to the alternative dimensionality methods in terms of performance when used with the GB model.

According to the results depicted in the tables, ICA outperformed the other methods in terms of enhancing the GB model's accuracy. The high performance of the GB classifier with ICA suggests that this combination expertly captured the underlying structure of the ultrasonic signals.

Implementation

Deploying the model on an MCU enables real-time fault detection, reducing the need for manual inspections and minimizing downtime. In this section, two approaches for MCU deployment are investigated: direct classification based on calculated features, and an alternative approach utilizing a dimensionality reduction method as the input to the classifier, as illustrated in Figure 4.13. The ICA method exhibiting a higher accuracy (based on Tables 4.2–4.5) was selected for implementation of the second approach. ICA was computed using the Fast-ICA function and then the 'components' and 'mixing' matrices were extracted and converted to C array format using the skit-learn library in Python. The models were deployed on a 64 MHz ARM Cortex-M4F MCU.

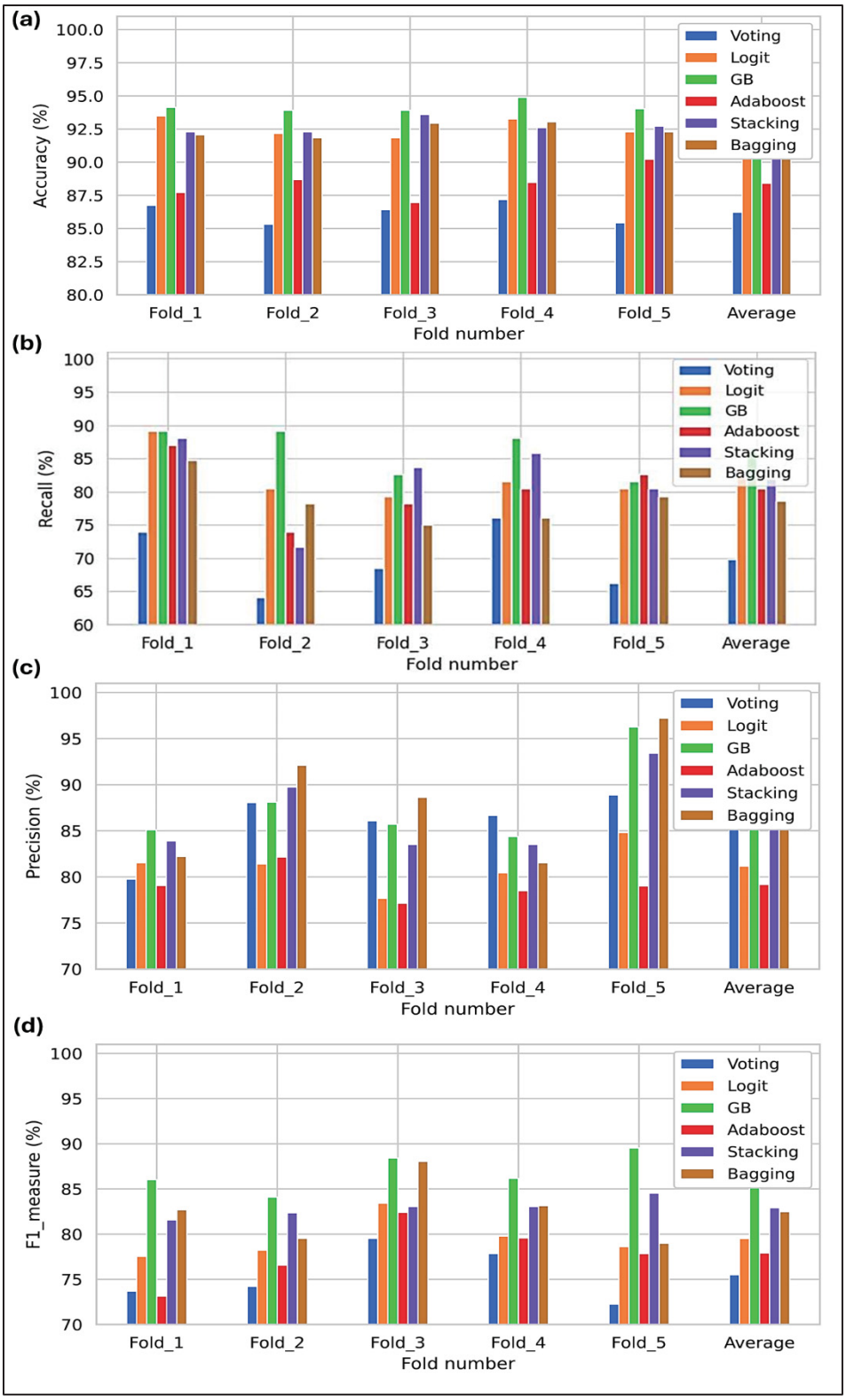

Figure 4.11 Barplot of 5-fold CV for different ensemble classifiers based on the (a) accuracy, (b) recall, (c) precision, and (d) F1 measure

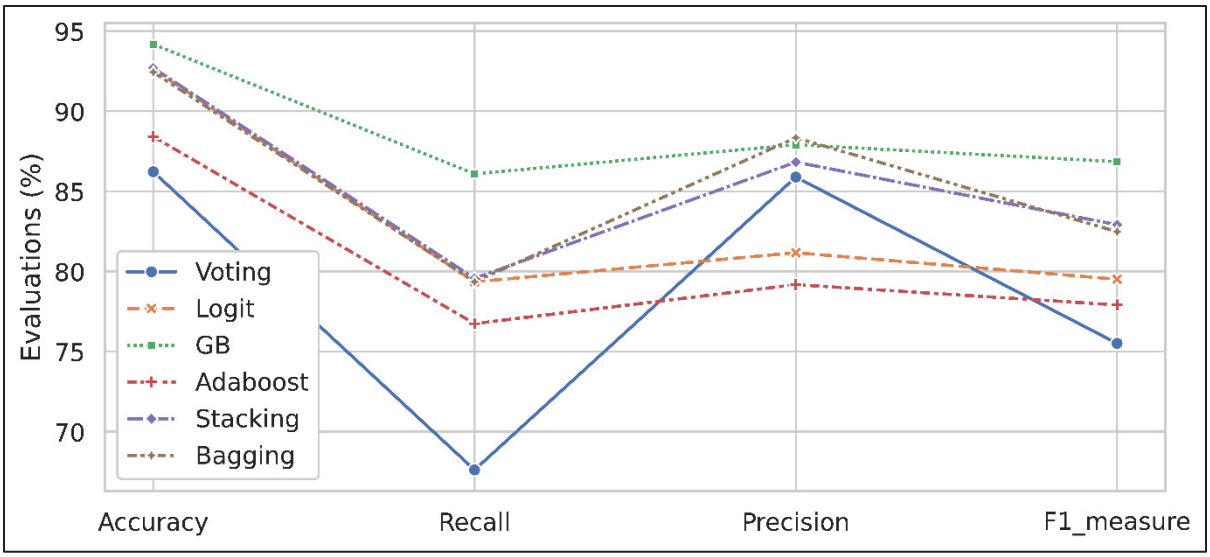

Figure 4.12 Evaluation results for the four metrics including accuracy, recall, precision, and F1-measure for different ensemble classifiers

Table 4.2 Accuracy of the GB model using various dimensionality reduction techniques including PCA, LDA, ICA, and UMAP

Fold number	PCA	LDA	ICA	UMAP
Fold_1	0.802173	0.872826	0.905434	0.726086
Fold_2	0.810869	0.891304	0.929347	0.735869
Fold_3	0.803261	0.875435	0.898913	0.727173
Fold_4	0.797826	0.859782	0.905434	0.713043
Fold_5	0.822826	0.885869	0.928267	0.759782
Average	**0.807391**	**0.876956**	**0.913478**	**0.732391**

Table 4.3 Recall of the GB model using various dimensionality reduction techniques including PCA, LDA, ICA, and UMAP

Fold number	PCA	LDA	ICA	UMAP
Fold_1	0.739130	0.543478	0.815217	0.528541
Fold_2	0.760869	0.663043	0.793478	0.489130
Fold_3	0.771739	0.543478	0.641304	0.467391
Fold_4	0.752961	0.597826	0.771739	0.576086
Fold_5	0.739130	0.608695	0.758061	0.535028
Average	**0.752173**	**0.591304**	**0.754347**	**0.506521**

Table 4.4 Precision of the GB model using various dimensionality reduction techniques including PCA, LDA, ICA, and UMAP

Fold number	PCA	LDA	ICA	UMAP
Fold_1	0.704225	0.809523	0.824175	0.511728
Fold_2	0.685393	0.843373	0.935897	0.584415
Fold_3	0.746268	0.788306	0.880597	0.632352
Fold_4	0.647058	0.741935	0.835294	0.638554
Fold_5	0.643678	0.809523	0.851851	0.547619
Average	**0.685324**	**0.798649**	**0.865563**	**0.582810**

Table 4.5 F1-measure of the GB model using various dimensionality reduction techniques including PCA, LDA, ICA, and UMAP

Fold number	PCA	LDA	ICA	UMAP
Fold_1	0.613496	0.772727	0.819672	0.505494
Fold_2	0.674033	0.872065	0.858823	0.532544
Fold_3	0.628930	0.780219	0.742138	0.537514
Fold_4	0.621468	0.745945	0.802259	0.605714
Fold_5	0.625698	0.772803	0.797687	0.522717
Average	**0.632725**	**0.774324**	**0.804116**	**0.540796**

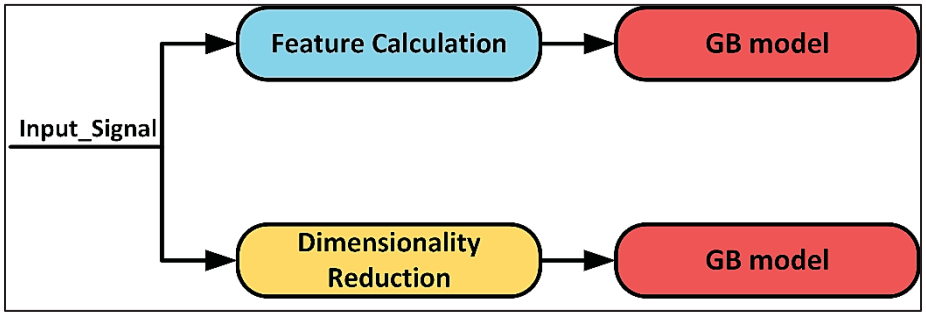

Figure 4.13 Diagram of the two deployed approaches

An LA104 Logic Analyzer with 4 channels and a sampling rate of up to 100 MSa/s along with Saleae Logic software were employed for the timing measurements. The first approach, with feature computation on the MCU, took 9.48 ms, while the second approach, with ICA computation on the MCU, took 315.44 ms. Both included 6.54 ms for data sampling and differed in their computation and prediction times, as shown in Figures 4.14 and 4.15. The first method was faster with a higher accuracy (94.2% compared to the second method with 91.35%) for our dataset, but the second method had more adaptability for diverse types of data due to the use of the ICA dimensionality reduction model. The choice of approach can vary

based on the user's criteria. Additionally, using ICA before the GB model can lead to better noise reduction and feature extraction, improving the robustness of the classifier in varying conditions. This also enhances the interpretability of the model by separating independent sources within the data, potentially revealing hidden structures in the data and improving the performance of the classifier on new, unseen data by reducing overfitting.

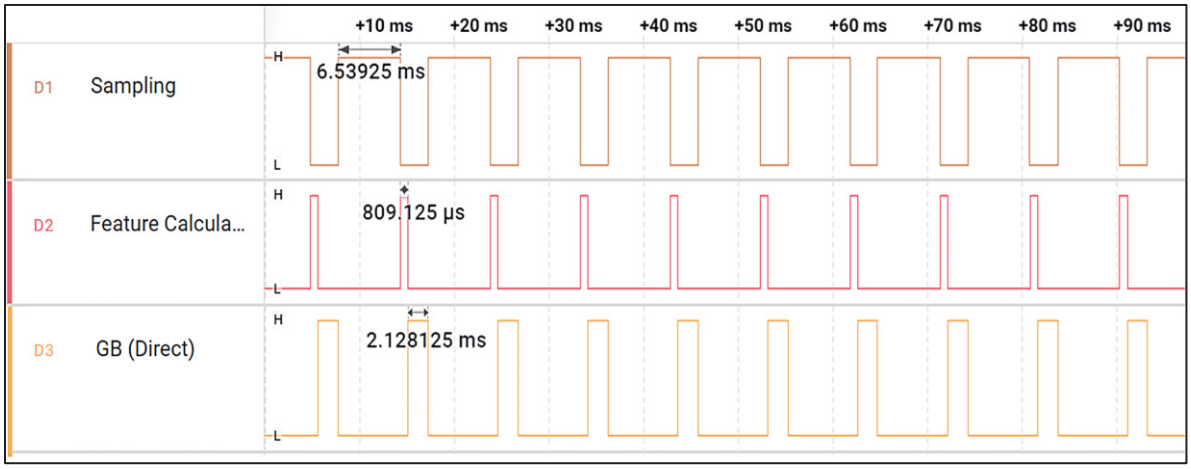

Figure 4.14 Execution time for the first approach deployed —direct classification

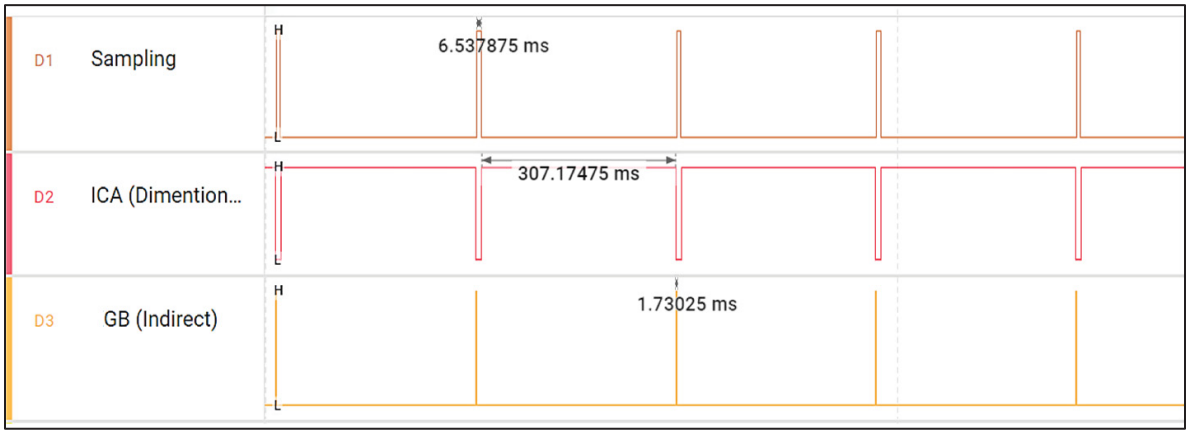

Figure 4.15 Execution time for the second deployed approach—ICA dimensionality reduction prior to classification

4.4 Conclusion

This paper presented a comprehensive model for ultrasonic industrial fault detection, targeting diverse applications such as bearings and pipelines using contact sensors. The model's

capability to evaluate and monitor the health of industrial equipment was assessed by detecting and classifying ten different ultrasonic signal conditions. Various dimensionality reduction techniques, including PCA, LDA, ICA, and UMAP, were explored, with ICA being selected for its superior performance. Ensemble classifiers such as voting, logistic regression, gradient boosting, Adaboost, stacking, and bagging were tested, demonstrating the effectiveness of the GB classifier based on performance metrics, confusion matrix, and ROC curves.

The k-fold CV technique was employed to rigorously evaluate the models' performance, ensuring robustness and generalizability. Experimental results confirmed that the GB classifier outperformed the other models in terms of accuracy, precision, recall, and F1-measure. Our results suggest that using ICA for dimensionality reduction can improve model robustness for different faults.

Advanced techniques like filtering, scaling, dimensionality reductions, and k-fold CV for ensuring evaluation can improve the signal quality for automatic defect recognition, reducing the reliance on skilled operators. Additionally, a data augmentation method is used, which helps improve the model's ability to generalize and perform well on unseen data.

Furthermore, the model's real-time applicability was demonstrated through deployment on an ARM Cortex-M4F MCU, showcasing its potential for practical industrial applications. In our study, we explored two approaches: The direct classification method proved to be quicker and more precise, whereas the ICA-based method offered greater adaptability due to its signal-dependent nature and independence from specific features. Based on the results, integrating ultrasonic signal processing with ensemble machine learning techniques improves the efficiency of industrial fault diagnosis. This study not only provides a robust framework for fault detection but also emphasizes the importance of dimensionality reduction and real-time deployment in industrial settings. However, the ICA computation time on the MCU was significantly longer than direct classification, and the dataset could be expanded for better generalizability. The focus on bearings and pipelines limited the scope of the study. Future work could expand to a greater diversity of industrial data classes, explore further optimization of MCU deployment for faster processing times, as well as developing an optimized PCB board and integrating with IoT for comprehensive fault monitoring management.

Author Contributions: Writing, software, hardware and original draft, A.M.; Supervision, review and editing, F.N. All authors have read and agreed to the published version of the manuscript.

Funding: Collaborative Research and Development Grant number CRDPJ 543712-19 and Discovery Grant RGPIN-2022-04228 from the Natural Sciences and Engineering Research Council of Canada (NSERC).

Institutional Review Board Statement: Not applicable.

Informed Consent Statement: Not applicable.

Data Availability Statement: The data presented in this study are openly available from UE Systems Co. Available online: https://www.uesystems.com/resources/sound-library/ (accessed on 1 January 2020) [UE Systems Co.].

Conflicts of Interest: The authors declare no conflicts of interest.

CONCLUSION

In conclusion, this thesis has made significant advancements in the integration of ultrasonic technology, signal processing, and machine learning, illustrating their transformative potential in various industrial and diagnostic applications. Through a series of detailed studies, this research has demonstrated how the synergy between these technologies can overcome limitations of traditional approaches, addressing critical challenges in accuracy, efficiency, and scalability.

1. **Ultrasonic Rangefinder Development**: This work introduced a novel high-accuracy ultrasonic rangefinder utilizing PMUT beams and deep learning techniques. The developed system achieved unprecedented accuracy in short-range distance measurements, proving ideal for applications in robotics, augmented reality, and safety systems. This advancement showcases ultrasonic technology's versatility across diverse fields, leveraging CNNs to push the boundaries of range-finding performance.
2. **Sensitive MEMS Cantilever Design**: The proposed piezoelectric cantilever structure offers a highly sensitive and cost-effective solution for airborne ultrasonic applications. Design C, with a smaller beam size, achieves greater displacement than design A due to its lower aspect ratio, making it more flexible and responsive for a specific amount of force or voltage. This design underscores the scalability of MEMS fabrication methods, combining trenching and array structures to enhance signal strength, leading to improved SNR and enabling more accurate signal detection in complex environments.
3. **Industrial Fault Detection**: This research developed a robust framework for detecting faults in industrial pipelines and motors by combining ultrasonic signal analysis with advanced machine learning. Utilizing ensemble models, the system demonstrated real-time fault classification with high accuracy, marking a significant step forward in predictive maintenance and industrial safety.
4. **Machine Learning Optimization**: A recurring theme across this thesis was the critical role of machine learning in refining ultrasonic signal processing. By applying dimensionality reduction techniques and recursive feature elimination, the research

improved model performance while reducing computational demands, making real-time analysis feasible on embedded systems.

5. **Integration and Scalability**: The successful deployment of ultrasonic transducers and their signal processing for fault detection on low-power MCUs validated the potential of ultrasonic technology for real-time monitoring in resource-constrained environments. This integration enables scalable, remote diagnostics for predictive maintenance in industries such as oil and gas, manufacturing, and infrastructure management.
6. **Ultrasonic Flow Meter Design (Appendix II)**: This work also presented an ultrasonic flow meter capable of accurate fluid flow measurements through non-intrusive methods. By utilizing time-of-flight principles and a unique microcantilever configuration, this design demonstrated reliable performance in industrial settings, laying groundwork for future advancements in flow measurement technologies.
7. **Optimized CMUT Design for Imaging (Appendix III)**: Finally, this thesis contributed to medical diagnostics by optimizing CMUT designs for high-resolution imaging. With a focus on noise reduction and artifact minimization, this advancement underscores the importance of clarity in diagnostic applications, reinforcing ultrasonic technology's value in healthcare.

This research underscores the transformative potential of ultrasonic MEMS systems, enhanced by machine learning, across various sectors. These findings not only provide a robust foundation for future work in ultrasonic communication and fault detection but also open avenues for integrating AI-driven analytics, multi-sensor data fusion, and wireless scalability into next-generation diagnostic and monitoring systems.

Future Directions:

1. **Multi-Sensor Integration**: Future research could explore combining ultrasonic sensors with additional modalities, such as optical or thermal sensors, to create comprehensive diagnostic tools that leverage data fusion for improved accuracy.

2. **Energy Optimization**: With practical applications in mind, future efforts should focus on developing ultra-low-power designs and efficient power management algorithms to extend battery life in portable devices.
3. **Adaptation for Extreme Environments**: Enhancing hardware for high-temperature, high-pressure, and underwater conditions could broaden ultrasonic technology's applications in challenging industrial settings.
4. **Industrial IoT and Cloud Integration**: Further scaling the system with cloud-based platforms and IoT frameworks would enable large-scale deployments, allowing multiple ultrasonic sensors to communicate in real time, integrating seamlessly into modern industrial IoT ecosystems.

This work lays a solid foundation for continued research, advancing the boundaries of ultrasonic technology in real-time monitoring, predictive maintenance, and fault diagnostics, thereby supporting the evolution of smarter, more resilient industrial and healthcare systems.

Academic Achievements:

Throughout this doctoral program, various academic accomplishments were achieved, categorized into two main types: journal articles and conference papers. These are outlined below.

Journal Papers:

1. Moshrefi, A., Ali, A., Balghari, S. T., & Nabki, F. (2024). High-accuracy airborne rangefinder via deep learning based on piezoelectric micromachined ultrasonic cantilevers. IEEE Transactions on Ultrasonics, Ferroelectrics, and Frequency Control.
2. Moshrefi, A., Tawfik, H. H., Elsayed, M. Y., & Nabki, F. (2024). Industrial fault detection employing meta ensemble model based on contact sensor ultrasonic signal. Sensors, 24(7), 2297.
3. Moshrefi, A., & Nabki, F. (2024). Advanced industrial fault detection: A comparative analysis of ultrasonic signal processing and ensemble machine learning techniques. Applied Sciences, 14(15), 6397.
4. (to be submitted) Moshrefi, A., Taghipour, P., Blaquiere. Y. Nabki, F. (2024). Enhancing the Quality of Ultrasound Medical Images Using Complementary Ensemble

Empirical Mode Decomposition with Adaptive Noise: FPGA Implementation, submitted to IEEE Transactions on Ultrasonics, Ferroelectrics, and Frequency Control.

Conference Papers:

1. Moshrefi, A., Kolahdouz. M., Pournaki, I. Ali, A., & Nabki, F. (2024, September). Advanced Design of Capacitive Micromachined Ultrasonic Transducers with Ultra-Low-Quality Factor. In 2024 IEEE International Ultrasonics Symposium (IUS) (pp. 1-3). IEEE.
2. Moshrefi, A., Blaquiere, Y., & Nabki, F. (2024, May). A precise and reliable engine knock detection utilizing meta classifier. In 2024 IEEE International Symposium on Circuits and Systems (ISCAS) (pp. 1-5). IEEE.
3. Moshrefi, A., Gratuze, M., Tawfik, H. H., Elsayed, M. Y., & Nabki, F. (2023, September). Ensemble AI fault diagnosis model using ultrasonic microphone. In 2023 IEEE International Ultrasonics Symposium (IUS) (pp. 1-3). IEEE.
4. Moshrefi, A., & Nabki, F. (2021, August). An efficient method to enhance the quality of ultrasound medical images. In 2021 IEEE International Midwest Symposium on Circuits and Systems (MWSCAS) (pp. 267-270). IEEE.
5. Moshrefi, A., & Nabki, F. (2020, June). A new method to improve the quality of embolic ultrasound signal detection. In 2020 18th IEEE International New Circuits and Systems Conference (NEWCAS) (pp. 198-201). IEEE.

APPENDIX I

CHAPTER 4

FAULT DETECTOR SYSTEM

This appendix details the components and functionality of the fault detector embedded system designed to ensure accurate monitoring and real-time fault detection, and which was presented in Chapter 4.

The system's core is the nRF52840 ARM Cortex M4F microcontroller, which supports TinyML libraries based on the written python code scikit-learn libraries (Pedregosa, F. (2011)) and is equipped with onboard sensors, including an MP34DT05 digital MEMS microphone. This microphone captures audio signals to detect industrial faults, while a u-blox Bluetooth module enables wireless data transmission, allowing alerts to be sent to connected devices, such as smartphones or PCs, for remote monitoring.

We opted for the on-chip digital microphone instead of our fabricated MEMS chip due to seamless microcontroller integration, built-in signal processing, and reduced calibration efforts. The MEMS chip required additional testing and signal conditioning, which would have introduced the complexities as a portable package. Additionally, the digital microphone's low power consumption and compact size aligned better with the system's design requirements, ensuring efficiency and reliability in the ultrasonic fault detection system.

The code captures raw 16-bit audio samples from a PDM digital microphone and converts them into a normalized 300-element array of float32 values. The neural network model originally trained in Python and converted via the TensorFlow Lite converter into a flat buffer format, is embedded as a C array for deployment. The model is loaded and executed using the Eloquent-TinyML library, which wraps TensorFlow Lite for Microcontrollers and operates using float32 data.

To validate the ML model on an MCU for 10 classes, a test file containing a diverse range of fault signals is fed into the model code running on the MCU, and the resulting class predictions are output through the MCU's GPIO pins. These outputs are then captured by the LA104 Logic Analyzer, which can sample up to 100 MSa/s and uses four channels to monitor the predicted

class signals. Using Saleae Logic software, the output signals are decoded and compared against the expected class numbers specified in the test file. Because the measured signals from the analyzer match the expected outputs, it confirms that the model is correctly detecting and predicting the corresponding faults and that the entire inference pipeline on the MCU is functioning accurately.

The system is powered by a 3.7V 3400mAh Lithium-Ion rechargeable battery, providing portability and continuous operation. Power management is handled by a TP4056 Lithium-Ion charging module, which ensures safe charging with overcharge and discharge protection. To stabilize the power supply, a large electrolytic capacitor is included, smoothing voltage fluctuations for reliable operation of the microcontroller and peripheral components.

For immediate status feedback, a 16x2 LCD display, controlled by the MCU, shows real-time information on the system's state. Messages like "No Fault!" appear during normal operation, while specific error notifications are displayed if a fault is detected. Upon activation, the MCU initializes, collects data from the microphone, and processes it to identify any abnormal patterns. If a fault is detected, the MCU triggers an alert on the LCD and transmits a notification to paired devices via Bluetooth.

This combination of components makes the fault detector system effective for real-time fault detection, with portability for field applications and dual feedback through local display and remote alerts, enhancing its practical usability in industrial environments.

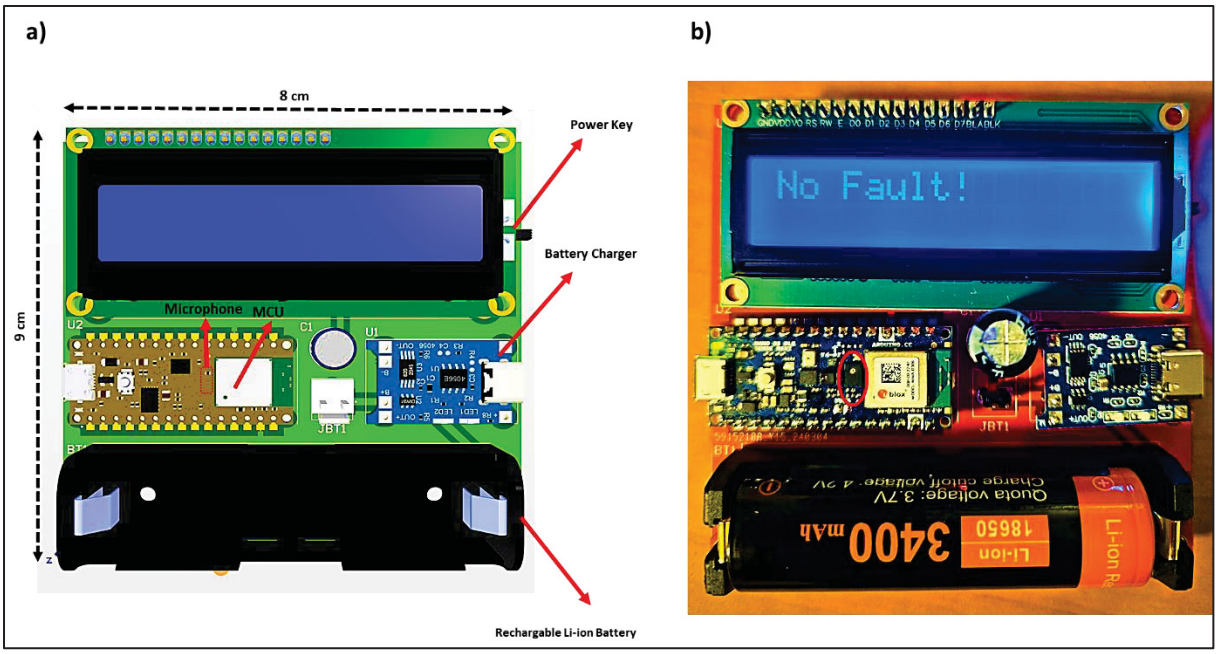

Figure A I-1 Fault detector system a) Schematic b) Fabricated and Assembled system

APPENDIX II

CHAPTER 2

ULTRASONIC FLOW METER

An ultrasonic flow meter measures fluid flow by using ultrasonic delays. It calculates flow velocity based on the time it takes for sound waves to travel between sensors. Non-intrusive and versatile, it's ideal for liquids, gases, and slurries in industrial settings.

To measure the flow, we have (Drenthen, J. G., & de Boer, G. (2001)).

$$V = \frac{\Delta t.D}{2.t_0.\sin(\theta)} \qquad \text{(A II-1)}$$

where Δt is the time difference between upstream and downstream transit times. D is the distance between the ultrasonic transducers (in meters). t_0 is the average transit time and the θ is the angle of the ultrasonic path relative to the flow direction. Therefore, the delay signal in the receiver side should be measured.

To measure the ultrasonic signals, the proposed setup involves positioning two Piezo-micro cantilever chips facing each other, with the flow passing between them at an angle. Figure A II-1 displays the designed PCB and 3D-printed components used in the measurement setup.

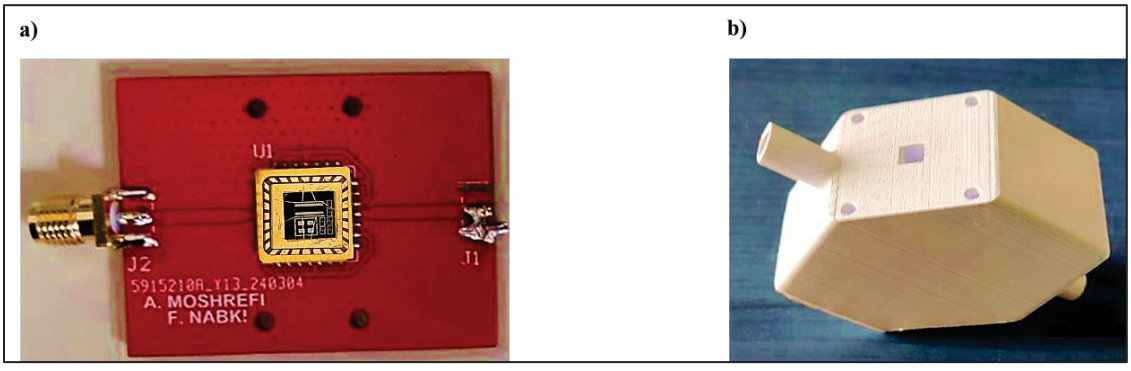

Figure A II-1 Ultrasonic Flow meter setup a) designed PCB b) designed 3D print

Finally, the setup, which consists of a Tektronix MD0405403 oscilloscope, a WA301 wideband amplifier, a Keysight 33600A function generator, and a QIUSUO gas flow rate as the reference were prepared as shown in Figure A II-2.

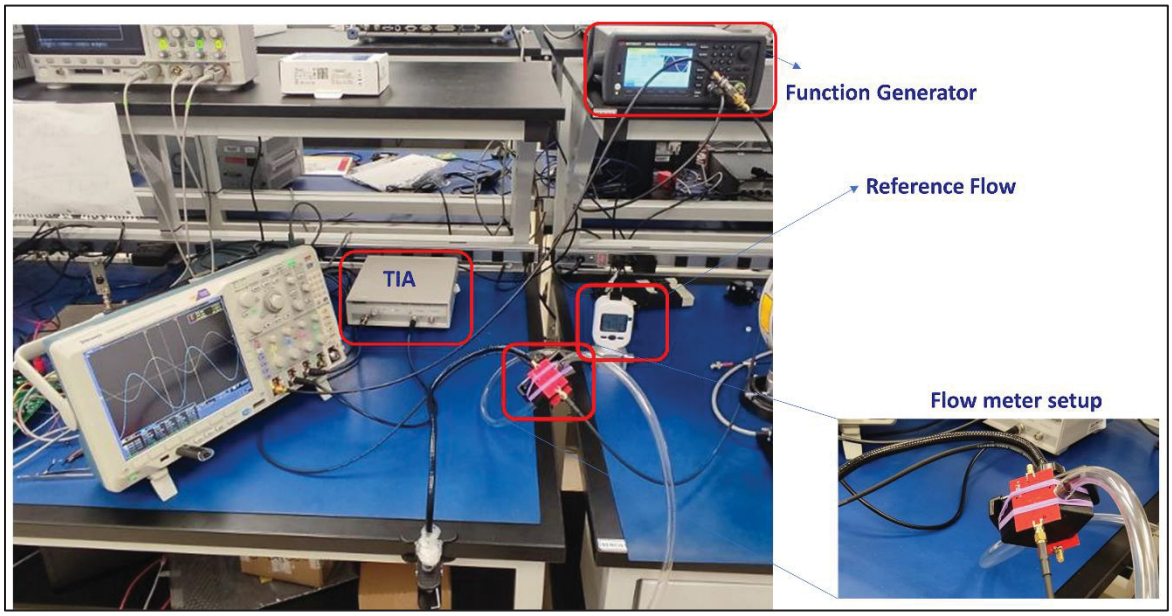

Figure A II-2 Ultrasonic Flow meter setup

It demonstrated a delay of approximately 2 μs for every 20 L/min of flow rate as shown in Figure A II-3.

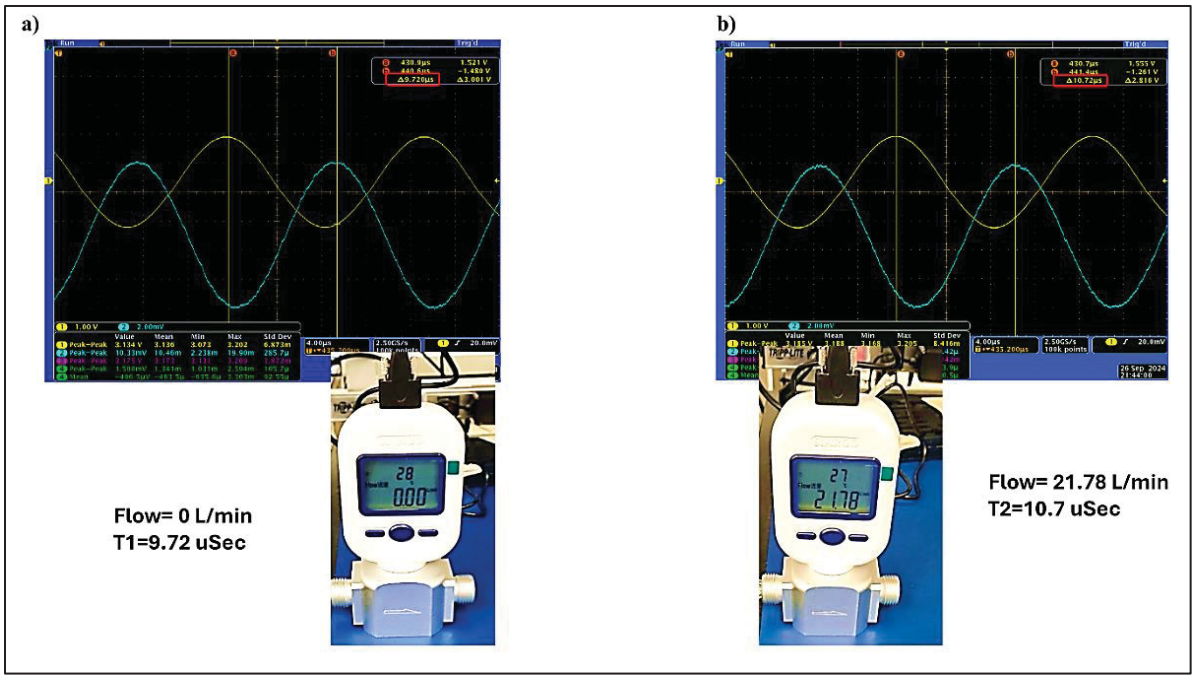

Figure A II-3 Flow rate results a) valve is closed b) valve is open

Conversely, the theoretical outcome (Figure A II-4) derived from formula (A II-1) demonstrated consistency between the practical and ideal values.

```
import math
# Given values
D = 4 / 100  # Convert cm to meters
sound_speed = 343 # m/s
theta = math. radians (60)  # Convert degrees to radians
deltaT = 2e-6 # 2 microseconds in seconds
# Calculate the average transit time t0 (for air at rest)
t0 = D / sound_speed
# Calculate flow velocity using the formula V = (Δt * D) / (2 * t0 * sin(theta))
V = (deltaT * D) / (2 * t0 * math.sin(theta))
# Convert velocity from m/s to L/min (1 m^3/s = 60 * 1000 L/min)
flow_velocity_L_min = V * 60 * 1000
print(flow_velocity_L_min)
>>
Theoretical Result: 23.763737079844997 L/min
```

Figure A II-4 Theorical result based on the setup

APPENDIX III

CHAPTER 2

ULTRA-LOW-QUALITY FACTOR CAPACITIVE MICROMACHINED ULTRASONIC TRANSDUCER

This appendix provides a detailed overview of the design and optimization of a capacitive micromachined ultrasonic transducer (CMUT) aimed at enhancing ultrasonic imaging for medical diagnostics. Ultrasonic imaging is widely utilized in healthcare due to its non-invasive, real-time imaging capabilities and high-resolution output. Applications range from cardiovascular assessments to prenatal examinations, where ultrasound enables detailed insights into soft tissue structures. However, maintaining high image quality is challenging due to issues such as noise, artifacts, and trade-offs between resolution and sensor performance (Hasegawa, 2021).

One major limitation in ultrasonic imaging is noise, which can obscure critical features, impacting diagnostic accuracy. This noise may arise from multiple sources, including electronic interference, material properties, and structural imperfections in the transducer. Additionally, artifacts like side lobes degrade image clarity by introducing false reflections or blurring fine details, particularly in high-frequency imaging where precision is essential (McDicken, 1991).

The quality factor (Q) of ultrasonic sensors is a key factor influencing both noise and image artifacts. High-Q sensors typically exhibit prolonged ringing times, leading to blurring and reduced temporal resolution, and broader side lobes that create unwanted reflections. To address these limitations, a lower-Q sensor with an optimized main lobe is essential. A lower Q reduces ringing, enhances the clarity of the primary reflection, and minimizes side lobes, leading to sharper and more accurate imaging (Tanter & Fink, 2014).

In this study, a CMUT with a low-Q factor is designed to improve image quality by balancing the sensor's mechanical and electrical properties. This optimization minimizes noise, reduces artifacts, and ensures a well-defined main imaging lobe, ultimately contributing to more reliable medical diagnostics (Tanter & Fink, 2014; Bayram et al., 2002).

Approach and Methodology

The design and validation process for the CMUT is divided into two phases:

1. Design Optimization: The initial phase involved designing a CMUT to achieve optimal imaging performance. Key objectives included balancing high-frequency operation with a low-quality factor (Q ~2), maximizing displacement, reducing side lobes, and enhancing the sharpness of the main lobe in the array.
2. Validation through Simulation and Fabrication: Following the optimization, finite element analysis (FEA) simulations were conducted using COMSOL to validate the performance improvements. This phase confirmed that the theoretical objectives—lower Q, increased displacement, and reduced side lobe levels—could be realized under practical conditions. Finally, the device was fabricated by PolyMUMPs technology, and the results were validated.

To design an optimal CMUT, it is essential to calculate parameters such as Q, frequency, and displacement. For a perforated CMUT membrane, the damping coefficient can be obtained using the approach outlined by Bao and Yang (2007). These calculations are foundational to ensuring that the CMUT achieves the desired balance of performance characteristics, ultimately improving the accuracy and reliability of ultrasonic imaging in medical applications. The governing equations are:

$$C = \frac{3\mu A^2}{2\pi d^3 N} k(\beta); \qquad \text{(A III-1)}$$

$$\beta = \frac{r_0}{r_c} \; ; k(\beta) = 4\beta^2 - \beta^4 - 4\ln(\beta) - 3$$

$$Q = \frac{\omega_0 m}{C} \qquad \text{(A III-2)}$$

where μ is the fluid's viscosity, A is the area, m is the effective mass of membrane, ω_0 is the resonance frequency, r_0 is the hole radius, and N is the number of holes influencing energy dissipation. β is the ratio of hole radius to cell radius and function $k(\beta)$ accounts for the fluid dynamics through the perforations, impacting the system's damping and Q.

The maximum displacement W_{max} of a CMUT membrane is given by (Bao, M. (2005))

$$W_{max} = \frac{\varepsilon_0 V^2 a^4}{128 D d^2} \qquad \text{(A III-3)}$$

$$D = \frac{E h^3}{12(1-\nu^2)}$$

where the ε_0 is the permittivity of free space, V is the applied voltage, a is the radius of the membrane, and d is the gap distance between the membrane and the substrate. D is the flexural rigidity, E is Young's modulus, h is the membrane thickness, and nu is Poisson's ratio. The formula shows how voltage and structural properties determine the membrane's maximum displacement.

For the array lobe optimization in an array structure, such as a CMUT array we have (Hansen, R. C. (2009))

$$\varphi_g = \sin^{-1}\left(\frac{\lambda}{s}\right) \qquad \text{(A III-4)}$$

where Φg is the grating lobe angle, which is the angle at which unwanted lobes (i.e., grating lobes) appear due to the spacing between elements. λ is the wavelength of the operating signal, and s is the distance between two adjacent cells. To ensure that grating lobes are minimized one needs to ensure $\lambda \geq s$. This prevents interference and unwanted artifacts in imaging or signal reception.

In addition, the main lobe represents the strongest part of the beam and the main lobe angle Φx, which defines the direction of the main lobe of the array is (Christensen, D. A. (1988))

$$\varphi_x = \sin^{-1}\left(\frac{\lambda}{L}\right) \qquad \text{(A III-5)}$$

where L is the total length of the array, and λ is the wavelength. A longer array L results in a narrower main lobe, improving directional resolution and reducing interference.

The main lobe optimization ensures that the strongest, sharpest beam is directed where it's needed, improving image or signal quality.

By combining these formulas, we can obtain an optimum point to have high frequency, low quality factor and high displacement which is shown in Figure A III-1.

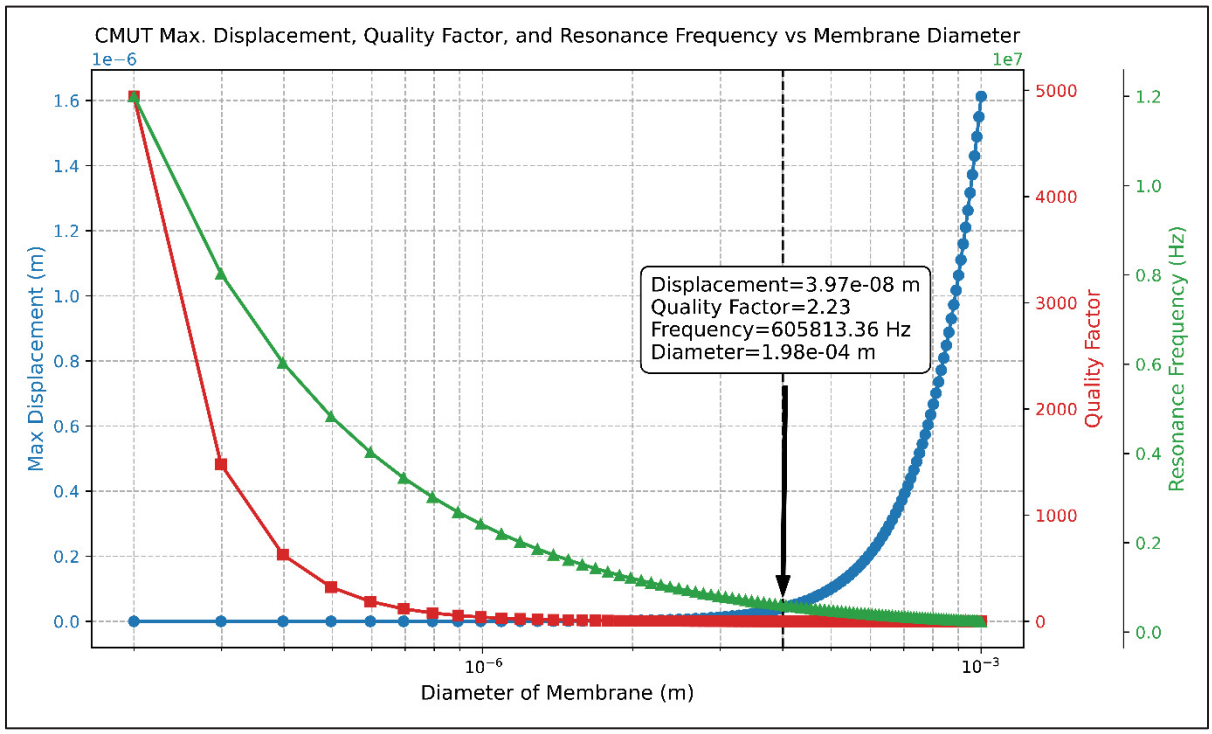

Figure A III-1 Design parameter optimization for displacement, quality factor and resonance frequency

Results

The COMSOL simulations were instrumental in refining the CMUT design, particularly in optimizing its mechanical and acoustic behavior to meet targeted performance goals. The simulations included thin film damping analysis to model the squeeze film effect between the vibrating membrane and the substrate. This analysis calculated key parameters such as the damping coefficient, membrane displacement, and pressure distribution, allowing precise optimization of the quality factor (Q) for enhanced CMUT performance. The simulation parameters were set with an applied voltage of 50 V and a permittivity of free space of 8.854×10^{-12} F/m. The initial gap height was defined as 2 μm, with silicon as the material,

characterized by a Young's modulus of 170 GPa and a Poisson's ratio of 0.22. Additionally, the design included 33 holes in the membrane structure. As shown in Figure A III-2, the optimized design achieved a measured Q of approximately 2, which minimizes ringing, improves primary reflection clarity, and reduces side lobe interference—critical for high-resolution ultrasonic imaging applications.

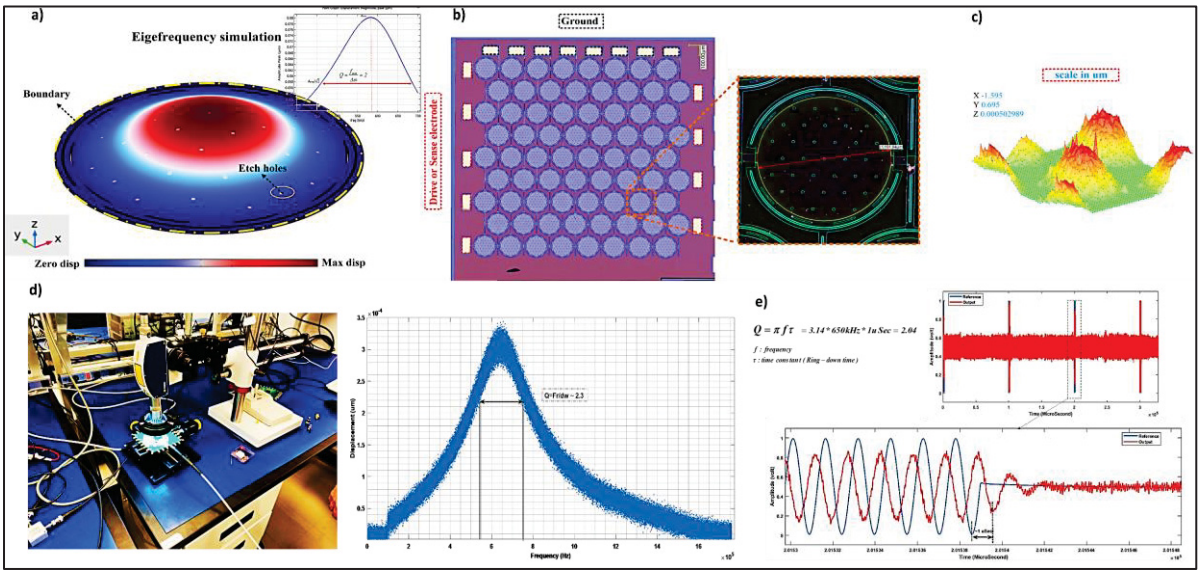

Figure A III-2 a) COMSOL simulation demonstrating that a Q of 2 results from the squeeze film damping effect. b) Fabricated CMUT array produced using the PolyMUMPS process. c) Mode shape results from vibrometer scanning, showing a 50 nm displacement, suitable for data transmission applications. d) Vibrometer measurement of Q (~2.3), validating the COMSOL simulation results. e) Ring-down time test confirming the low Q (~2.04) in the fabricated chip

BIBLIOGRAPHY

Abdelrhman, A. M., Ying, L., Ali, Y. H., Ahmad, I., Georgantopoulou, C. G., Nor, F. M., & Kurniawan, D. (2020). Diagnosis model for bearing faults in rotating machinery by using vibration signals and binary logistic regression. In AIP Conference Proceedings (Vol. 2262). https://doi.org/10.1063/5.0015150.

Adebiyi, M. O., Arowolo, M. O., Mshelia, M. D., & Olugbara, O. O. (2022). A linear discriminant analysis and classification model for breast cancer diagnosis. Applied Sciences, 12, 11455. https://doi.org/10.3390/app122211455.

Agis, D., & Pozo, F. (2019). A frequency-based approach for the detection and classification of structural changes using t-SNE. Sensors, 19, 5097. https://doi.org/10.3390/s19235097.

Aguayo-Tapia, S., Avalos-Almazan, G., Rangel-Magdaleno, J. D. J., & Ramirez-Cortes, J. M. (2023). Physical variable measurement techniques for fault detection in electric motors. Energies, 16, 4780. https://doi.org/10.3390/en16094780.

Al-Sabaeei, A. M., Alhussian, H., Abdulkadir, S. J., & Jagadeesh, A. (2023). Prediction of oil and gas pipeline failures through machine learning approaches: A systematic review. Energy Reports, 10, 1313–1338. https://doi.org/10.1016/j.egyr.2022.09.002.

Al-Sagheer, R. H. A., Mohammed, K. I., Mezher, A. A. H., & Habeeban, K. A. M. (2019). Impact of crack length into pipe conveying fluid utilizing fast Fourier transform computer algorithm. International Journal of Electrical and Computer Engineering, 9, 2541. https://doi.org/10.11591/ijece.v9i5.pp2541-2549.

Ali, A., & Lee, J. E.-Y. (2019). Fully differential piezoelectric button-like mode disk resonator for liquid phase sensing. IEEE Transactions on Ultrasonics, Ferroelectrics, and Frequency Control, 66(3), 600–608.

Bao, M. (2005). Analysis and design principles of MEMS devices. Elsevier.

Bao, M., & Yang, H. (2007). Squeeze film air damping in MEMS. Sensors and Actuators A: Physical, 136(1), 3-27.

Banik, P. P., Saha, R., & Kim, K.-D. (2020). An automatic nucleus segmentation and CNN model based classification method of white blood cell. Expert Systems with Applications, 149, Article 113211.

Bayram, B., Hsu, W., Ergun, A. S., Huang, Y., & Khuri-Yakub, B. T. (2002). Capacitive micromachined ultrasonic transducer (CMUT) design for high-frequency applications. In Proceedings of the IEEE Ultrasonics Symposium (Vol. 1, pp. 417-420). https://doi.org/10.1109/ULTSYM.2002.1193412.

Becker, V., Schwamm, T., Urschel, S., & Antonino-Daviu, J. (2021). Fault detection of circulation pumps on the basis of motor current evaluation. IEEE Transactions on Industrial Applications, 57, 4617–4624. https://doi.org/10.1109/TIA.2021.3092644.

Bui, G. T., Jiang, Y. T., & Pang, D. C. (2016). Two capacitive micro-machined ultrasonic transducers for wind speed measurement. Sensors, 16(6), 814.

Cai, L., Diao, Z., Chen, F., Guan, L., & Xu, G. (2024). Identification method of circumferential declination based on amplitude reduction of pipeline ultrasonic internal inspection signals. Nondestructive Testing and Evaluation, 37, 1–17. https://doi.org/10.1080/10589759.2023.2049870.

Carrera-Avendaño, E., Urquiza-Beltrán, G., Trutié-Carrero, E., Nieto-Jalil, J. M., Carrillo-Pereyra, C., & Seuret-Jiménez, D. (2022). Detection of crankshaft faults by means of a modified Welch-Bartlett periodogram. Engineering Failure Analysis, 132, 105938. https://doi.org/10.1016/j.engfailanal.2021.105938

Chandra, M. A., & Bedi, S. S. (2021). Survey on SVM and their application in image classification. International Journal of Information Technology, 13, 1–11. https://doi.org/10.1007/s41870-020-00530-1.

Chen, X., Xu, J., Chen, H., Ding, H., & Xie, J. (2019). High-accuracy ultrasonic rangefinders via pMUTs arrays using multi-frequency continuous waves. Journal of Microelectromechanical Systems, 28(4), 634–642.

Chen, Y., Zhou, Z., Zhang, W., Li, J., & Feng, L. (2023). Measurement of the instantaneous acoustic power of diagnostic ultrasound equipment by piezoelectric-array acoustic power meter. IEEE Transactions on Instrumentation and Measurement, 72, 1–9.

Christensen, D. A. (1988). Ultrasonic bioinstrumentation. Wiley.

Coelho, J. A., Glória, A., & Sebastião, P. (2020). Precise water leak detection using machine learning and real-time sensor data. IoT, 1, 474–493. https://doi.org/10.3390/iot1020030.

Cowen, A., Hames, G., Glukh, K., & Hardy, B. (2014). PiezoMUMPs design handbook. MEMSCAP Inc.

Dastres, R., & Soori, M. (2021). A review in advanced digital signal processing systems. International Journal of Electrical and Computer Engineering, 1(1), 1–23.

Datta, S., & Sarkar, S. (2016). A review on different pipeline fault detection methods. Journal of Loss Prevention in the Process Industries, 41, 97–106. https://doi.org/10.1016/j.jlp.2016.01.005.

Devassy, B. M., George, S., & Nussbaum, P. (2020). Unsupervised clustering of hyperspectral paper data using t-SNE. Journal of Imaging, 6, 29. https://doi.org/10.3390/jimaging6050029.

Ding, H., Liang, Z., Qi, L., Sun, H., & Liu, X. (2021). Spacecraft leakage detection using acoustic emissions based on empirical mode decomposition and support vector machine. In Proceedings of the 2021 IEEE International Instrumentation and Measurement Technology Conference (I2MTC), Glasgow, UK, IEEE (p. 5). https://doi.org/10.1109/I2MTC50364.2021.9460058.

Dong, X., Yu, Z., Cao, W., Shi, Y., & Ma, Q. (2020). A survey on ensemble learning. Frontiers of Computer Science, 14, 241–258. https://doi.org/10.1007/s11704-019-8153-2.

Drenthen, J. G., & de Boer, G. (2001). The manufacturing of ultrasonic gas flow meters. Flow Measurement and Instrumentation, 12(2), 89-99.

Dunbabin, M., & Marques, L. (2012). Robots for environmental monitoring: Significant advancements and applications. IEEE Robotics & Automation Magazine, 19(1), 24–39.

Faudzi, A. A. M., Sabzehmeidani, Y., & Suzumori, K. (2020). Application of micro-electro-mechanical systems (MEMS) as sensors: A review. Journal of Robotics and Mechatronics, 32(2), 281-288.

Gandomzadeh, D., Rohani, A., & Abbaspour-Fard, M. H. (2023). Future of Ultrasonic Transducers: How Machine Learning Is Driving Innovation. Industrial & Engineering Chemistry Research, 62(49), 21222-21236.

Gao, M., Wu, Z., Tong, Z., Zhang, Z., & Lou, L. (2023, May). An ultrasonic target identification system based on piezoelectric micromachined ultrasonic transducers. In Journal of Physics: Conference Series (Vol. 2483, No. 1, p. 012058). IOP Publishing.

Gao, M., Wu, Z., Tong, Z., Zhang, Z., & Lou, L. (2023). An ultrasonic target identification system based on piezoelectric micromachined ultrasonic transducers. Journal of Physics: Conference Series, 2483(1), Article 012058.

Gaal, M., Caldeira, R., Bartusch, J., Schadow, F., Vössing, K., & Kupnik, M. (2019). Air-coupled ultrasonic ferroelectret receiver with additional bias voltage. IEEE Transactions on Ultrasonics, Ferroelectrics, and Frequency Control, 66(10), 1600–1605.

Gerardo, C. D., Cretu, E., & Rohling, R. (2018). Fabrication and testing of polymer-based capacitive micromachined ultrasound transducers for medical imaging. Microsystems & Nanoengineering, 4(1), 19.

Ghahramani, A., Alizadeh, A., Ahmadi, M., & Anvari, M. (2019). Measuring air speed with a low-power MEMS ultrasonic anemometer via adaptive phase tracking. IEEE Sensors Journal, 19(18), 8136–8145.

González, S., García, S., Del Ser, J., Rokach, L., & Herrera, F. (2020). A practical tutorial on bagging and boosting based ensembles for machine learning: Algorithms, software tools, performance study, practical perspectives, and opportunities. Information Fusion, 64, 205–237. https://doi.org/10.1016/j.inffus.2020.07.009.

Granitto, P. M., Furlanello, C., Biasioli, F., & Gasperi, F. (2006). Recursive feature elimination with random forest for PTR-MS analysis of agroindustrial products. Chemometrics and Intelligent Laboratory Systems, 83, 83–90. https://doi.org/10.1016/j.chemolab.2006.02.013.

Hansen, R. C. (2009). Phased array antennas. Wiley.

Hasegawa, H. (2021). Advances in ultrasonography: Image formation and quality assessment. Journal of Medical Ultrasonics, 48(4), 377-389.

He, Q., Liu, J., Yang, B., Wang, X., Chen, X., & Yang, C. (2014). MEMS-based ultrasonic transducer as the receiver for wireless power supply of the implantable microdevices. Sensors and Actuators A: Physical, 219, 65–72.

Hosur, P., Shettar, R. B., & Potdar, M. (2016). Environmental awareness around vehicle using ultrasonic sensors. In Proceedings of the International Conference on Advanced Computing, Communication and Informatics (ICACCI) (pp. 1154–1159).

Iniewski, K. (Ed.). (2017). Smart sensors for industrial applications. CRC Press.

Jackson, J. C., Summan, R., Dobie, G. I., Whiteley, S. M., Pierce, S. G., & Hayward, G. (2013). Time-of-flight measurement techniques for airborne ultrasonic ranging. IEEE Transactions on Ultrasonics, Ferroelectrics, and Frequency Control, 60(2), 343–355.

Jaafar, N. S. M., Aziz, I. A., Jaafar, J., & Mahmood, A. K. (2019). An approach of filtering to select IMFs of EEMD in signal processing for acoustic emission (AE) sensors. In Intelligent Systems in Cybernetics and Automation Control Theory 2 (pp. 100–111). Springer. https://doi.org/10.1007/978-3-030-11680-4_10.

Jia, W., Sun, M., Lian, J., & Hou, S. (2022). Feature dimensionality reduction: A review. Complex & Intelligent Systems, 8, 2663–2693. https://doi.org/10.1007/s40747-021-00594-1.

Jiang, Q., Dai, J., Shao, F., Song, S., & Meng, F. (2022). Bearing early fault diagnosis based on an improved multiscale permutation entropy and SVM. Shock and Vibration, 2022, 2227148. https://doi.org/10.1155/2022/2227148.

Ju, X., & Salibián-Barrera, M. (2021). Robust boosting for regression problems. Computational Statistics & Data Analysis, 153, 107065. https://doi.org/10.1016/j.csda.2021.107065.

Kaminski, B., Jakubczyk, M., & Szufel, P. (2018). A framework for sensitivity analysis of decision trees. Central European Journal of Operations Research, 26, 135–159. https://doi.org/10.1007/s10100-017-0471-2.

Khan, A., Sohail, A., Zahoora, U., & Qureshi, A. S. (2020). A survey of the recent architectures of deep convolutional neural networks. Artificial Intelligence Review, 53(8), 5455–5516.

Kurita, T. (2019). Principal component analysis (PCA). Computer Vision: A Reference Guide, 19, 303–342. https://doi.org/10.1007/978-1-4899-7565-3_505.

Lamothe-Fernández, P., Alaminos, D., Lamothe-López, P., & Fernández-Gámez, M. A. (2020). Deep learning methods for modeling Bitcoin price. Mathematics, 8(8), 1245.

Laredo, D., Ma, S. F, Leylaz, G., Schutze, O., & Sun, J.-Q. (2020). Automatic model selection for fully connected neural networks. International Journal of Dynamics and Control, 8(4), 1063–1079.

Levinzon, F. A. (2004). Fundamental noise limit of piezoelectric accelerometer. IEEE Sensors Journal, 4(1), 108–111. https://doi.org/10.1109/78.678985.

Li, J., Ma, Y., Zhang, T., Shung, K. K., & Zhu, B. (2022). Recent advancements in ultrasound transducer: From material strategies to biomedical applications. BME Frontiers, 2022(1), 1–23. https://doi.org/10.3389/fbioe.2022.123456

Lin, H. C., & Ye, Y. C. (2019). Reviews of bearing vibration measurement using fast Fourier transform and enhanced fast Fourier transform algorithms. Advances in Mechanical Engineering, 11, 1687814018816751. https://doi.org/10.1177/1687814018816751.

Luijten, B., Chennakeshava, N., Eldar, Y. C., Mischi, M., & van Sloun, R. J. (2023). Ultrasound signal processing: from models to deep learning. Ultrasound in medicine & biology, 49(3), 677-698.

Luo, G., He, K., Wang, Y., Zhou, W., Chen, K., Zhao, L., ... & Jiang, Z. (2023). Small blind-area, high-accuracy ultrasonic rangefinder using a broadband multi-frequency piezoelectric micromachined ultrasonic transducer array. Measurement Science and Technology, 34(12), Article 125140.

Luo, G., Liu, Y., Li, X., Zhang, H., & Wang, X. (2023). Small blind-area, high-accuracy ultrasonic rangefinder using a broadband multi-frequency piezoelectric micromachined ultrasonic transducer array. Measurement Science and Technology, 34(12), 125140.

Maadi, M. (2020). Large-scale multi-frequency capacitive micromachined ultrasonic transducer (CMUT) arrays for ultrasound medical imaging and therapeutic applications.

Marcot, B. G., & Hanea, A. M. (2021). What is an optimal value of K in K-fold cross-validation in discrete Bayesian network analysis? Computational Statistics, 36, 2009–2031. https://doi.org/10.1007/s00180-021-01090-7.

Mazzilli, F., & Dehollain, C. (2020). Ultrasound Energy and Data Transfer for Medical Implants (pp. 1-143). Cham, Switzerland: Springer.

McConn, J. L., Lamoureux, C. R., Poudel, S., Palsson, B. O., & Sastry, A. V. (2021). Optimal dimensionality selection for independent component analysis of transcriptomic data. BMC Bioinformatics, 22, 584. https://doi.org/10.1186/s12859-021-04434-1.

McDicken, W. N. (1991). Diagnostic ultrasonics: Principles and use of instruments. Journal of Medical Engineering & Technology, 15(4), 161-170. https://doi.org/10.3109/03091909109025512.

Mello, R. G. T., Oliveira, L. F., & Nadal, J. (2007). Digital Butterworth filter for subtracting noise from low magnitude surface electromyogram. Computer Methods and Programs in Biomedicine, 87(1), 28–35.

Meribout, M., Azzi, A., Ghendour, N., Kharoua, N., Khezzar, L., & AlHosani, E. (2020). Multiphase flow meters targeting oil & gas industries. Measurement, 165, 108111.

Messer, A. (2015). Solutions for improved equipment reliability. Available online: https://www.bearing-news.com/mechanical-remote-monitoring-with-ultrasound/ (accessed on 30 November 2015).

Mohapatra, S., Maneesha, S., & Patra, P. K. (2023). Heart diseases prediction based on stacking classifiers model. Procedia Computer Science, 218, 1621–1630. https://doi.org/10.1016/j.procs.2023.01.201.

Moshrefi, A., Gratuze, M., Tawfik, H. H., Elsayed, M. Y., & Nabki, F. (2023). Ensemble AI fault diagnosis model using ultrasonic microphone. In Proceedings of the 2023 IEEE International Ultrasonics Symposium (IUS), Montreal, QC, Canada, 3–8 September 2023 (pp. 1–3). https://doi.org/10.1109/IUS2023.2023.1034861.

Moshrefi, A., Tawfik, H. H., Elsayed, M. Y., & Nabki, F. (2024). Industrial fault detection employing meta ensemble model based on contact sensor ultrasonic signal. Sensors, 24, 2297. https://doi.org/10.3390/s24082297.

Nihtianov, S., & Luque, A. (2018). Smart sensors and MEMS: Intelligent sensing devices and microsystems for industrial applications. Wood.

Norli, P., Frijlink, M., Standal, Ø. K.-V., Bjåstad, T. G., Prieur, F., & Vallée, E. (2018). Ultrasonic detection of stress corrosion cracks in pipe samples using guided waves. In Proceedings of the 2018 IEEE International Ultrasonics Symposium (IUS), Kobe, Japan, 22–25 October 2018 (pp. 1–4). https://doi.org/10.1109/IUS.2018.8570002.

Nti, I. K., Nyarko-Boateng, O., & Aning, J. (2021). Performance of machine learning algorithms with different K values in K-fold cross-validation. International Journal of Information Technology and Computer Science, 13, 61–71. https://doi.org/10.5815/ijitcs.2021.06.07.

Ohsaki, M., Wang, P., Matsuda, K., Katagiri, S., Watanabe, H., & Ralescu, A. (2017). Confusion-matrix-based kernel logistic regression for imbalanced data classification. IEEE Transactions on Knowledge and Data Engineering, 29, 1806–1819. https://doi.org/10.1109/TKDE.2017.2654459.

Ontivero-Ortega, M., Lage-Castellanos, A., Valente, G., Goebel, R., & Valdes-Sosa, M. (2017). Fast Gaussian naive Bayes for searchlight classification analysis. NeuroImage, 163, 471–479. https://doi.org/10.1016/j.neuroimage.2017.09.041.

Pandey, S., Kumar, P. S., Amarnath, M., Kumar, T. T., & Rakesh, P. (2021). Incipient fault detection in roller bearing using ultrasonic diagnostic technique. In Advances in Metrology and Measurement of Engineering Surfaces: Select Proceedings of ICFMMP 2019 (pp. 243–251). Springer. https://doi.org/10.1007/978-981-15-6193-4_24.

Park, J. H. (2010). Development of MEMS piezoelectric energy harvesters [Ph.D. thesis, Auburn University].

Patil, S. M., Malagi, R. R., Desavale, R. G., & Sawant, S. H. (2022). Fault identification in a nonlinear rotating system using Dimensional Analysis (DA) and central composite rotatable design (CCRD). Measurement, 200, 111610. https://doi.org/10.1016/j.measurement.2022.111610.

Patro, S. G. K., & Sahu, K. K. (2015). Normalization: A preprocessing stage. arXiv preprint arXiv:1503.06462.

Pedregosa, F., Varoquaux, G., Gramfort, A., Michel, V., Thirion, B., Grisel, O., ... & Duchesnay, É. (2011). Scikit-learn: Machine learning in Python. the Journal of machine Learning research, 12, 2825-2830.

Przybyla, R. J., Horsley, D. A., & Boser, B. E. (2011). In-air rangefinding with an AlN piezoelectric micromachined ultrasound transducer. IEEE Sensors Journal, 11(11), 2690–2697.

Przybyla, R. J., Shelton, S. E., Guedes, A., Izyumin, I. I., Kline, M. H., Horsley, D. A., & Boser, B. E. (2011). In-air rangefinding with an AlN piezoelectric micromachined ultrasound transducer. IEEE Sensors Journal, 11(11), 2690–2697.

Pyle, R., Wilcox, P., Hughes, R. R., & Bevan, R. L. (2023). Application of machine learning to ultrasonic nondestructive evaluation (Doctoral dissertation, University of Bristol).

Quy, T. B., & Kim, J. M. (2021). Real-time leak detection for a gas pipeline using a k-nn classifier and hybrid AE features. Sensors, 21, 367. https://doi.org/10.3390/s21020367.

Rai, A., & Kim, J. M. (2021). A novel pipeline leak detection approach independent of prior failure information. Measurement, 167, 108284. https://doi.org/10.1016/j.measurement.2020.108284.

Raišutis, R., Tumšys, O., Žukauskas, E., Samaitis, V., Draudviliene, L., & Jankauskas, A. (2023). An inspection technique for steel pipes wall condition using ultrasonic guided helical waves and a limited number of transducers. Materials, 16, 5410. https://doi.org/10.3390/ma16155410.

Ranjan Laha, S., Pattanayak, B. K., & Pattnaik, S. (2022). Advancement of environmental monitoring system using IoT and sensor: A comprehensive analysis. AIMS Environmental Science, 9(6), 771–800.

Robichaud, A., Deslandes, D., Cicek, P.-V., & Nabki, F. (2020). Electromechanical tuning of piecewise stiffness and damping for long-range and high-precision piezoelectric ultrasonic transducers. Journal of Microelectromechanical Systems, 29(5), 1189–1198.

Roy, K., Lee, J. E.-Y., & Lee, C. (2023). Thin-film PMUTs: A review of over 40 years of research. Microsystems & Nanoengineering, 9(1), 95.

Salunkhe, V. G., Khot, S. M., Desavale, R. G., & Yelve, N. P. (2023). Unbalance bearing fault identification using highly accurate Hilbert-Huang transform approach. Journal of Nondestructive Evaluation, Diagnostics and Prognostics of Engineering Systems, 6, 031005. https://doi.org/10.1115/1.4055262.

Saucedo-Dorantes, J. J., Jaen-Cuellar, A. Y., Delgado-Prieto, M., de Jesus Romero-Troncoso, R., & Osornio-Rios, R. A. (2021). Condition monitoring strategy based on an optimized selection of high-dimensional set of hybrid features to diagnose and detect multiple and combined faults in an induction motor. Measurement, 178, 109404. https://doi.org/10.1016/j.measurement.2020.109404.

Sharma, A. (2022). Fault diagnosis of bearings using recurrences and artificial intelligence techniques. Journal of Nondestructive Evaluation, Diagnostics and Prognostics of Engineering Systems, 5, 031004. https://doi.org/10.1115/1.4054821.

Shahrivari, S. (2014). Beyond batch processing: Towards real-time and streaming big data. Computers, 3(4), 117–129.

Shinde, P. V., & Desavale, R. G. (2022). Application of dimension analysis and soft competitive tool to predict compound faults present in rotor-bearing systems. Measurement, 193, 110984. https://doi.org/10.1016/j.measurement.2022.110984.

Selesnick, I. W., & Burrus, C. S. (1998). Generalized digital Butterworth filter design. IEEE Transactions on Signal Processing, 46, 1688–1694. https://doi.org/10.1109/78.678985.

Soomro, A. A., Mokhtar, A. A., Kurnia, J. C., Lashari, N., Lu, H., & Sambo, C. (2022). Integrity assessment of corroded oil and gas pipelines using machine learning: A systematic review. Engineering Failure Analysis, 131, 105810. https://doi.org/10.1016/j.engfailanal.2021.105810.

Song, C., Chen, J., Lu, Z., Li, F., & Liu, Y. (2023). Steel surface defect detection via deformable convolution and background suppression. IEEE Transactions on Instrumentation and Measurement, 72, 1–9.

Sonmezoglu, S., Arslan, Y., & Erkan, H. (2017). Passive signal amplification via series-piezoelectric read-out. In Proceedings of the 19th International Conference on Solid-State Sensors, Actuators, and Microsystems (pp. 155–158).

Sravani, S., & Karthikeyan, P. R. (2023). Detection of cardiovascular disease using KNN in comparison with naive Bayes to measure precision, recall, and F-score. In AIP Conference Proceedings (Vol. 2821). https://doi.org/10.1063/5.0138947.

Sultana, N., & Islam, M. M. (2020). Meta classifier-based ensemble learning for sentiment classification. In Proceedings of the International Joint Conference on Computational Intelligence: IJCCI 2018 (pp. 73–84). Springer. https://doi.org/10.1007/978-3-030-38133-2_5.

Tanha, J., Abdi, Y., Samadi, N., Razzaghi, N., & Asadpour, M. (2020). Boosting methods for multi-class imbalanced data classification: An experimental review. Journal of Big Data, 7, 1–47. https://doi.org/10.1186/s40537-020-00307-0.

Tanter, M., & Fink, M. (2014). Ultrafast imaging in biomedical ultrasound. IEEE Transactions on Ultrasonics, Ferroelectrics, and Frequency Control, 61(1), 102-119. https://doi.org/10.1109/TUFFC.2014.6689779

Thara, D. K., PremaSudha, B. G., & Xiong, F. (2019). Auto-detection of epileptic seizure events using deep neural network with different feature scaling techniques. Pattern Recognition Letters, 128, 544–550. https://doi.org/10.1016/j.patrec.2019.06.009.

Tharwat, A., Gaber, T., Ibrahim, A., & Hassanien, A. E. (2017). Linear discriminant analysis: A detailed tutorial. AI Communications, 30, 169–190. https://doi.org/10.3233/AIC-170428.

Ting, L. L. (2017). Detection of water pipeline leakage using time and frequency signal. UTAR: Tartu, Estonia.

Toa, M., & Whitehead, A. (2020). Ultrasonic sensing basics. Texas Instruments Technical Report SLAA907, 53–75.

Toma, R. N., & Kim, J. M. (2022). Bearing fault classification of induction motor using statistical features and machine learning algorithms. Lecture Notes in Networks and Systems, 418, 243–254. https://doi.org/10.1007/978-3-030-95235-7_22.

Toma, R. N., Piltan, F., & Kim, J. M. (2021). A deep autoencoder-based convolution neural network framework for bearing fault classification in induction motors. Sensors, 21, 8453. https://doi.org/10.3390/s21248453.

Ullah, S., Ahmad, Z., & Kim, J. M. (2024). Fault Diagnosis of a Multistage Centrifugal Pump Using Explanatory Ratio Linear Discriminant Analysis. Sensors, 24(6), 1830.

UE Systems. (2020). Sound library. Available online: https://www.uesystems.com/resources/sound-library/ (accessed on 1 January 2020).

Van Der Maaten, L., Postma, E. O., & Van Den Herik, H. J. (2009). Dimensionality reduction: A comparative review. Journal of Machine Learning Research, 10(66-71), 13.

Veroniki, A. A., Hutton, B., Stevens, A., McKenzie, J. E., Page, M. J., Moher, D., ... & Tricco, A. C. (2025). Update to the PRISMA guidelines for network meta-analyses and scoping reviews and development of guidelines for rapid reviews: a scoping review protocol. JBI evidence synthesis, 10-11124.

Vishwendra, M. A., Salunkhe, P. S., Patil, S. V., Shinde, S. A., Shinde, P. V., Desavale, R. G., Jadhav, P. M., & Dharwadkar, N. V. (2022). A novel method to classify rolling element bearing faults using K-nearest neighbor machine learning algorithm. ASCE-ASME Journal of Risk and Uncertainty in Engineering Systems Part B: Mechanical Engineering, 8, 031202. https://doi.org/10.1115/1.4055112.

Wang, H., Chen, Z., Yang, H., Jiang, H., & Xie, H. (2020). A ceramic PZT-based PMUT array for endoscopic photoacoustic imaging. Journal of Microelectromechanical Systems, 29(5), 1038–1043.

Wang, H., Fan, Z., Chen, X., Cheng, J., Chen, W., Wang, Z., & Bu, Y. (2022). Automated classification of pipeline defects from ultrasonic phased array total focusing method imaging. Energy, 5, 8272. https://doi.org/10.1016/j.energy.2022.04.025.

Wang, H., Ma, Y., Yang, H., Jiang, H., Ding, Y., & Xie, H. (2020). MEMS ultrasound transducers for endoscopic photoacoustic imaging applications. Micromachines, 11(10), 928.

Wei, M., Miao, Q., & Jiang, L. (2024). Feature extraction method for ultrasonic pipeline defects based on fractional-order VMD. Nondestructive Testing and Evaluation, 39, 1–20. https://doi.org/10.1080/10589759.2023.2056567.

Wong, T.-T., & Yeh, P.-Y. (2019). Reliable accuracy estimates from k-fold cross validation. IEEE Transactions on Knowledge and Data Engineering, 32, 1586–1594. https://doi.org/10.1109/TKDE.2019.2903502.

Yadav, S., & Shukla, S. (2016). Analysis of K-fold cross-validation over hold-out validation on colossal datasets for quality classification. In Proceedings of the 2016 IEEE 6th International Conference on Advanced Computing (IACC), Bhimavaram, India, 27–28 February 2016 (pp. 78–83). https://doi.org/10.1109/IACC.2016.19.

Yadavendra, S. (2020). A comparative study of breast cancer tumor classification by classical machine learning methods and deep learning method. Machine Vision and Applications, 31, 46. https://doi.org/10.1007/s00138-020-01071-6.

Yates, L. A., Aandahl, Z., Richards, S. A., & Brook, B. W. (2023). Cross validation for model selection: A review with examples from ecology. Ecological Monographs, 93(1), Article e1557.

Yole Group. (2023, October 10). Ultrasound: More than a choice, a strategic positioning for players. Yole Group. Retrieved October 24, 2024, from https://www.yolegroup.com/press-release/ultrasound-more-than-a-choice-a-strategic-positioning-for-players/

Yu, Y., Safari, A., Niu, X., Drinkwater, B., & Horoshenkov, K. V. (2021). Acoustic and ultrasonic techniques for defect detection and condition monitoring in water and sewerage pipes: A review. Applied Acoustics, 183, 108282. https://doi.org/10.1016/j.apacoust.2021.108282.

Yuan, J., Mao, W., Hu, C., Zheng, J., Zheng, D., & Yang, Y. (2023). Leak detection and localization techniques in oil and gas pipeline: A bibliometric and systematic review. Engineering Failure Analysis, 146, 107060. https://doi.org/10.1016/j.engfailanal.2023.107060.

Zhang, M., Guo, Y., Xie, Q., Zhang, Y., Wang, D., & Chen, J. (2022). Defect identification for oil and gas pipeline safety based on autonomous deep learning network. Computer Communications, 195, 14–26. https://doi.org/10.1016/j.comcom.2022.02.001.

Zhang, Q., Ruan, W., Wang, H., Zhou, Y., Wang, Z., & Liu, L. (2010). A self-bended piezoresistive microcantilever flow sensor for low flow rate measurement. Sensors and Actuators A: Physical, 158(2), 273–279.